2012

THE EFFECT OF SPILLOVER ONTO IONOTROPIC GLUTAMATE RECEPTORS AT THE SCHAFFER-CA1 SYNAPSE IN HIPPOCAMPAL SLICE

Katie Marie Hoffman
The University of Montana

THE EFFECT OF SPILLOVER ONTO IONOTROPIC GLUTAMATE RECEPTORS AT THE SCHAFFER-CA1 SYNAPSE IN HIPPOCAMPAL SLICE

By

Katie Marie Hoffman

BA in Psychology, University of Montana, Missoula, MT, 2005
BS in Microbiology, University of Montana, Missoula, MT, 2007

Dissertation

presented in partial fulfillment of the requirements
for the degree of

Doctor of Philosophy
in Neuroscience

The University of Montana
Missoula, MT

July 2012

Approved by:
Sandy Ross, Associate Dean of The Graduate School
Graduate School

Dr. Michael P. Kavanaugh, Chair
Department of Biomedical and Pharmaceutical Sciences

Dr. Richard J. Bridges
Department of Biomedical and Pharmaceutical Sciences

Dr. Charles M. Thompson
Department of Biomedical and Pharmaceutical Sciences

Dr. J. Josh Lawrence
Department of Biomedical and Pharmaceutical Sciences

Dr. Emily F. Stone
Department of Mathematical Science

Hoffman, Katie, Ph.D., July 2012 Major
Neuroscience

THE EFFECT OF SPILLOVER ONTO IONOTROPIC GLUTAMATE RECEPTORS AT THE SCHAFFER-CA1 SYNAPSE IN HIPPOCAMPAL SLICE

Chairperson: Michael P. Kavanaugh, Ph.D.

Abstract

Glutamate is the major excitatory neurotransmitter in the brain and is crucial for processes such as learning and memory. Due its importance as a signaling molecule, the extracellular glutamate concentration is tightly regulated, largely by the excitatory amino-acid transporters (EAATs). In these studies, we investigated the role of EAAT1-3 in synaptic transmission at the Schaffer-CA1 synapse in acute hippocampal brain slices. My results demonstrated that transport block by L-TBA resulted in glutamate spillover and activation of NMDARs. Further investigation showed that L-TBA-mediated activation of NMDARs was facilitated by the Mg^{2+} unblock of the receptor. Furthermore our data indicate that NMDAR signaling was controlled by the interplay between several factors, including synaptic frequency, glutamate transport, Mg^{2+} block, and NMDAR channel kinetics. We propose that the observed theta frequency threshold for enhanced NMDAR signaling observed in physiological conditions is a consequence of a phase shifted signal at rhythms limited by NMDAR channel kinetics. We also found that dense fiber recruitment created conditions of spillover and glutamate pooling and therefore resulted in an increase in AMPAR desensitization at the hippocampal Schaffer-CA1 synapse. Overall my studies focused on the effects of glutamate spillover onto both NMDA and AMPA receptors at the Schaffer-CA1 synapse in hippocampal slice.

Acknowledgements

I would like to thank all those who contributed to my path as a scientist and a person at the University of Montana. First and foremost is my advisor, Michael Kavanaugh, who pushed me to become a dedicated and meticulous scientist in my words and actions, and see the beauty in an elegantly designed experiment. I would also like to thank my committee members; Dr. Bridges, Dr. Thompson, Dr. Lawrence, Dr. Stone, for their commitment and guidance to my educational development. I would like to thank the administrators: Dr. Sandy Ross, Dr. Vernon Grund, and Dr. Lori Morin for always having an open door and keeping my best interest in mind. My formation as a scientist would not have been the same without my labmates and friends: Carla Burgess, Valerie Mosser, Kami Chiotti, Phillip Beske, Loretta Bolyard, Alicia Angell, Gregory Leary, Weinan Sun, and Avi Rascoe. I would like to thank Sarj Patel and Fred Rhodrick for always being there for me. I cherish my time spent at the University of Montana and in Missoula. I can attest that the person I am today is because of my experiences there.

This work is dedicated to JSR, who was always there for me.

Table of Contents

LIST OF FIGURES

CHAPTER 1 : BACKGROUND AND SIGNIFICANCE

Presynaptic Release

During normal excitatory synaptic transmission, an action potential (AP) travels down the axon and arrives at the presynaptic terminal. Upon arrival at the presynaptic terminal, voltage-gated Ca^{2+} channels are opened and the influx of Ca^{2+} leads to the fusion and release of neurotransmitter vesicle(s) (Miledi and Slater, 1966). When two successive stimuli are received by the presynaptic terminal within a brief interval (i.e. 50 milliseconds), the presence of residual Ca^{2+} from the first AP results in an increased release probability and a facilitation of the amplitude of the second excitatory post synaptic potential (EPSP;Katz and Miledi,1968, reviewed in Thomson 2000). This observation is now known as paired-pulse facilitation and is reported as the average amplitude of the second EPSP divided by the average amplitude of first EPSP or paired-pulse ratio (PPR). The PPR has primarily been utilized as an indication of the probability of presynaptic release due to its inverse correlation with modifications in intracellular calcium concentration in the terminal, while possible postsynaptic contributions to the PPR are not well established (Katz and Miledi, 1968; Dobrunz and Stevens, 1997; Debanne et al. 1996; Manita et al. 2007).

Glutamate Concentration in the Synaptic Cleft

Glutamate is the major excitatory neurotransmitter and therefore the maintenance of its extracellular concentration is critical due to its' role as a signaling molecule. The concentration of extracellular basal glutamate in the hippocampal slice has only recently been estimated to be in the nanomolar range as a consequence of the equilibrium thermodynamics of glutamate transporters (~25 nM, Herman and Jahr, 2007; Zerangue and Kavanaugh, 1996). Following vesicle fusion, glutamate diffuses across the synaptic cleft onto the postsynaptic cell where millimolar concentrations occur for a brief time (Clements et al, 1992). The glutamate concentration that is 'sensed' by postsynaptic receptors is altered by a number of factors (e.g.

neuronal and glial glutamate transporters, synaptic architecture, diffusion rate, number of vesicles released).

Glutamate Transporters

In the hippocampus, there are three subtypes of excitatory amino acid transporters (EAAT1-3) that are expressed on different cell types; EAAT1/2 are expressed on glia and EAAT3 is expressed on neurons (Danbolt, 2001). Interestingly, non-specific block of glutamate uptake in the hippocampus has revealed cooperation between independent excitatory synapses (Asztely et al. 1997, Arnth-Jensen et al. 2002). The development of high affinity subtype specific pharmacological blockers has not been completely successful, and therefore characterization of novel EAAT blockers is an important step in understanding subtype specific effects on synaptic signaling. β-threo-benzyloxy-aspartate (TBOA) is one of the most frequently used non-specific transport blockers and shows similar action among all of the EAAT subtypes, yet its related aspartate analogue L-β-threo-benzyl-aspartate (L-TBA) exhibits its highest affinity at EAAT3 compared to EAAT1 and EAAT2 (K_D:2μM,12μM,9μM, respectively; Esslinger et al. 2005). Dihydrokainate (DHK) is a derivative of EAA receptor agonist kainate and is the most commonly used selective EAAT2 blocker (K_i:3mM,23μM,3mM at EAAT1, EAAT2, and EAAT3 respectively, Arriza et al. 1994). Only until recently had an EAAT1 specific blocker has been reported, UCPH-101 (EAAT1 IC_{50}=0.66μM, Jensen et al. 2009). Although the affinities of the aforementioned transport blockers are in the micromolar range, not all of them have been throughly characterized in brain slice.

Postsynaptic response

Spatial effects

In recent years, evidence has accumulated that suggests that extrasynaptic signaling may occur at a single synapse or cross-talk may occur between groups of synapses onto glutamate receptors. One example of extrasynaptic signaling occurs when a single synapse releases neurotransmitter that spills onto neighboring synapses, resulting in what has been

termed “spillover” (Kullmann et al. 1996, Scimemi et. al 2004, Bailey et al. 2000, Pankratov and Krishtal 2003). Another type of extrasynaptic signaling occurs heterosynaptically when the residual glutamate concentration is elevated between multiple release sites and is referred to as “glutamate pooling”(Otis et al. 1996). Glutamate pooling between synapses and the subsequent crosstalk between release sites has been demonstrated in large calyceal synapses containing large numbers of neurotransmitter release sites (Otis et al. 1996).

Ionotropic glutamate receptors

As stated above, glutamate is the primary excitatory neurotransmitter within the central nervous system. The presynaptically released glutamate has been shown to bind postsynaptic N-methyl-D-aspartic acid (NMDA) and alpha-amino-3-hydroxy-5-methyl-4-isoxazole-propionic acid (AMPA) receptors.

AMPARs

When glutamate arrives at the postsynaptic density, it binds to two subtypes of ionotropic glutamate receptors, the AMPAR and the NMDAR, which shape the kinetics of the EPSP. AMPA receptors display fast decay kinetics in which they are rapidly activated, desensitized, and deactivated, and have a low affinity (EC_{50}=46 μM) for glutamate (Attwell & Gibb, 2005; Weston et al. 2006, Jones & Westbrook 1996). Although AMPARs were originally hypothesized to be insensitive to glutamate pooling and spillover (Kullman & Asztely, 1998), models of intersynaptic pooling due to multiple vesicular release sites and pharmacological blockade of glutamate uptake have demonstrated resultant AMPAR activation and desensitization (Otis et al. 1996). AMPAR desensitization occurs when glutamate is bound to the receptor yet the cation channel is conformationally altered by relaxation of the dimer interface into the ‘inactive’ desensitized state (Weston et al. 2006). CA1 pyramidal neurons in the hippocampus have displayed a lack of AMPAR desensitization after a single excitatory post synaptic current (EPSC) during basic synaptic transmission (Hjelmstad et al. 1999) yet when high-frequency repetitive stimuli were applied to CA1 patches, evidence of AMPAR desensitization occurred (Arai & Lynch 1998). Specifically, Arai and Lynch (1998) demonstrated that stimuli administered

at 50 Hz to CA1 patches led to a decrease in the amplitude of the subsequent pulses, which was reversed by the AMPA-desensitization blocker cyclothiazide. Additionally, it has been argued that the rapid clearance of glutamate from the synapse via diffusion and transporter uptake limits the decay of the AMPAR response by the desensitization and dissociation of glutamate from the receptor (Tong & Jahr 1994). A majority of the evidence for the spatial role of release site proximity and short-term plasticity has been reported in the calyceal synapse of Held and in the chick brainstem (See review von Gersdorff & Borst 2002, Otis et al.1996). This synapse exhibits a high probability of multivesicular release (MVR) from multiple release sites that results in a low concentration of glutamate pooling from neighboring sites which appears to desensitize AMPARs (Otis et al. 1996). In other cases, the concentration time course of glutamate in the cleft has been prolonged by an increased number of presynaptic release sites and leads to glutamate pooling (Otis & Trussell 1996).

NMDARs

The NMDA receptors have a voltage-dependent magnesium block (Mayer et al. 1984), a high affinity for glutamate, a slow glutamate unbinding rate, and are slow to desensitize (Attwell and Gibb, 2005). NMDARs are particularly sensitive to the effects of glutamate spillover because of the high affinity for glutamate and the slow desensitization rates (Diamond 2001, Asztely et al. 1997, Scimemi et al. 2004). Although a general consensus from work at the hippocampal Shaffer-CA1 pyramidal synapse is that transporter activity does not acutely modify synaptic AMPAR responses (Isaacson and Nicoll, 1993; Sarantis et al., 1993); rather, inhibition of transport leads to glutamate spillover and activation of extrasynaptic NMDAR receptors (Asztely et al., 1997; Lozovaya et al., 1999; Diamond, 2001, Arnth-Jensen et al. 2002; Tsukada et al., 2005; Scimemi et al., 2009). This evidence comes primarily from voltage-clamp recordings to investigate the effects of glutamate transport blockers on postsynaptic NMDAR currents. A notable limitation of previous studies examining the influence of glutamate transport on NMDAR EPSCs arises from the necessity of recording in non-physiological voltage clamp conditions due to voltage-dependent block by Mg^{2+} (Mayer et al. 1984). Under these voltage

clamp conditions cells are held at -60mV, near the cells normal resting potential, yet are unable to undergo the voltage changes that occur during depolarization. In these studies we recorded NMDA-EPSCs in CA1 pyramidal neurons with the selective glutamate transporter blocker L-threo-beta-benzylaspartate (TBA; Esslinger et al. 2005; Sun et al, 2011) and confirmed the contribution of transport to restricting glutamate diffusion to extrasynaptic NMDARs.

Evidence has accumulated for extrasynaptic signaling in the CA1 region of the hippocampus (Kullmann et al. 1996, Kullmann and Asztely, 1998, Diamond 2001, Scimemi et. al. 2009). This diffusion of glutamate out of the synapse is hypothesized to result in extrasynaptic NMDAR activation (Scimemi et al. 2004, Lui et al. 2004, Bartlett et al. 2007). This phenomenon has been referred to as glutamate "spillover" (reviewed in Diamond 2002) and is dependent upon the presynaptic release probability and glutamate uptake by the excitatory amino acid transporters (EAATs; Lozovaya et al. 1999, Asztely et al 1997). Although previous research suggests that spillover onto NMDARs is mediated by the neuronal EAAT3 subtype (Scimemi et. al 2009), we provide evidence that spillover may be mediated by another EAAT subtype in the following chapters.

Long-term Potentiation

Within the field of synaptic physiology, it has been long postulated that neurotransmitter released from a single presynaptic site activates post-synaptic receptors only within that synapse, resulting in synaptic specificity (Hebb,1949). The principles of "homosynaptic" signaling provided the initial framework to identify and understand a variety of synapse modification mechanisms, including long-term potentiation (LTP) within the Schaffer collateral pathway of the hippocampus is mediated by NMDA receptors (Bliss and Lomo, 1973; Bliss and Collinridge, 1993; Malenka and Nicoll, 1999). In a study that investigated the role of the NMDARs in an LTP synaptic transmission protocol, glutamate spillover onto postsynaptic NMDARs was observed (Kullmann et al. 1996). Using voltage-clamp experiments, Diamond (2001) demonstrated that neuronal glutamate transporters limit glutamate spillover onto extra-synaptic NMDARs within CA1 hippocampal slice preparations. In fact, the NR2B subunit of the

NMDAR has been shown to be affected preferentially by glutamate spillover in hippocampal synapses and mediates LTP (Scimemi et al. 2004, Lui et al. 2004, Bartlett et al. 2007).

LTP is input specific and requires the activation of NMDARs due to their co-incident detection properties. NMDARs require the binding of glutamate and a postsynaptic depolarization to free the Mg^{++} block from the pore (Attwell and Gibb, 2005). Activation of the NMDAR and the opening of its pore leads to the influx of Ca^{++} and Na^{+} into the post-synaptic cell. The influx of calcium leads to the activation of several protein kinases including the calcium/calmodulin-dependent protein kinase II (CaMKII). Activation of these calcium sensitive kinases eventually lead to downstream effectors and transcriptional pathways that effect the expression and placement of AMPA receptors and in turn long term plasticity (Bailey et al. 2000). The most effective LTP induction protocols are generally brief periods of intense stimulation. The most widely used and most effective protocols for LTP induction are administered at theta frequency (5-7Hz), which also is the endogenous frequency at which neurons fire during periods of learning and memory (Stella and Treves, 2011).

Frequency dependence

The NMDA receptors have a high affinity for glutamate, are slow to desensitize, a slow glutamate unbinding rate, and a voltage-dependent magnesium block (Attwell and Gibb, 2005). In contrast, AMPARs have a low affinity for glutamate, quickly desensitize, a quick unbinding rate, and are non-voltage gated. Although during synaptic transmission the binding rate of glutamate for AMPARs and NMDARs are $4x10^{6}M^{-1}s^{-1}$ and $5x10^{6}M^{-1}s^{-1}$ respectively, their unbinding rates differ drastically (AMPAR K_{off} = $2{,}000s^{-1}$, NMDAR K_{off}=$5s^{-1}$; Attwell and Gibb, 2005). The slow unbinding rate of glutamate and the unbinding rate of Mg^{++} from the NMDAR assist in its function as a coincidence detector. The high-affinity NMDARs are able to temporally integrate the information from the low-affinity and quickly activated AMPARs (Attwell and Gibb, 2005). NMDARs participate in high-frequency synaptic transmission, yet their involvement in low-frequency transmission is greatly suppressed by the time course of Mg^{2+} block (Herron et al. 1986).

In order to study the physiologically relevant conditions, i.e. normal extracellular [Mg^{2+}] without voltage clamp, we isolated AMPAR- and NMDAR-mediated components of extracellular fEPSPs in hippocampal slices. In the following studies we found that at low frequencies of synaptic activity, the influence of glutamate transport on synaptic signaling at the Shaffer-CA1 pyramidal cell synapse was minimal. At frequencies greater than ~5Hz (Theta frequency) NMDAR signaling was facilitated due to relief of Mg^{2+} block from glutamate-occupied NMDARs, and this effect was greatly increased by inhibition of glutamate transport by L-TBA. The data suggest that NMDAR signaling and LTP is controlled by the interaction of factors including synaptic frequency, transport, Mg^{2+} block, and NMDAR channel kinetics.

Pathological Significance

Epileptic seizures are a pathological condition that occur when a large ensemble of excitatory presynaptic sites synchronously release. Administration of the AMPA antagonist NBQX in the first 48 hours after seizures attenuates a long-term increase in seizure susceptibility and seizure-induced neuronal injury in hippocampus (Koh et al. 2004). Alternatively, application of an AMPAR desensitization blocker cyclothiazide leads to an increase in seizure behavior in hippocampal neurons (Kong et al. 2010, Lasztoczi and Kardos, 2006, Qi et al., 2006). Therefore, the negative feedback of AMPAR desensitization is an intrinsic receptor property of AMPAR receptors that prevents epileptiform activity in the hippocampus. Although the pathological effects of non-specific and excessive glutamatergic signaling is observed in epilepsy, it also occurs during stroke, traumatic brain injury, and Alzheimer's disease (reviewed by Bert and O'Shea, 2007); and therefore understanding the underlying molecular events is critical.

CHAPTER 2: METHODS

Solutions. Artificial cerebrospinal fluid (ASCF; mM): 126 NaCl, 2.5 KCl, 1.2 $MgCl_2$, 2.4 $CaCl_2$, 1.2 NaH_2PO_4, 21.4 $NaHCO_3$, 11.4 glucose, pH 7.15-7.30. ACSF was bubbled to saturation with 95%O_2/5%CO_2. Partial sucrose cutting ringer (mM): 79.9 NaCl, 2.5 KCl, 70 sucrose, 1.25 NaH_2PO_4, 0.5 CaCl, 7.0 $MgCl_2$, 24.9 glucose, 25.2 $NaHCO_3$, 1.0 Kynurenic acid, 1.0 NaOH maintained at <4℃ (modified from Geiger et al. 2000; Bischofberger et al. 2006)

Hippocampal slice preparation. Rodents were anesthetized with isofluorane and decapitated in accordance with IACUC approved guidelines. The brain is rapidly dissected out and placed in ice cold cutting ringer (see above). Transverse hippocampal slices (350 μm thick) were cut using a VT1000S vibrating microtome (Leica, Germany), then hemisected and placed in ACSF (see previous description) and maintained at 30° C (pH 7.3). Slices are allowed at least 1 hour to recover before being placed in a submersion type recording chamber constantly perfused (1.6-1.9 ml/min) with saturated ACSF at 30°C.

Animals. Rats were obtained from... EAAT3-KO mice were obtained from Dr. Ray Swanson (UCSF).

*Electrophysiological recordings.*Field excitatory post synaptic potentials (fEPSPs) were recorded using glass stimulating electrodes (X Mohm) filled with ACSF (pH 7.3) solution and induced by stimulating in S. radiatum of CA1 (vendor and catalog number of stimulating device(s)). Stimulation strength was adjusted to a range of subthreshold fiber volley amplitudes. A stable baseline was acquired for at least 20 minutes before further treatments were applied. fEPSP responses were monitored at 0.05 Hz. Paired-pulse stimulation was delivered at a 50 msec interval. fEPSPs were recorded using a Geneclamp 500 amplifier (Molecular Devices, Sunnyvale, CA, USA, country) and AxographX software (version 1.1.6, John Clements, Berkely, CA, USA).

Whole-cell recordings. Slices were visualized on an upright fixed-stage microscope (Olympus BX51WI) equipped with infrared differential interference contrast optics. CA1 pyramidal cells were voltage clamped at -60 to -70mV. The whole recording pipette (3-6MΩ resistance) was

filled with internal solution containing (in mM): K-gluconate 150, HEPES 10, NaCl 8, EGTA 0.5, MgATP 4, and NA_3GTP 0.3, QX314 5. Recordings were made with an Axopatch 200B amplifier (Axon Instruments, Foster City, CA), and data were acquired (sample frequency, 5-10 kHz; filter frequency, 2-5 kHz) and analyzed with AxographX. .

Data analysis. All acquisition and analysis protocols were created using AxographX and Kaleidagraph (version 4.04, Synergy Software, Reading , PA, USA). Paired-pulse ratios were calculated by averaging five pulses at each stimulus strength, in order to protect against spurious PPF that can mask the intrinsic paired-pulse property of the synapse (Kim & Alger, 2001). The mean paired-pulse ratio was obtained by dividing the second fEPSP by the first fEPSP t. Statistical comparisons of differences between experimental groups were performed using a Student's t-test.

*Ethics statement.*Mice and frogs used in this study were treated in a manner to minimize suffering, and were anesthetized with isofluorane or Tricaine respectively, and decapitated in accordance with NIH and University of Montana regulations. The study was approved by the University's IACUC (protocol approval 03905).

Chemicals and reagents.

Reagents were purchased from Sigma, except CNQX and DL-APV (Tocris) and DL-TBOA (Ascent). Stock solutions of TBOA was dissolved in DMSO at 50mM. L-TBA was synthesized and purified as described (Esslinger et al. 2005) and a stock solution was dissolved in DMSO at 50mM. Data are presented as mean ± SEM and statistical significance evaluated by Student's paired (drug effects) or unpaired (transgenic effect).

Oocyte recording.

Stage V *Xenopus* oocytes were microinjected with approximately 50 ng of human EAAT1, EAAT2, or EAAT3 cRNA and two-microelectrode voltage clamp recordings were made 3-5 days later at 22° with Molecular Devices amplifiers and A/D interfaces. Oocytes were superfused with Ringer containing (in mM) 96 NaCl, 4 KCl, 1.8 $CaCl_2$, 1.0 $MgCl_2$, 5 HEPES pH 7.4 and were voltage clamped at -30 mV.

Computational modeling.

Human EAAT3 sequence (GenBank http://www.ncbi.nlm.nih.gov) was aligned with the Protein Data Bank (PDB) sequence of the archaeal homologue Glt_{Ph} (2NWW.pdb) according to Boudker et al.. The EAAT3 homology model was constructed by threading the aligned sequence along PDB coordinates using the SwissProt server (http://swissmodel.expasy.org//SWISS-MODEL.html). The resulting model was optimized through local energy minimizations of regions with high steric and electrostatic interference using the AMBER7 force field in the Tripos SYBYL8.0 platform. Representations of L-TBA and L-TBOA were docked using GOLD v.3.0.1 (http://www.ccdc.cam.ac.uk/) into the EAAT3 model and evaluated using the ChemScore scoring function. Structures were seeded within a sphere of radius 8Å from the α-carbon of L-3-Br-TBOA in 2NWW. The structures from three separate docking run (30 seeds/run) were evaluated for electrostatic interactions with residues that have been shown to confer substrate and inhibitor specificity. We screened docked structures for two interactions between EAAT3 R447 and inhibitor distal oxygens and between EAAT3 D444 and the inhibitor α-amino group. Structures with the lowest estimated ΔG values were incorporated into the homology model and represented using PyMol1.3.

Mouse hippocampal slice preparation and recording

P18-26 CD1 wild-type or EAAT3 (-/-) siblings (Raymond Swanson, UCSF) were anesthetized with isofluorane and decapitated in accordance with University of Montana IACUC regulations (protocol approval number 039 05). The brain was rapidly dissected and placed in ice-cold solution containing (in mM): 80 NaCl, 24 $NaHCO_3$, 25 glucose, 75 sucrose, 2.5 KCl, 1.25 NaH_2PO_4, 0.5 $CaCl_2$, 5 $MgCl_2$, 1 ascorbic acid, 3 Na pyruvate. The solution was saturated with 95% O_2 and 5% CO_2 (pH 7.3). Coronal hippocampal slices (300μm thick) were cut using a vibratome (VT1200S, Leica, Germany), then hemisected and placed in artificial cerebral spinal fluid (ACSF) containing (in mM): 126 NaCl, 2.5 KCl, 1.2 $MgCl_2$, 2.4 $CaCl_2$, 1.2 NaH_2PO_4, 11.4 glucose, and 21.4 $NaHCO_3$ saturated with 95%O_2 and 5% CO_2 (pH 7.3) and maintained at

30°C. Slices were allowed at least 1 hour to recover before being placed in a submersion-type recording chamber perfused at 1.6-2.0 ml/minute with ACSF at 30°C. Slices were visualized on an upright fixed-stage microscope (Olympus BX51WI) equipped with infrared-differential interference contrast optics. The recording pipettes (3-6MΩ resistance) were filled with internal solution containing (in mM): 110 Cs methanesulfonate, 38 CsCl, 10 HEPES, 10 Na-phosphocreatine, 0.1 EGTA, 4.0 Mg-ATP, 0.3 GTP, 5 QX-314, pH=7.3. Series resistance (typically 15-20 MOhm), was monitored at regular intervals. The recording was terminated if a change of >20% was observed. Holding potential was -60 to -70 mV. 100μM picrotoxin was added to the ACSF for whole-cell recordings and a cut was made between CA3 and CA1.

Whole cell recordings of synaptically activated transport currents (STCs) in astrocytes in CA1 stratum radiatum were made with assistance of fluorescence visualization following incubation in 2 μM SR-101 (20 min; Sigma) and 1h washout. Recordings were made in ACSF including (in μM) 100 picrotoxin, 50 DL-APV, 20 CNQX, 10 8-CPT. Astrocytes were clamped at -90 mV (resting potential -80 ± 1.5 mV; 9.1 ± 0.8 MOhm input resistance, n=4). Peak current amplitudes were determined following baseline subtraction of persistent current at 200 ms following stimulation. Stimulation intensity was 80-100 μA and the stimulating electrode was approximately 100 μm from the recording site.

Extracellular field excitatory post synaptic potentials (fEPSPs) recordings

Extracellular field excitatory post synaptic potentials (fEPSPs) were recorded using glass electrodes filled with ACSF. Recordings were made with analog-digital converters and amplifiers from Molecular Devices, and data were acquired at 20kHz and filtered at 5-10 kHz. Acquisition and analysis software was AxographX (Sydney, Australia, version 1.1.6). EPSCs and fEPSPs were induced with 100 μs current pulses between 100-400 μA administered through ACSF-filled stimulating pipettes placed in CA1 stratum radiatum. EPSC charge transfer changes and fEPSP prolongation were quantified by integrating the area from the peak of the response (normalized to control) to 100 ms after the peak. Areas of the fEPSPs elicited by a burst of 2 or 3 stimuli were calculated after subtraction of responses to 1 and 2 stimuli, respectively.

Outside-out patch recordings

Outside-out patches were pulled from the soma of CA1 pyramidal neurons from CD1 mice (P9-22) identified under transmitted IR DIC optics. Patches were held at -60mV with a pipette solution containing (in mM): 150 K-gluconate, 10 HEPES, 8 NaCl, 0.5 EGTA, 4 MgATP, and 0.3 NaGTP, pH 7.3. Patch recordings were made at room temperature. Drug solution was applied through a 200μm diameter theta tube attached to a piezoelectric bimorph. Solution change kinetics were estimated following patch rupture by measuring junction currents during switches between iso- and hypo-osmotic solutions as shown above current records. NMDAR currents were recorded in nucleated patches with Mg^{2+}-free ACSF containing 20 μM CNQX and 20 μM glycine. L-glutamate with or without L-TBA (each at 100μM) were applied in alternating order for 100 ms or 400 ms to induce AMPAR or NMDAR currents respectively. Averages of 5-10 responses to repetitive application are shown with an interpulse interval of 3 sec for AMPAR experiments and 10 sec for NMDAR experiments.

Nucleated outside-out patch recordings

Nucleated patches were pulled from the soma of CA1 pyramidal neurons of CD1 mice (P10-12) identified under transmitted IR-DIC optics. Intracellular pipette solution contained (in mM): 60 Cs-methanesulfonate, 38 CsCl, 20 Cs_4BAPTA (4*CsOH+BAPTA), 10 HEPES, 10 Na-phosphocreatine, 4 MgATP, and 0.3 NaGTP, 5 QX-314, pH 7.3 (adjusted by HCl or CsOH). Patch recordings were made at 25° in the presence of 20 μM CNQX. L-glutamate (1 mM) was applied for 1 ms through a 200 μm diameter double-barreled theta tube attached to a piezoelectric bimorph. Solution change kinetics were estimated following patch rupture by measuring junction currents during switches between iso- and hypoosmotic solutions as shown above current records. To investigate the kinetics of Mg^{2+}- blocked channels, 5 ms voltage pulses from -60mV to -20mV or +40mV were applied at varying intervals as indicated following the glutamate pulse. NMDAR-mediated currents were also recorded at -60 mV in Mg^{2+}-free

ACSF containing 20 μM CNQX and 20 μM glycine. Control voltage jump recordings without a glutamate pulse were made to subtract leak and capacitance currents. Averages of 5-10 responses to repetitive application are shown.

CHAPTER 3: SPECIFICITY AND ACTIONS OF AN ARYLASPARTATE INHIBITOR OF GLUTAMATE TRANSPORT AT THE SCHAFFER COLLATERAL-CA1 PYRAMIDAL CELL SYNAPSE

Weinan Sun*, Katie M. Hoffman*, David C. Holley, and Michael P. Kavanaugh[1]
Center for Structural and Functional Neuroscience, The University of Montana, Missoula, MT, 59812

*these authors contributed equally to this work
[1]author for correspondence:
Michael Kavanaugh, Ph.D.
Center for Structural and Functional Neuroscience
University of Montana
390 Skaggs
Missoula, MT 59812
michael.kavanaugh@umontana.edu
tel 406 243 4398
fax 406 243 4888

Running title: L-TBA effects on glutamate transport and signaling

text pages: 14
figures: 5
tables: 1
abstract: 294 words
introduction: 468 words
discussion: 760 words
abbreviations used:
L-TBA, L-threo-ß-benzylaspartate;

Abstract

In this study we characterized the pharmacological selectivity and physiological actions of a new arylaspartate glutamate transporter blocker, L-threo-ß-benzylaspartate (L-TBA). At concentrations up to 100 μM, L-TBA did not act as an AMPA receptor (AMPAR) or NMDA receptor (NMDAR) agonist or antagonist when applied to outside-out patches from mouse hippocampal CA1 pyramidal neurons. L-TBA had no effect on the amplitude of field excitatory postsynaptic potentials (fEPSPs) recorded at the Schaffer collateral-CA1 pyramidal cell synapse. Excitatory postsynaptic currents (EPSCs) in CA1 pyramidal neurons were unaffected by L-TBA in the presence of physiological extracellular Mg^{2+} concentrations, but in Mg^{2+}-free solution, EPSCs were significantly prolonged as a consequence of increased NMDAR activity. Although L-TBA exhibited approximately four-fold selectivity for neuronal EAAT3 over glial EAAT1/EAAT2 transporter subtypes expressed in *Xenopus* oocytes, the L-TBA concentration-dependence of the EPSC charge transfer increase in the absence of Mg^{2+} was the same in hippocampal slices from EAAT3 +/+ and EAAT3 -/- mice, suggesting that TBA effects were primarily due to block of glial transporters. Consistent with this, L-TBA blocked synaptically evoked transporter currents in CA1 astrocytes with a potency similar to its block of heterologously expressed glial transporters. Extracellular recording in the presence of physiological Mg^{2+} revealed that L-TBA prolonged fEPSPs in a frequency-dependent manner by selectively increasing the NMDAR-mediated component of the fEPSP during short bursts of activity. The data indicate that glial glutamate transporters play a dominant role in limiting extrasynaptic transmitter diffusion and binding to NMDARs. Furthermore, NMDAR signaling is primarily limited by voltage-dependent Mg^{2+} block during low-frequency activity while the relative contribution of transport increases during short bursts of higher frequency signaling.

Introduction

Five major subtypes of excitatory amino acid transporters exist in the CNS, and three of these (EAAT1-3; also known as GLAST, GLT-1, and EAAC1) are expressed in forebrain with distinct distribution patterns on astrocytes (EAAT1 and EAAT2) and neurons (EAAT3) (Furuta et al. 1997). Studies utilizing glutamate uptake inhibitors broadly indicate that the transporters play key roles in glutamate homeostasis, and that they can in some cases shape receptor dynamics during synaptic transmission (Tzingounis & Wadiche 2007). While the synaptic effects of glutamate transport inhibition vary widely in different brain regions, studies at the hippocampal Schaffer collateral-CA1 pyramidal cell (SC-PC) synapse generally indicate that transporter activity does not strongly modify synaptic AMPAR responses [Isaacson & Nicoll, 1993; Sarantis et al. 1993; but see Tong & Jahr,1994; Tsukada et al., 2005]. In contrast, extrasynaptic NMDAR activity is enhanced by glutamate uptake block in this region (Asztely et al., 2007; Lozovaya et al., 1999; Diamond, 2001; Arnth-Jensen et al., 2002; Scimemi et al. 2009).

The relative contributions of the glial EAAT1 and EAAT2 and neuronal EAAT3 subtypes to restricting the spread of synaptically released glutamate from the SC-PC synapse is presently unclear. EAAT2 and EAAT3 are the dominant transporters in forebrain astrocytes and neurons, respectively, while EAAT1 is found on forebrain astrocytes at lower levels (Lehre & Danbolt, 1998). The widely used glutamate uptake blocker DL-TBOA blocks EAAT2 and EAAT3-mediated [^{3}H]L-Glu uptake with IC_{50} values approximately seven-fold lower than for EAAT1 (Shimamoto et al., 2000), and studies utilizing DL-TBOA indicate that it can induce spillover of synaptic glutamate onto NMDARs in hippocampus (Asztely et al., 2007; Lozovaya et al., 1999; Diamond, 2001; Arnth-Jensen et al., 2002; Scimemi et al. 2009). More selective inhibition of the postsynaptic neuronal transporter EAAT3 by intracellular ion substitution during whole

cell recording or genetic manipulation also leads to augmentation of NMDAR-mediated EPSCs as well as changes in synaptic plasticity (Diamond, 2001; Scimemi et al. 2009). In addition to uncertainty surrounding the detailed roles of individual EAAT subtypes in hippocampus, another issue concerns the general role of glutamate transport in restricting NMDAR signaling in the hippocampus under physiological conditions, since this effect has only been reported in conditions permissive for channel activity, i.e. voltage clamp of the postsynaptic neuron at positive potentials or in Mg^{2+}-free ACSF (Asztely et al., 2007; Lozovaya et al., 1999; Diamond, 2001; Arnth-Jensen et al., 2002; Scimemi et al. 2009).

Threo-ß-benzylaspartate (TBA) is a new arylaspartate derivative that is structurally related to TBOA, but with a shorter aryl linkage. In contrast to DL-TBOA, L-TBA displays moderate selectivity for the neuronal EAAT3 subtype over EAAT1 and EAAT2 (Esslinger et al., 2005). In this work we show that L-TBA is highly selective for glutamate transporters over ionotropic glutamate receptors expressed on CA1 pyramidal cells and examined its effects on NMDAR activity during synaptic transmission at the Schaffer-CA1 synapse in wild-type and transgenic mice lacking the neuronal EAAT3 glutamate transporter to gain insights into the respective roles of glial and neuronal transporters. We also compared its actions on postsynaptic signaling using voltage clamp as well as extracellular recording to gain insights into the role of transporters in physiological conditions. The data suggest that glial transporters restrict synaptically released transmitter binding to NMDARs to a significantly greater extent than neuronal transporters. Further, voltage-dependent Mg^{2+} block plays a dominant role in limiting NMDAR signaling during low-frequency activity, while the relative influence of transport increases during short bursts of activity.

Results

Computational docking of TBA with glutamate transporters

We constructed an EAAT3 model using published homologous archaeal Glt_{Ph} structures (Boudker et al., 2007, Yernool et al., 2004) and docked aryl-aspartate analogs in order to identify and compare plausible structural interactions. A single Na^+ ion was positioned in the structure according to the structural determination of a Tl^+ ion in the Glt_{Ph}/L-3-Br-TBOA complex (Boudker et al., 2007) and corresponding to electrostatic predictions of Na^+ ion binding sites in EAAT3 (Holley & Kavanaugh, 2009). The EAAT3 residues R447 and D444 interact with the γ-carboxylate and the α-amino group of transported glutamate and determine substrate specificity (Bendahan et al., 2000; Teichman & Kanner, 2007). The computationally docked L-TBA complex suggested corresponding electrostatic interactions between the blocker carboxyl and amino groups with the R447 and D444 residues in EAAT3 (Figure 1A). The most energetically favorable L-TBA complexes corresponded to the benzyl group orientation of L-3-Br-TBOA that was determined in the Glt_{Ph} crystal structure, with interactions between the ring and non-polar residues near the tip of HP2. Interestingly, when computational docking of L-TBOA was performed, an energetically favorable conformation was observed that involved an interaction of R447 with the ether group of the blocker. This alternate orientation positions the benzyl group in an ‘up’ conformation perpendicular to the membrane and parallel to TMD7, and aligns it with non-polar residues in TM7, TM8 and HP2 (Figure 1B). Docking energies (Table 1) predict that L-3-Br-TBOA could orient in either conformation while L-TBOA is predicted to predominantly align in the perpendicular, ‘up’ orientation, and L-TBA aligns predominantly in the ‘down’ conformation parallel to the membrane plane.

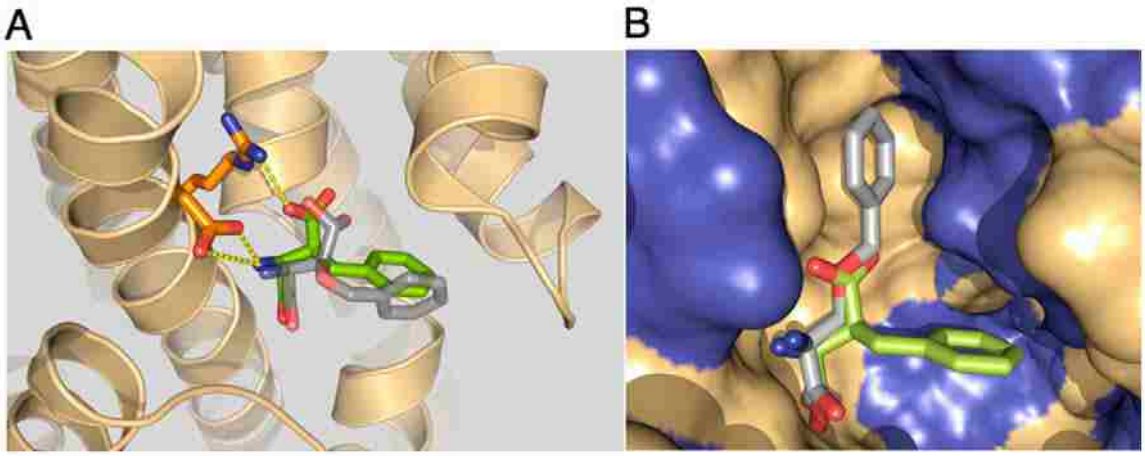

Figure 3.1. Interaction of L-TBA with EAATs. (A) Docking of L-TBA (green) and L-TBOA (gray) in EAAT3 model showing overlap of functional groups interacting with R447 and D444, with benzyl groups oriented toward extracellular loop HP2 as seen in (Esslinger et al., 2005). (B) Surface depiction of the transporter binding site (hydrophobic regions blue) showing L-TBA and alternate docking orientation of L-TBOA with benzyl ring aligned in alternate hydrophobic pocket.

Interaction of L-TBA with glutamate transporters

L-TBA inhibits uptake mediated by heterologously expressed EAATs, with preference for the neuronal glutamate transporter subtype EAAT3 (Esslinger et al. 2005). However, transport currents mediated by the major glial subtypes are also blocked in *Xenopus* oocytes expressing the transporters (Figure 2A,B). To examine the actions of L-TBA on glial transporters in situ, synaptically activated transport currents (STCs) were recorded in astrocytes in stratum radiatum of area CA1 in mouse hippocampal slices. Currents evoked by stimulation in the presence of ionotropic blockers CNQX (20 μM) and DL-APV (50 μM) revealed a current with properties consistent with glial transporters EAAT1 and EAAT2 together with a slowly decaying potassium current as previously described (Bergles & Jahr, 1997). The STC, or transporter-mediated component of the evoked current, peaked and decayed within approximately 20 ms (Figure $2C_2$). The peak STC was blocked 67±10% by 30 μM L-TBA (n=4; Figure 2C).

Effects of TBA on fast excitatory synaptic transmission

Because the potential actions of L-TBA on ionotropic glutamate receptors have not been examined, its functional effects on receptor currents recorded in outside-out patches from CA1 pyramidal neurons were first evaluated. Fast application of 100 μM L- Glu alone induced robust AMPAR and NMDAR currents, while application of 100 μM L-TBA alone failed to induce measurable currents (Figure 3). Co-application of 100 μM L-TBA showed no antagonism of the AMPAR (101.2±2.0% of control; n=4; p>0.6) or NMDAR currents (98.7±2.3% of control; n=5, p=0.59; Fig. 3C) induced by 100 μM L-Glu.

The amplitude of fEPSPs elicited by .05 Hz stimulation in stratum radiatum was not affected by application of 30 μM L-TBA (100±3% of control; n=41 slices). There was also no significant change in the 50 ms paired-pulse facilitation of the peak amplitude of fEPSPs induced by L-TBA (control, 1.72±.03; TBA, 1.60±.08; p>.05). In whole cell voltage clamp recordings from CA1 pyramidal neurons, the effect of L-TBA on EPSC kinetics was highly $[Mg^{2+}]$-dependent (Figure 4).

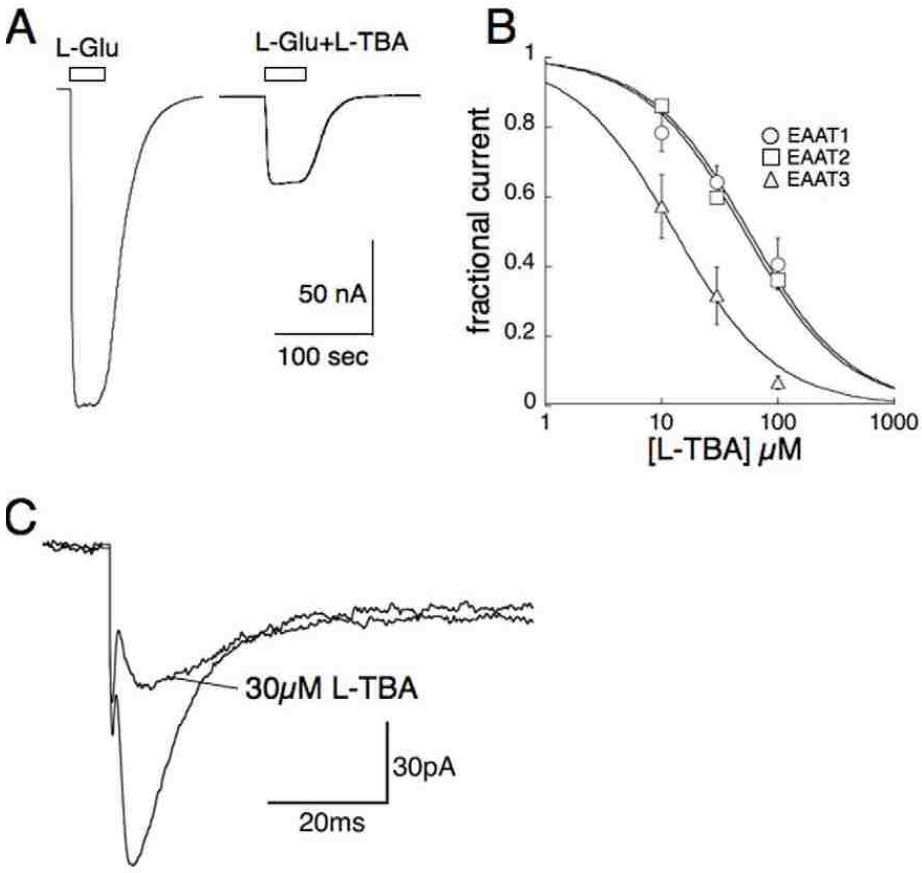

Figure 3.2. Effects of L-TBA on native and recombinant transporters. (A) Effect of 30μM L-TBA on synaptically activated transport current (STC) in hippocampal CA1 astrocyte. (A_1) Currents in the presence or absence of L-TBA were evoked by stimulation in stratum radiatum in the continuous presence of ionotropic receptor antagonists (see methods). (A_2) Subtracted current (control - L-TBA). 30μM L-TBOA blocked 66.7±10.4 of the peak STC (n=4). (B) Representative recording from voltage-clamped Xenopus oocyte expressing astrocyte transporter subtype EAAT2. 100 μM L-TBA partially blocks equimolar L-Glu uptake current mediated by EAAT2. (C) Summary of L-TBA concentration-dependence of block of 100 μM L-Glu currents in oocytes expressing EAAT1-3, showing approximately four-fold selectivity for EAAT3 by least-squares minimized fits to mean data generating IC_{50} values of 56, 52, and 13 μM, respectively.

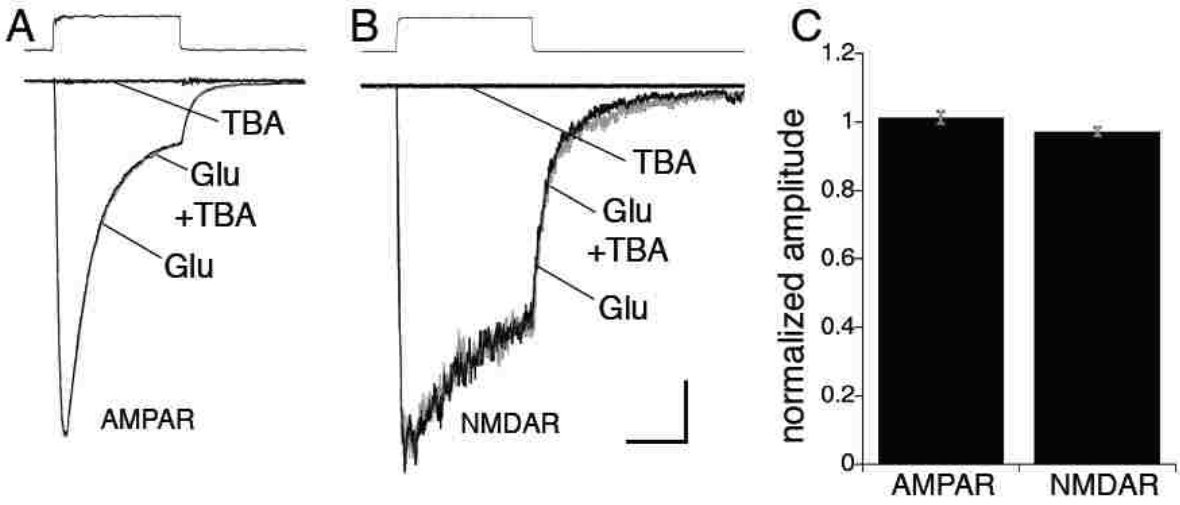

Figure 3.3. Representative recordings from outside-out patches excised from CA1 pyramidal neurons illustrating AMPAR and NMDAR responses to rapid application of 100 μM L-glutamate and/or 100μM L-TBA for durations indicated by solution exchange traces above. Responses at -60mV showing lack of agonist or antagonist actions of L-TBA on AMPARs (A; with 1.2 mM Mg^{2+}) and NMDARs (B; with 0 mM Mg^{2+}/20μM glycine/20μM CNQX). Scale bars are 50/200 ms and 50/100 pA for AMPAR/NMDAR responses respectively. (C) Summary of mean effects of 100μM L-TBA on 100μM L-Glu AMPAR and NMDAR responses.

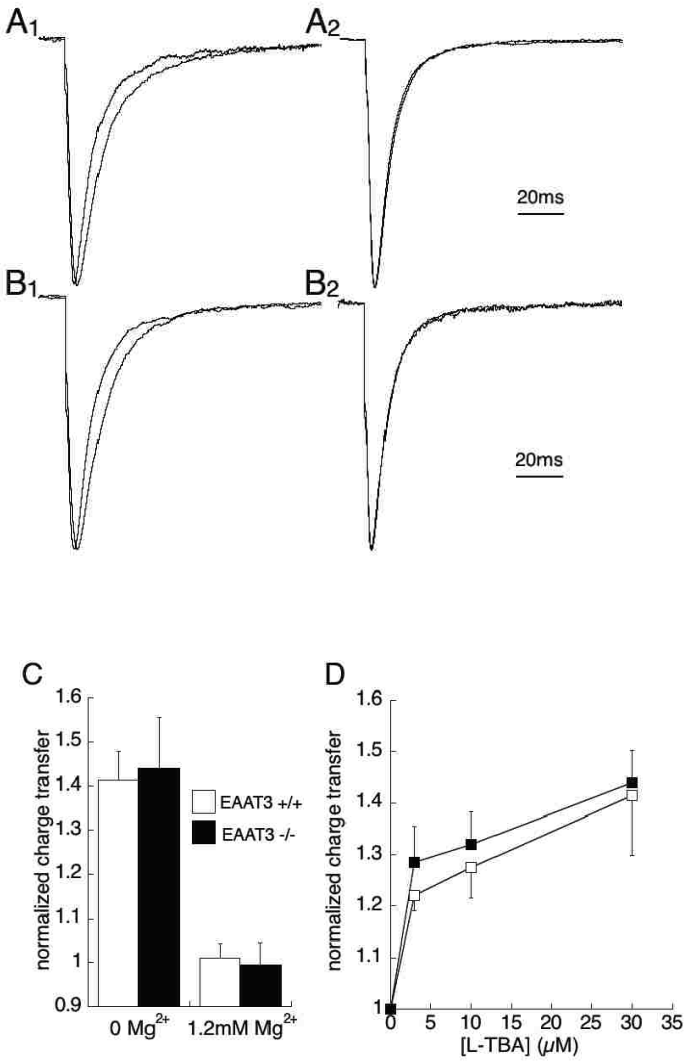

Figure 3.4. Actions of L-TBA (30 μM) on postsynaptic responses at the CA1 Schaffer collateral-pyramidal neuron synapse of EAAT3 +/+ (A) and EAAT3 -/- (B) mice. Representative whole cell recordings (-60 mV) showing effect of L-TBA on EPSCs evoked by stimulation in stratum radiatum in the presence (A_1, B_1) and absence (A_2, B_2) of physiological extracellular Mg^{2+} (1.2 mM). (C) Summary of data showing EPSC charge transfer increase in slices from EAAT3 (+/+) and (-/-) mice by 30 μM L-TBA in the absence and presence of Mg^{2+} (n=5-7 slices; $p<0.05$). (D) Summary of data showing statistically identical L-TBA concentration-dependence of EPSC charge transfer increase (normalized to control) for EAAT3 +/+ (open squares) and EAAT3 -/- (filled squares) (n=4).

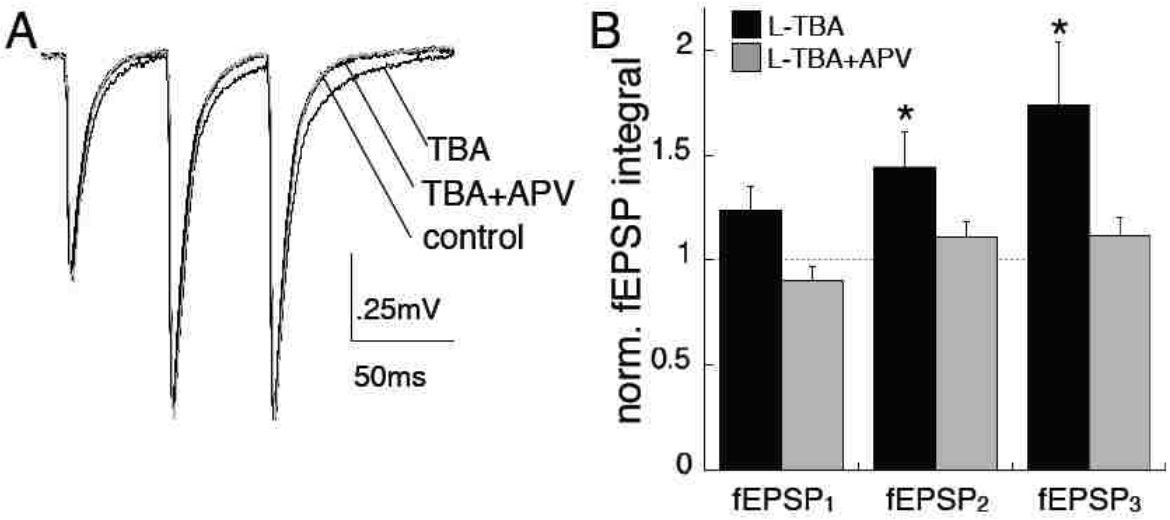

Figure 3.5. Actions of L-TBA on field responses at the CA1 Schaffer collateral-pyramidal neuron synapse. (A) Representative field EPSPs elicited in response to three stimuli delivered at 20 Hz in stratum radiatum. 30 μM L-TBA (black trace) prolonged fEPSPs relative to control (gray trace) in an activity-dependent manner (p=0.02). The TBA prolongation was inhibited by co-application of 50μM DL-APV (2nd black trace). (B) Summary of effects on fEPSP time-integrals elicited by 1, 2 and 3 stimuli normalized to corresponding fEPSPs in control ACSF (*p<.05 paired t-test; n=9 slices for one and two stimuli, n=5 slices for three stimuli).

In Mg^{2+}-free ACSF, 30 μM L-TBA significantly prolonged evoked EPSCs. The charge transfer in the presence of L-TBA was 141±6% of that without drug (n=6; p<.05), with no significant effect on the peak amplitude (102±7% of control, n=6). The effect of L-TBA on EPSC kinetics was presumed to be mediated by NMDAR activity, because in the presence of physiological (1.2 mM) Mg^{2+}, 30 μM TBA had no effect on the time course of the EPSC (charge transfer 101±3%; p=.78, n=4; Fig.$4A_1$). The prolongation was also not seen in the presence of 50 μM DL-APV in the absence of Mg^{2+} (data not shown). The effects of L-TBA on the EPSC charge transfer were concentration-dependent and not statistically different for EAAT3 (+/+) and EAAT3 (-/-) mice (Figure 4C,D).

Extracellular recording in the presence of physiological (1.2 mM) Mg^{2+} revealed an effect of L-TBA on fEPSP kinetics that exhibited pronounced frequency-dependence. L-TBA (30 μM) slightly prolonged fEPSPs elicited by low-frequency (.05Hz) stimulation, while time-integrals of fEPSPs recorded during a brief 20Hz burst prolonged the time course of the fEPSP significantly further (Figure 5; 31±7% vs 69±21% for the first and second fEPSPs, respectively, n=9, p=.02). Increasing stimulus strength to increase the fEPSP magnitude by an amount comparable to the frequency facilitation had no effect on the time course of the fEPSP (data not shown). The L-TBA-induced prolongation at both low and high frequencies was not observed in the presence of 50 μM APV (Figure 5).

Discussion

Selective glutamate uptake blockers are critical tools for studying the roles of glutamate transporters in modulating synaptic activity (Asztely et al., 2007; Lozovaya et al., 1999; Diamond, 2001; Arnth-Jensen et al., 2002; Scimemi et al. 2009). Both the widely used DL-TBOA and the newer analog characterized in this study are ß-substituted aryl aspartate analogs. The data presented demonstrate that L-TBA is selective for glutamate transporters over ionotropic glutamate receptors expressed on pyramidal neurons, as it neither antagonized ionotropic receptor responses to equimolar glutamate nor activated responses at concentrations up to 100μM. Unlike TBOA, TBA

lacks an ether linkage between the aryl group and the amino acid, resulting in a slight change in distance and bond angle of the benzyl ring relative to the aspartyl group (Figure 2A). The computationally predicted docking orientation of L-TBA was similar to the reported structure of L-3-Br-TBOA complexed with the archaeal homolog Glt_{Ph} (Boudker et al., 2007), with key electrostatic interactions involving R447 and D444 in TMD7 of EAAT3. Predicted interactions of the benzyl group with hydrophobic regions of EAAT3 were also in agreement with the structure of L-3-Br-TBOA complexed with Glt_{Ph}. In this conformation, the blocker prevents closure of the extracellular-facing HP2 loop which normally occludes bound L-aspartate (Yernool et al. 2004). Interestingly, a distinct orientation was predicted for L-TBOA because of the alternate interaction of R447 with the ether oxygen of L-TBOA. This interaction preserves the α-amino group interaction with D444 but causes the benzyl group to rotate to an orientation perpendicular to the membrane plane, fitting into a hydrophobic domain bordered by TMDs 7/8 and HP2 (Figure 2B). These predicted conformations suggest that the HP2 loop position in the L-TBA and L-TBOA transporter complexes may slightly differ. In terms of transporter selectivity, L-TBOA and L-TBA exhibit moderate selectivity for the the glial EAAT2 and neuronal EAAT3 subtypes, respectively (Shimamoto et al., 2000; Esslinger et al., 2005). While L-TBA and DL-TBOA differ in subtype selectivity, each exhibits significant subtype cross-reactivity at concentrations typically used. Because the effects of L-TBA on EPSC and fEPSP kinetics observed in this study were not significantly different in wild-type and transgenic mice lacking the EAAT3 gene, we conclude that they were primarily mediated by inhibition of glial transporters EAAT1 and/or EAAT2, which would be predicted to be approximately 75% occupied at the inhibitor concentration used (30μM) based on the K_D values of 12 μM and 9 μM for EAAT1 and EAAT2, respectively. This prediction is consistent with the 67±10% observed block of the peak synaptic transporter currents in astrocytes by L-TBA. While the glial transporter-dependent effects of L-TBA in increasing synaptic glutamate reaching NMDARs appear to dominate the results we observed, it is

important to note that the selective loss of neuronal transport has been reported to result in changes in both synaptic transmission and plasticity that were not addressed here (Diamond, 2001; Scimemi et al., 2009).

Past work has generally examined transporter control of extrasynaptic glutamate spillover onto NMDARs under voltage clamp by examining the effect of transporter block on EPSCs elicited under conditions where NMDAR activity is enabled (i.e. depolarized potentials or Mg^{2+}-free solution). Consistent with work from several groups (Asztely et al., 2007; Lozovaya et al., 1999; Diamond, 2001; Arnth-Jensen et al., 2002; Scimemi et al. 2009), we found that EAAT inhibition significantly prolonged EPSCs recorded at the Schaffer-CA1 pyramidal cell synapse in Mg^{2+}-free conditions due to enhanced NMDAR signaling. L-TBA had no effect on postsynaptic responses in voltage clamp conditions with NMDARs blocked by physiological [Mg^{2+}]. Because voltage-dependent Mg^{2+} block of NMDARs is dynamic during synaptic transmission, gaining greater insight into the role of glutamate transport in modulating synaptic activity will require the use of selective transport blockers in physiological conditions without voltage clamp. In this study we have begun to address this issue and have shown that NMDAR-mediated components of fEPSPs can be isolated that are dependent on glutamate transporter activity in a frequency-dependent manner. The effect of L-TBA on the kinetics of fEPSPs elicited by low-frequency stimulation in physiological Mg^{2+} was increased during brief bursts of higher frequency synaptic activity, and this prolongation was blocked by the NMDAR antagonist APV. This effect was not likely to be due simply to frequency-facilitation of transmitter release, because increasing stimulus strength did not affect the kinetics of fEPSPs elicited by low frequency stimulation. The data suggest that the influence of glial glutamate transporters on NMDAR signaling are likely to vary with synaptic frequency through postsynaptic voltage responses. A deeper quantitative understanding of the role of glutamate transporters in excitatory synaptic transmission will require further studies accounting for these variables.

Acknowledgements

1. This work is dedicated to the memory of Sean Esslinger
2. This work was supported by the National Institutes of Health/NINDS [grant NS33270]

Participated in research design: Sun, Holley, Hoffman, Kavanaugh
Conducted experiments: Sun, Holley, Hoffman
Contributed new reagents or analytic tools: Esslinger
Performed data analysis: Sun, Holley, Hoffman, Kavanaugh
Wrote or contributed to the writing of the manuscript: Sun, Hoffman, Holley, Kavanaugh

Table 1. Computational docking results

	ChemScore	ΔG(kJ mol^{-1})	orientation
L-TBOA	18.07	-22.14	perpendicular
L-TBOA	15.01	-18.62	parallel
L-TBA	-	-	perpendicular*
L-TBA	19.70	-23.62	parallel
L-3-Br-TBOA	20.19	-23.09	perpendicular
L-3-Br-TBOA	18.04	-23.90	parallel

*structure not found by energy minimization

CHAPTER 4: EFFECTS OF SYNAPTIC FREQUENCY AND GLUTAMATE TRANSPORT ON NMDAR ACTIVITY AT THE SCHAFFER-CA1 SYNAPSE

Abstract

NMDARs are high-affinity iontropic glutamate receptors which play a critical role in the induction synaptic plasticity. The activation and channel opening of NMDARs is dependent upon glutamate binding and depolarization due to Mg^{+2} blockade of the channel. NMDARs can become activated by low concentrations of glutamate and therefore have been utilized as sensors for spillover events at the synapse. Glutamate transporters are thought to help maintain synapse specificity in the hippocampus by limiting spillover of glutamate. While inhibition of glutamate transport has been shown to cause increased NMDAR activity in conditions permissive for signaling, such as in the absence of extracellular Mg^{2+}, the roles of transport in physiological conditions are less well understood. In this work we show that in Mg^{2+}-free conditions, increasing release site density prolonged the time course of EPSCs and fEPSPs evoked at low frequency by enhancing NMDAR activity, while in physiological [Mg^{2+}], this effect was not observed. NMDAR fEPSPs were selectively enhanced by repetitive activity in a frequency range that closely matched the decay kinetics of [Mg^{2+}]-blocked NMDAR channels monitored with depolarizing voltage pulses. Glutamate transporter inhibition in physiological [Mg^{2+}] increased NMDAR signaling in the same frequency-dependent manner. The data suggest that at low frequencies, Mg^{2+} block rather than glutamate transport plays a dominant role in restricting extrasynaptic NMDAR activity. This pool of glutamate-bound and Mg^{2+}-blocked NMDARs signal in a phase-shifted manner during repetitive synaptic activity at frequencies governed by channel desensitization and transmitter unbinding. The data also suggest a potential mechanism contributing to theta frequency-dependent associative LTP.

Introduction

Glutamate, the primary excitatory neurotransmitter in the CNS, binds to a variety of ligand gated ion channels and G-protein coupled receptors with differing affinities and spatial distributions. In addition to these targets, synaptically released glutamate also interacts with glutamate transporters. Five major subtypes of excitatory amino acid transporters exist in the CNS, and three of these (EAAT1-3; also known as GLAST, GLT1, and EAAC1) are expressed in forebrain with primary distribution patterns on astrocytes (EAAT1/2) and neurons (EAAT3) (Furuta et al. 1997). Studies with glutamate transporter blockers indicate that the transporters play key roles in controlling glutamate homeostasis in the CNS.In some cases, transport shapes glutamate dynamics during synaptic transmission, though the latter effect is synapse-specific (Marcaggi and Attwell, 2004; Tzingounis and Wadiche, 2007). A general consensus from work at the hippocampal Shaffer-CA1 pyramidal synapse is that transporter activity does not acutely modify synaptic AMPAR-mediated responses (Isaacson and Nicoll, 1993; Sarantis et al., 1993). However, inhibition of transport leads to glutamate spillover and activation of extrasynaptic NMDAR receptors (Asztely et al., 1997; Lozovaya et al., 1999; Diamond, 2001, Arnth-Jensen et al. 2002; Tsukada et al., 2005; Scimemi et al., 2009). This evidence comes primarily from voltage-clamp recordings to investigate the effects of glutamate transport blockers on postsynaptic NMDAR currents.

A notable limitation of studies examining the influence of glutamate transport on NMDAR EPSCs arises from the necessity of recording in non-physiological conditions due to voltage-dependent block by Mg^{2+} (Mayer et al. 1984). In this study, we recorded EPSCs in CA1 pyramidal neurons with the selective glutamate transporter blocker L-threo-beta-benzylaspartate (L-TBA; Esslinger et al. 2005; Sun et al, 2011) and confirmed that transport activity limits glutamate diffusion to extrasynaptic NMDARs. To extend these studies to physiologically relevant conditions (i.e. normal extracellular [Mg^{2+}] without voltage clamp), we isolated AMPAR- and NMDAR-mediated components of

extracellular fEPSPs in stratum radiatum. We found that at low frequencies of synaptic activity, the influence of glutamate transport on synaptic signaling at the Shaffer-CA1 pyramidal cell synapse was minimal. At frequencies greater than ~5Hz, NMDAR signaling was facilitated due to relief of Mg^{2+} block from glutamate-occupied receptors, an effect that was greatly increased by inhibition of glutamate transport. Our findings suggest that NMDAR signaling is controlled by the interplay of many several factors including; synaptic frequency, transport, Mg^{2+} block, and NMDAR channel kinetics. We propose that the observed theta frequency threshold for enhanced NMDAR signaling observed in physiological conditions is a consequence of a phase shifted signal at rhythms limited by NMDAR channel kinetics.

Results

Physiological Mg2+ prevents NMDAR activation and EPSC prolongation during repetitive stimulation. In conditions that relieve voltage-dependent Mg^{2+} block, NMDAR-mediated EPSCs at the Schaffer-CA1 pyramidal cell synapse are enhanced by spillover when transport is blocked (Asztely and Kullman. 1997, Diamond 2001, Scimemi et al, 2004) or when glutamate release is increased (Christie and Jahr, 2006; Kullman and Asztely, 1998). In order to examine the role of Mg^{2+} in limiting the effects of spillover with transport intact, we first examined Mg^{2+} effects on postsynaptic response kinetics when transmitter release was increased by frequency facilitation. This form of short-term plasticity increases the probability of multivesicular release at this synapse in addition to increasing release site density (Christie and Jahr, 2006). Paired-pulse stimulation (50 ms interpulse interval) facilitated the response amplitude with no effect on EPSC kinetics in the presence of physiological Mg^{2+} (1.2 mM; Figure 1B), but a marked prolongation was observed in Mg^{2+}-free ACSF (Figure 1A,D). As expected from relief of voltage-dependent Mg^{2+} block of NMDARs, Mg^{2+} removal prolonged EPSCs elicited by single stimuli. The effect of Mg^{2+} removal was significantly greater in the frequency-facilitated second EPSC (Figure 1C,E). The effects of increased presynaptic glutamate release on the EPSC kinetics were mediated solely by

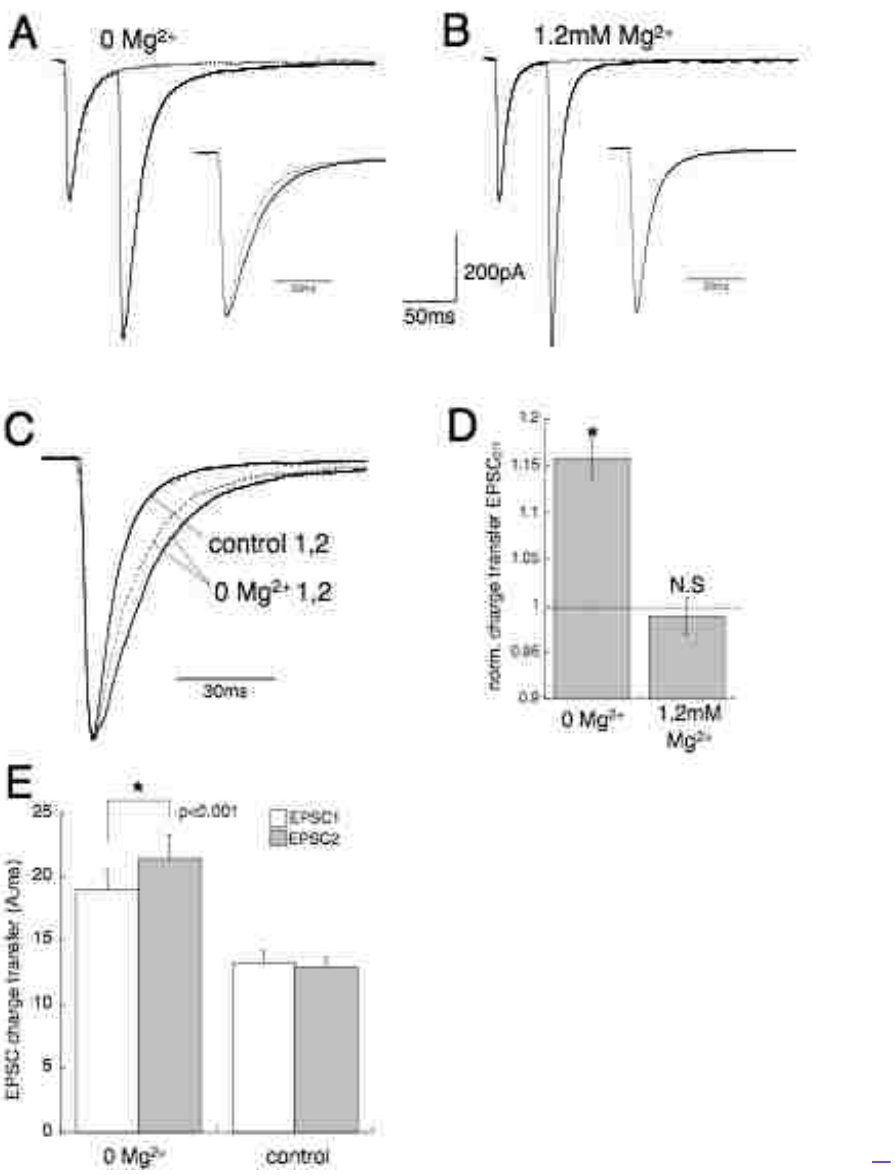

Figure 4.1. Physiological Mg2+ prevents NMDAR activation and EPSC prolongation during repetitive stimulation. A) EPSC induced by a paired pulse stimulation with 50ms interpulse interval in 0 Mg ACSF (containing 1.2mM Mg^{2+}), the recording 1st EPSC only. Inset: normalized 1st and 2nd EPSCs showing the 2nd EPSC is prolonged comparing with the 1st EPSC, 2nd EPSC normalized charge transfer is 115±2.0% of 1st EPSC, n=14, p<0.0001. B) EPSC induced by a paired pulse stimulation with 50ms interpulse interval in control ACSF (containing 1.2mM Mg^{2+}), the dotted line indicates the recording of 1st EPSC only. Inset: normalized 1st and 2nd EPSCs showing the 1st and 2nd EPSC kinetics are not different, 2nd EPSC normalized charge transfer is 98.9±1.9% of 1st EPSC , n=7, p=0.5815. C) Normalized 1st and 2nd EPSCs for both recordings in control ACSF and in 0 Mg^{2+} ACSF. D) Quantification of the charge transfer ratio (2nd/1st, Charge transfer is measured by integrating the normalized EPSCs from the peak to 200ms after the peak). E) Average charge transfer of EPSC1 and EPSC2 in both control and 0 Mg^{2+} ACSF.

NMDARs, as there was no difference in the kinetics of the first and second EPSC in either physiological Mg^{2+} or in the absence of Mg^{2+} with 50μM APV present (supplementary Figure 1). These results indicate that facilitated release of glutamate results in a significant increase in transmitter binding to NMDARs, even with glutamate transport intact, and that the physiological response to this increased binding will depend critically on the degree of voltage-dependent Mg^{2+} block.

To investigate the role of Mg^{2+} in controlling activation of NMDARs by glutamate spillover in more physiologically relevant conditions, we utilized extracellular recording with Mg^{2+} present or absent and analyzed AMPAR and NMDAR fEPSP changes as release site density varied. We first established that NMDAR fEPSPs could be detected by evoking responses in the presence of CNQX (10μM) and in the absence of Mg^{2+} (Figure 2A). These responses were blocked by APV (50μM), confirming that they were NMDAR-mediated (Figure 2A). In comparison with the fEPSP kinetics in physiological ACSF, the NMDAR fEPSPs isolated in the absence of Mg^{2+} displayed slower kinetics, as would be expected from the difference in channel kinetics and glutamate affinity between NMDARs and AMPARs (Figure 2B; 20-80% rise time 1.5 ± x ms n=16, 5.7 ± y ms n=17 p<.001). The kinetics of NMDAR fEPSPs isolated in 0 Mg^{2+} also displayed a sensitivity to release site density and became slower as stimulus strength was increased, in contrast to the fEPSPs recorded in physiological Mg^{2+} (Figure 2C,D). The normalized time-integrals of the control fEPSPs were constant over a range of stimulus strengths, while the NMDAR fEPSP decay times increased over the same range (Figure 2E).

Cooperation of voltage-dependent Mg^{2+} block and glutamate transport in limiting NMDAR responses to glutamate spillover.

We examined the effects of the glutamate transporter blocker L-TBA on EPSCs and fEPSPS to explore how glutamate transport and Mg^{2+} block might interact in controlling the response of NMDARs to transmitter spillover. L-TBA is an aspartate derivative with high selectivity for glutamate transporters over ionotropic glutamate receptors expressed on CA1 pyramidal neurons (Sun et al. 2011). In the absence of Mg^{2+}, partial block of glutamate

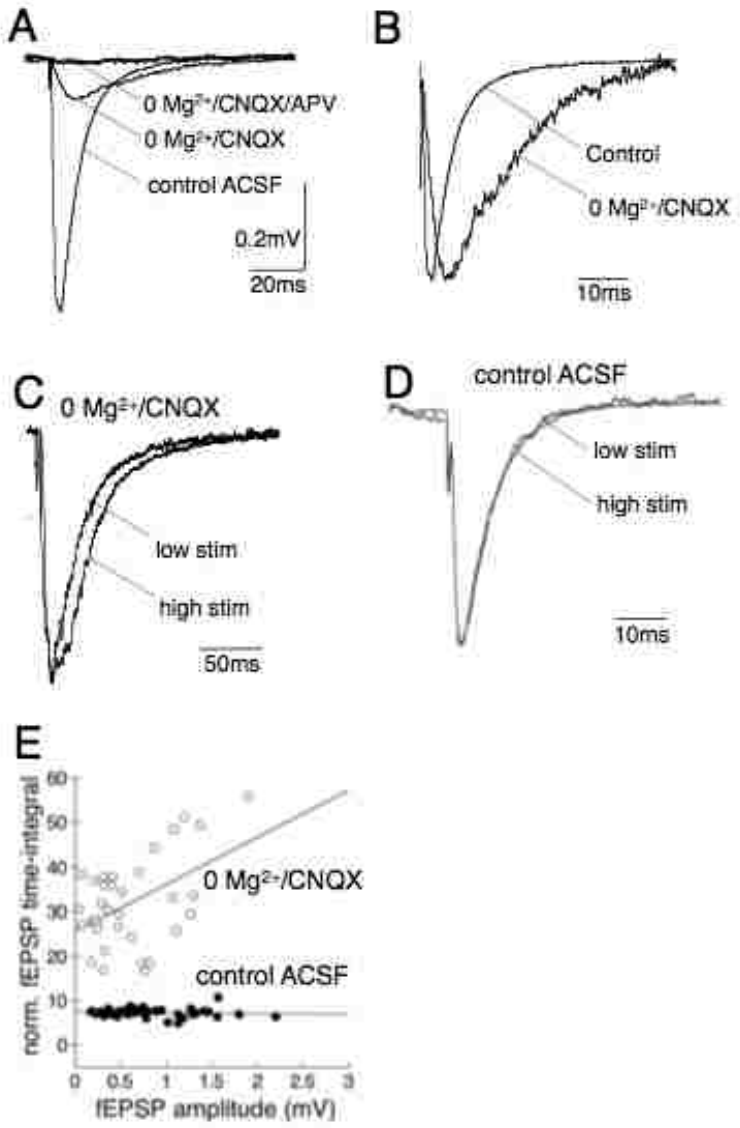

Figure 4.2. Isolated NMDAR (0 Mg^{2+}/10μM CNQX) fEPSPs display slower decay kinetics under conditions of dense fiber recruitment at the CA1 Schaffer collateral-pyramidal neuronal synapse. (A) Bath application of 0 Mg^{2+} ACSF and 10μM CNQX isolate a NMDAR-mediated fEPSP confirmed by complete block with the NMDAR antagonist DL-APV (50μM), representative trace. (B) The normalized Mg^{2+}/10μM CNQX (NMDAR) fEPSP rise time is slowed and decay kinetics are prolonged as compared to the fEPSP in control ACSF (1.2mM Mg^{2+}, representative trace.) (C) NMDAR (0 Mg^{2+}/10μM CNQX) fEPSP decay kinetics become more prolonged as stimulation strength increases, representative trace. (D) Dense fiber recruitment elicited at high stimulation strength does not alter control field EPSP decay kinetics, representative trace. (E) Normalized fEPSP time-integral (0-200ms) of individual experiments in control (n=44,17 slices) and NMDAR (0 Mg^{2+}/10μM CNQX, n=33,13 slices) conditions as a function of the first fEPSP amplitude.

transport with 30μM L-TBA prolonged EPSCs by selectively enhancing NMDAR signaling, with no effect on AMPAR responses (Sun et al. 2011). L-TBA had a similar effect on frequency-facilitated EPSCs, in which the charge transfers in the first and second EPSCs induced by paired pulse stimulation were increased to 141±6.3% (n=6, $p<0.01$) and 163±9% (n=6, $p<0.001$) of control, respectively (Figure 3A-C). Although the mean prolongation induced by L-TBA was greater in the facilitated EPSC, this difference did not reach statistical significance (p=0.08, Figure 3C).

These data confirm that in conditions permissive for NMDAR signaling, increases in release site density (Christie and Jahr, 2006) or reduction of glutamate transport (Asztely and Kullman. 1997, Diamond 2001, Scimemi et al, 2004) induce transmitter spillover with consequent effects on postsynaptic responses. However, the implications for physiological signaling are unclear because of the expected attenuation of NMDAR signaling by voltage-dependent Mg^{2+} block. We therefore sought to characterize NMDAR responses to spillover in physiological ACSF containing 1.2 mM Mg^{2+} using extracellular recording. In physiological ACSF, the primary component of the Schaffer-CA1 fEPSP arises from AMPAR signaling, but frequency facilitation revealed an NMDAR-mediated component of the fEPSP detectable by increased rate of decay in the presence of 50μM APV (Figure 3D,E). The change in the fEPSP kinetics induced by APV was assessed by measuring the time integral of the fEPSP responses after normalizing peak amplitudes. The NMDAR-mediated field signal was selectively enhanced relative to the AMPAR signal by paired-pulse facilitation (p=0.001; Figure 3E). Inhibition of glutamate transport by 30 μM L-TBA slowed the fEPSP decay kinetics, and this effect was also greater in the frequency-facilitated fEPSP relative to the response elicited at low frequency (p=.001; Figure 3D,E). This effect of L-TBA was reversed by co-application with 50 μM DL-APV (p=0.50, 0.37 respectively; Figure 3D,E), indicating that NMDAR signaling in the frequency-facilitated fEPSP was selectively enhanced by L-TBA-induced spillover. Paired-pulse facilitation could potentially increase NMDAR signaling in several ways; including increasing

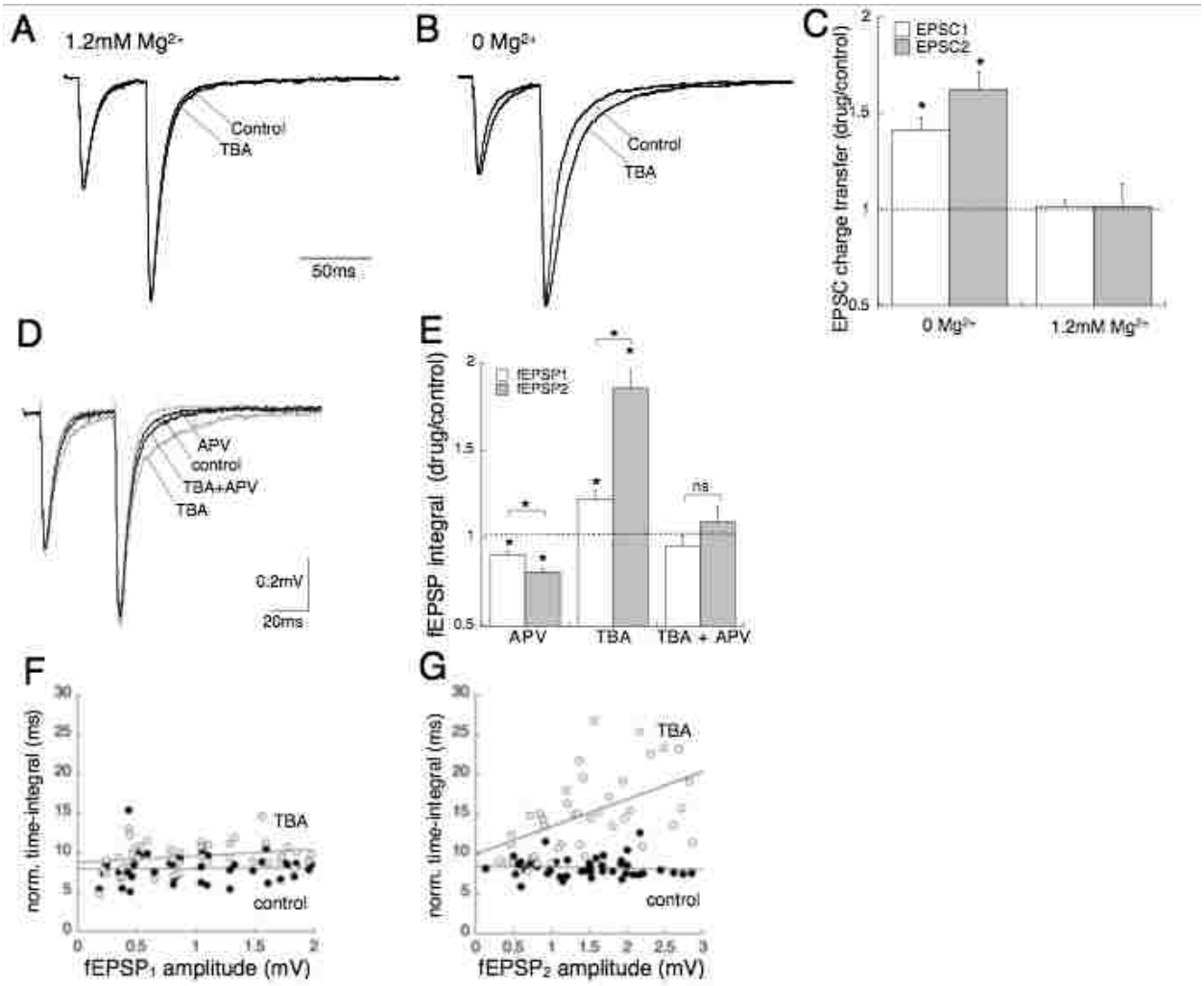

Figure 4.3. Physiological Mg^{2+} limits the enhancement of NMDAR activation induced by either transport block or increased fiber recruitment in a frequency dependent manner in non-voltage clamp recordings. (A,B) EPSC induced by a paired pulse stimulation in the presence or the absence of 30μM TBA in ACSF containing 1.2mM Mg^{2+} (A) or 0 Mg^{2+} (B), the charge transfer of 1st and 2nd EPSC after TBA were 141.4±6.3% (n=6, $p<0.01$) and 162.7±8.9% (n=6, $p<0.0001$) of control for 0 Mg^{2+} group, 101.1±3.3% (n=4, $p>0.7$) and 101.4±11.8% (n=4, $p>0.9$) for 1.2mM Mg^{2+} group. TBA's prolongation effect on 1st EPSC and 2nd EPSC in 0 Mg^{2+} solution are not significant different ($p>.05$). (C) Summary of data for experiments shown in (A) and (B). (D) 30 μM L-TBA prolonged fEPSPs in a frequency-dependent manner that was reversed by co-application of 50μM DL-APV (gray trace). (E) Summary of mean effects in 50μM DL-APV(n=44, 9slices), 30μM TBA (n=42, 9 slices) and 50μM DL-APV and 30μM TBA (n=9, 9 slices) in a single and paired-pulse protocol; * denotes $p<.05$. (F, G) Field EPSP time-integral of Individual experiments (all peaks were normalized to 1, 0-200ms after peak) in control and 30μM TBA as a function of first (F) and second (G) fEPSP amplitude (n=43).

presynaptic release probability and overall release site density, increasing multivesicular release from a subset of individual synapses , and/or by overwhelming glutamate transport (Christie and Jahr, 2006). To examine the potential effect of increased release site density in the selective increase in NMDAR signaling seen during frequency facilitation, stimulus strength was changed during a paired-pulse paradigm in the presence or absence of 30μM L-TBA. In the presence or absence of L-TBA, the normalized time-integral of the first fEPSP elicited by paired-pulse stimulation did not change with stimulation strength, even as fEPSP amplitudes varied over a range exceeding the peak facilitation ratio (Figure 3F,G). This suggests that during low frequency signaling, one or more mechanism(s) are in place to limit NMDAR activation as release site density increases, even when glutamate transport is inhibited. In contrast, with frequency facilitation, inhibition of glutamate transport resulted in a significant positive slope of the facilitated fEPSP time integral as function of fEPSP amplitude (Figure 3G; least-squares linear regression/slope analysis L-TBA: r =.43, p=0.004; control: r = 0.076, p=0.650).

Mechanism of frequency-dependent NMDAR facilitation- To examine the mechanism underlying the observed difference in frequency facilitation of AMPAR and NMDAR fEPSPs, we isolated NMDAR fEPSPs elicited by paired-pulse stimulation in either the presence or absence of extracellular Mg^{2+}. In the first set of experiments, NMDAR responses were isolated by recording fEPSPs in control ACSF containing 1.2 mM Mg^{2+} and subtracting responses in the presence of 50 μM APV. In the latter case, NMDAR fEPSPs were recorded in extracellular solution containing 20 μM CNQX with 0 Mg^{2+} (see Figure 2). The peak amplitude facilitation ratios of the fEPSP in control ACSF, the AMPAR-mediated fEPSP recorded in the presence of 50μM APV, and the NMDAR fEPSP recorded with CNQX in the absence of Mg^{2+} were not significantly different (Figure 4A-C). In contrast, the facilitation ratio of the NMDAR fEPSP isolated by APV during recording in physiological ACSF with Mg^{2+} was significantly greater (Figure 4D; p<.001). Interestingly, the rise time of the second fEPSP was also

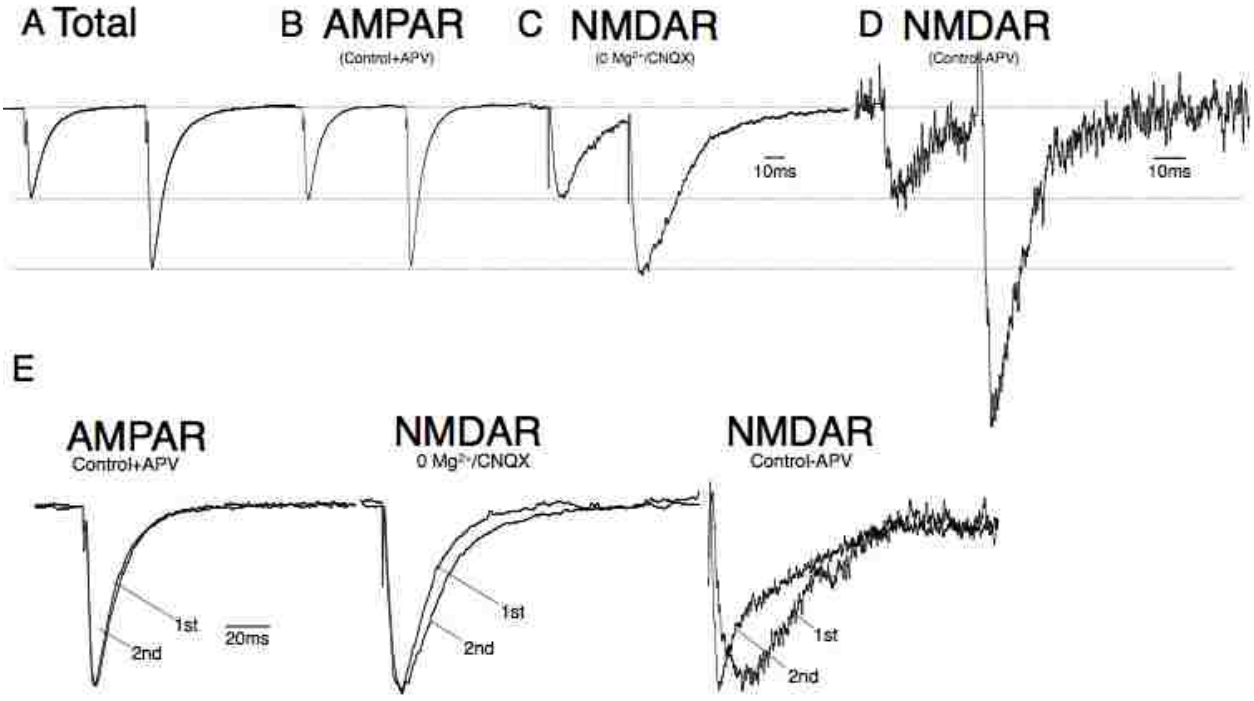

Figure 4.4. Paired pulse facilitation of NMDAR at the CA1 Schaffer collateral-pyramidal neuron synapse in the presence and absence of magnesium. Normalized fEPSPs of (A) fEPSP in control ACSF (representative trace) (B) AMPAR (50μM DL-APV, representative trace), (C) Mg-free +10μM CNQX (mean 40 traces, 4 slices), and (D) NMDAR (Control trace-DL APV, mean 80 traces, 8 experiments) responses elicited by a paired pulse (50ms) protocol. (E) Summary of paired pulse ratios calculated following subtraction of the 1st fEPSP of Total (n=45, 9 slices), AMPAR (n=45, 9 slices), Mg-free CNQX (n=34, 13 slices), and Control-APV (n=28, 8 slices) ** indicates a P<.001. (F) An overlay of the 1st and 2nd fEPSPs of the AMPARs (50μM APV, representative trace), isolated NMDARs (0Mg+2 and CNQX, representative trace), and APV-sensitive NMDARs (Control-APV, mean of 90 traces, 3 slices) indicate a significant shift in the rise time (10-90%) only under conditions of NMDAR isolation in the presence of Mg+2 (p<. 05).

significantly faster as compared to the first fEPSP in only the APV-sensitive component (Figure 4E). These data suggested the possibility that selective enhancement of NMDAR signaling during repetitive activity may be due to a postsynaptic effect of Mg^{2+}.

To compare the interpulse interval-dependence of the NMDAR facilitation with that of the presynaptic release change reflected in facilitation of the AMPAR fEPSP, paired stimuli were delivered at varying interpulse intervals (Figure 5). The time-dependent facilitation of the NMDAR signal was divided by that of the AMPAR signal to account for the presynaptic facilitation that occurs due to residual calcium. The time-dependence of their mean relative amplitudes revealed that the NMDAR-selective frequency-enhancement decayed with a time constant of 194 ms (Figure 5B). We used the same analysis to compare the interpulse interval-dependence of the NMDAR signal isolated in the absence of Mg^{2+} with CNQX. In this case, the frequency dependence of facilitation were not different for NMDAR and AMPAR fEPSPs, suggesting a key role for physiological Mg^{2+} in generating the time course of NMDAR-selective frequency facilitation. The NMDAR signal was also isolated in the presence of L-TBA which revealed a significantly longer time constant of 1348.6 ms (Figure 5C). The increase in time constant is most likely a reflection of the effect of glutamate transporters on t glutamate diffusion time course.

Frequency- and Mg^{2+}-dependent enhanced synaptic NMDAR signaling correlates with channel deactivation/desensitization kinetics

NMDAR receptors display slow decay kinetics following glutamate binding (Lester and Jahr 1992; Mayer et al. 1984). We sought to test the possibility that Mg^{2+} played a role in the NMDAR-selective frequency facilitation through voltage-dependent unblock of receptors occupied by a previous synaptic glutamate transient. Using nucleated patches from CA1 pyramidal cells, we compared the paired-pulse interval-dependence of this synaptic facilitation with the time-dependence of responses to brief voltage pulses relieving Mg^{2+} unblock from

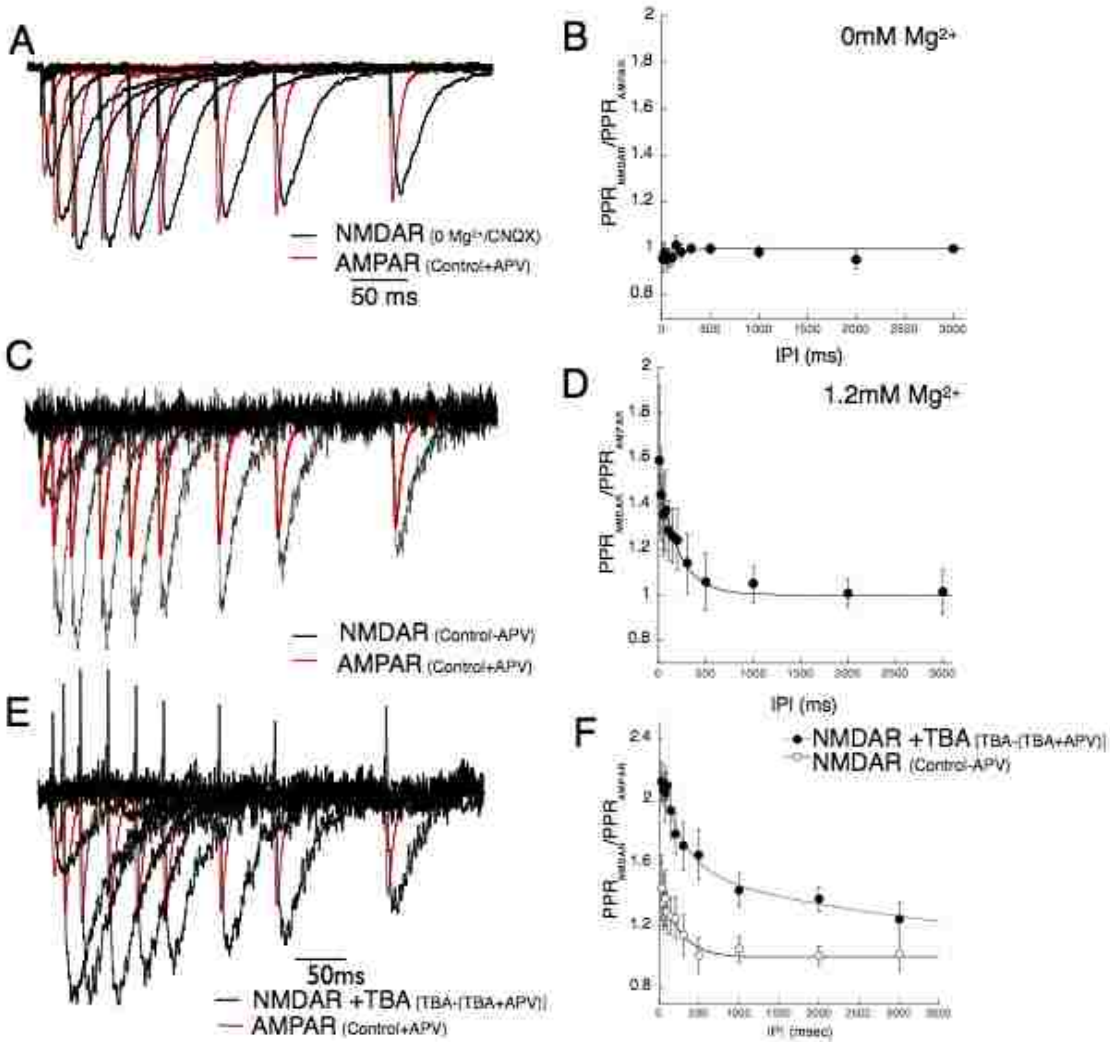

Figure 4.5. Magnesium-dependence of facilitation at the CA1 Schaffer collateral-pyramidal neuron synapse. (A) Mean fEPSPs trace (60 traces, n=6 slices) of APV-sensitive NMDA (Control trace -DL APV Traces) at interpulse intervals from 0 to 500ms (n=6). (B) Summary of mean NMDAR (Control-APV) PPR normalized to AMPAR PPR (n=9) fit to a single exponential. (C) Representative field EPSPs of NMDAR (0 Mg^{2+}+10μM CNQX) at interpulse intervals from 0 to 500 msecs (40 traces mean trace n=4). (D)Summary of mean NMDAR (0 Mg^{2+}) PPR normalized to AMPAR PPR (n=6). Interpulse interval experiments were done at a stimulus strength that elicited 60% of the maximum response. (E) Representative field EPSPs of NMDAR in 30μM TBA [TBA-(TBA+APV)] at interpulse intervals from 0 to 500 msecs (40 traces mean trace n=4). (F) Summary of mean NMDAR in 30μM TBA [TBA-(TBA+APV)] PPR normalized to AMPAR PPR (n=6) and mean NMDAR (Control-APV) PPR normalized to AMPAR PPR (n=9). Interpulse interval experiments were done at a stimulus strength that elicited 60% of the maximum response.

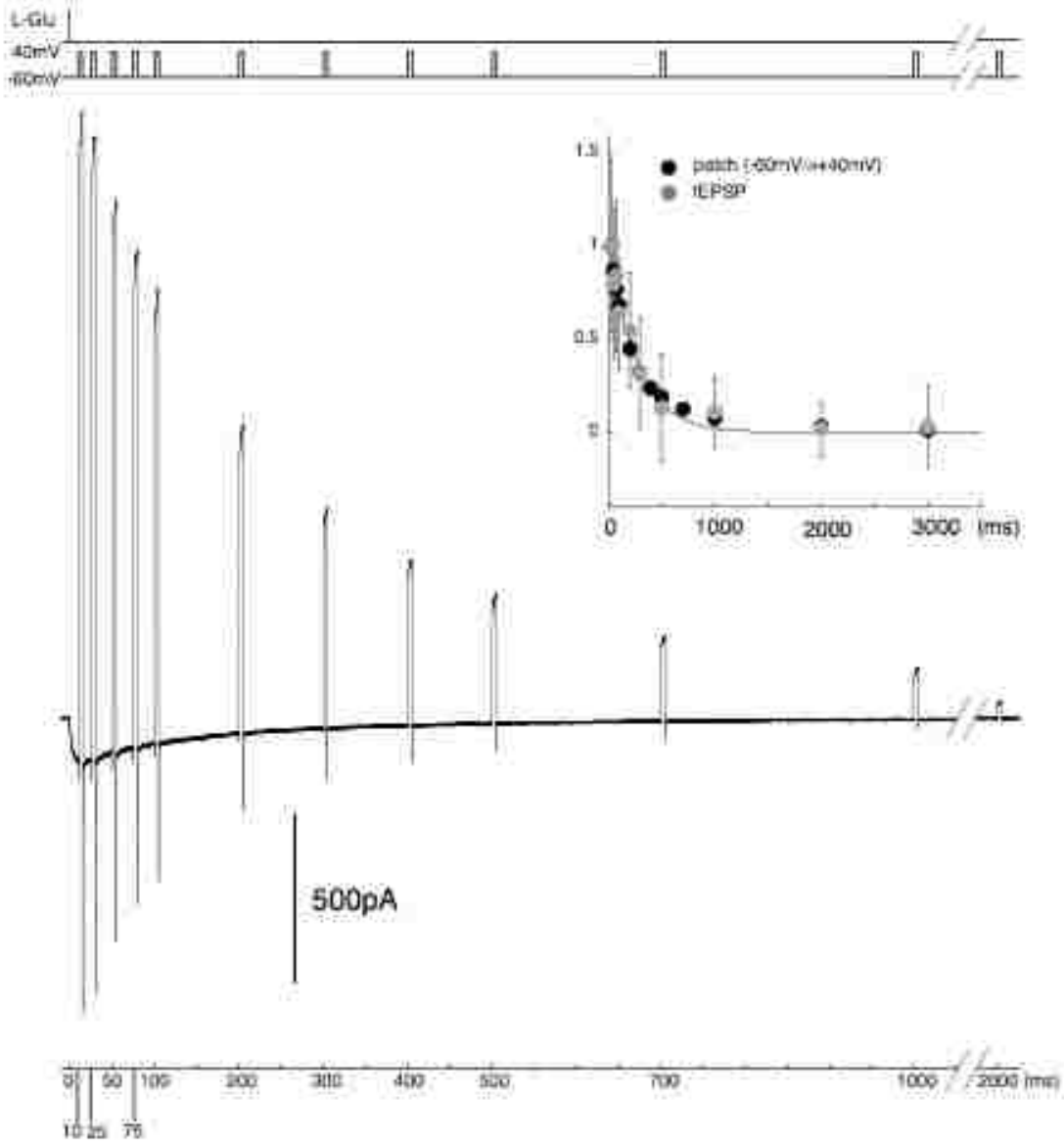

Figure 4.6. NMDAR currents recorded from nucleated patches with 1ms L-Glu application under continuous +40mV holding potential (top trace) or -60mV to +40mV 5ms voltage jumps (bottom trace). (B) Single exponential fitting of decay kinetics. Grey symbols, decay of voltage jump currents from outside out patches. Black symbols, decay kinetics of normalized APV sensitive fEPSP.

NMDAR channels at varying intervals following exposure to a transient glutamate concentration application. The response to 5 ms voltage jumps relieving Mg^{2+} block slowly decayed as a function of the time interval following a 1ms exposure to 1 mM L-Glu (Figure 6). The decay time course of the voltage jump currents matched the time-interval dependence of the synaptic facilitation reasonably well, with a fast time constant 148±12ms and a slow time constant of 521±73ms (Fig.6 inset).

Discussion

In these studies, we determined the effects of spillover and Mg++ unbinding on NMDAR signaling. We used whole-cell recording from CA1 pyramidal cells and extracellular field recording in stratum radiatum to investigate the effect of glutamate transport inhibition on synaptic NMDAR activity as a function of release site density, release frequency, and Mg^{2+} block. Our results demonstrate that glutamate spillover onto NMDARs can be facilitated by increasing release site density and release frequency.

As reported for NMDAR EPSCs in whole-cell voltage clamp studies (Arnth-Jensen et al. 2002), NMDAR field responses were prolonged by increasing stimulus strength, presumably due to spatiotemporal effects arising from transmitter pooling as release site density increases (Figure 3B,E; Otis et al., 1996). In dramatic contrast to results in Mg^{2+}-free conditions, fEPSP kinetics in physiological ACSF were not altered by varying stimulus intensity (Figure 3C,E). Furthermore, addition of APV had no effect on fEPSP kinetics in the presence of Mg^{2+} (Figure 3D). With increasing input density, more receptors bind glutamate but Mg^{2+} maintains this block (Figure 3C,D). In contrast, brief repetitive activity induced by as few as two stimuli (50ms inter-pulse interval) effectively activated NMDAR signaling, because the second fEPSP displayed pronounced APV-sensitivity even in the presence of physiological Mg^{2+}. Together these data suggest that even during sparse low-frequency synaptic activity with glutamate transport intact, significant transmitter binding to NMDARs occurs, but signaling is substantially prevented by Mg^{2+} block. The voltage-dependent Mg2+ block has previously been implicated in spike-timing

dependent plasticity (Kampa et al. 2004), yet the role of transporters has not yet been investigated. It is important to note that the mechanism underlying the NMDAR signaling induced by frequency facilitation in physiological ACSF was not likely amplitude-dependent, since increases in low-frequency stimulus strength that resulted in equivalent or greater increases in fEPSP amplitude than caused by frequency-facilitation had no effect on kinetics.

The involvement of glutamate transporters in limiting the frequency-enhancement of NMDAR activity was examined by testing the effect of 30μM L-TBA on fEPSPs. In the presence of physiological Mg^{2+}, neither the amplitude nor the facilitation ratio of fEPSPs was significantly changed by TBA (100±2% and 97±3% of control, respectively; n=29). TBA slightly prolonged the kinetics of the fEPSP elicited by low frequency stimulation, but it had a more pronounced effect on the frequency-facilitated fEPSP (Figure 4A,B). The prolongation induced by TBA was mediated by NMDARs, as it was reversed by APV (Figure 4B). The effect of transport inhibition on the second fEPSP was also selectively enhanced by increasing release site density (Figure 4C,D).

We further examined Mg^{2+} and glutamate transporter actions on synaptic NMDAR activity by whole cell recording from CA1 pyramidal cells. Consistent with field recording results, removal of Mg^{2+} with transport intact resulted in prolongation of the EPSC, with greater prolongation of the second EPSC evoked in a paired-pulse stimulation (Figure 3). While in physiological Mg^{2+} the normalized charge transfer in the second EPSC was the same as the first. In addition L-TBA prolonged EPSCs evoked in Mg^{2+}-free ACSF by either single stimuli or paired pulse stimulation. In this study we confirmed the contribution of transport to restricting glutamate diffusion to extrasynaptic NMDARs. We extended these studies to physiologically relevant conditions by isolating AMPAR- and NMDAR-mediated components of extracellular fEPSPs in stratum radiatum in normal extracellular [Mg^{2+}] without voltage clamp. These experiments found that the influence of glutamate transport on synaptic signaling at the Shaffer-CA1 pyramidal cell synapse was minimal at low frequencies of synaptic activity. At frequencies greater than ~5Hz NMDAR signaling was facilitated due to relief of Mg^{2+} block from

glutamate-occupied receptors. This phenomenon was greatly increased by inhibition of glutamate transport by L-TBA as apparent by the increase in the time constant. The data suggest that NMDAR signaling is controlled by the interaction of several factors. We conclude that NMDA signaling and the induction of LTP is dependent upon synaptic frequency, transport, Mg^{2+} block, and NMDAR channel kinetics. We propose that the observed theta frequency threshold for enhanced NMDAR signaling observed in physiological conditions is a consequence of a phase-shifted signal at rhythms, specifically theta, limited by NMDAR channel kinetics.

ARTICLE IN PRESS

Mathematical Biosciences xxx (2012) xxx–xxx

Contents lists available at SciVerse ScienceDirect

Mathematical Biosciences

journal homepage: www.elsevier.com/locate/mbs

Identifying neurotransmitter spill-over in hippocampal field recordings

Emily Stone [a,b,*], Katie Hoffman [b], Michael Kavanaugh [b]

[a] Department of Mathematical Sciences, The University of Montana, Missoula, MT 59812, United States
[b] Center for Structural and Functional Neuroscience, The University of Montana, Missoula, MT 59812, United States

ARTICLE INFO

Article history:
Received 17 November 2011
Received in revised form 19 July 2012
Accepted 20 July 2012
Available online xxxx

Keywords:
Neurotransmitter spill-over
Hippocampus
NMDA receptors
AMPA receptors
Glutamate transporters

ABSTRACT

A model of synaptic and extra-synaptic excitatory signaling in the hippocampus is presented. The model is used to analytically evaluate the potential contributions of homosynaptic and heterosynaptic glutamate spill-over to receptor signaling during an electrophysiological experiment in which glutamate transporters are pharmacologically blocked. Inhibition of glutamate uptake selectively prolongs the decay kinetics of the second field excitatory postsynaptic potential evoked by paired pulse stimulation of Schaffer collateral axons in area CA1. The model includes AMPA and NMDA glutamate receptors, and the removal of glutamate by transporters and diffusion. We establish analytically that the prolongation cannot be caused by local effects, i.e., the transporters acting within or near the synapse. In contrast, a time profile of glutamate consistent with spill-over from adjacent synapses can explain the effect. The different reaction kinetics of AMPA and NMDA receptors have a significant role in reproducing the experimental results, as explained by analysis of the ODEs governing the reactions.

1. Introduction

The hippocampal region of the brain is believed to play a major role in information storage, and understanding its structure and function is central to understanding mechanisms of memory and learning. The hippocampus is organized in layers of pyramidal neurons, and the connectivity of different cells has been partially mapped. In particular, principal neurons in the part of the hippocampus called CA3 send long axonal processes (Schaffer collaterals) to synapse on dendrites of pyramidal cells and interneurons in the CA1 region. But morphological connectivity of these neurons only partly determines the characteristics of neural networks. The actual functional connectivity must be flexible, i.e. have time dependent features, for information processing such as memory and learning to occur. In part, this flexibility is obtained through long and short term synaptic plasticity, and possibly variable connectivity through synaptic spill-over of neurotransmitter in particular conditions.

Early studies of spill-over in the neuromuscular junction showed a slowed decay of synaptic current when acetylcholinesterase was blocked, evidence of prolonged acetylcholine presence [14,22]. In contrast to acetylcholine, the actions of most other neurotransmitters are terminated by reuptake mediated by plasma membrane transporters. Reviews of experimental results relating to synaptic spill-over and the role of neurotransmitter transporters can be found in Barbour and Hausser [4], Kullman and Asztely [18], Holmseth, et al. [10], Attwell and Gibb [2], and Tzingounis and Wadiche [34]. Spillover has been presented as an explanation of prolongation of decay of inhibitory post-synaptic currents (IPSCs) when GABA uptake is blocked in hippocampal inhibitory synaptic currents [16], while in the cerebellum, compound parallel fiber-Purkinje cell excitatory synaptic currents show delayed decay that could be explained by spill-over [27,19]. Also in the cerebellum, spill-over of glutamate is inferred at the cerebellar mossy fiber-granule cell connection in DiGregorio et al. [13]. In the hippocampus, evidence for spill-over at excitatory synapses is presented in, for example, Arnth-Jensen et al. [1], Vogt and Nicoll [37], Asztely et al. [3], Lozovaya et al. [21], Tsukada et al.[33], and Diamond [11]. The action of neurotransmitter transporters is key in many of these studies, since the inhibition of these transporters can lead to excess neurotransmitter in the extracellular space. More recent studies of this phenomenon include Scimemi et al. [30] and Sun et al. [31]. An overview of glutamate spill-over and transporter action is given in Diamond [12].

Recently, it has been reported that spill-over from climbing fibers onto glutamate receptors on interneurons in the cerebellum may be a central mechanism of activation at this unique connection (Szapiro and Barbour [32]). Technological advances, such as glutamate sensing fluorescent reporters, have been developed to directly detect concentrations of glutamate in extra-synaptic spaces. In Hires et al. [15], these are used to measure the time course of glutamate propagation after synaptic release. Here they demonstrate that submicromolar glutamate persists along dendritic surfaces for hundreds of milliseconds, and depends upon coordination of release from adjacent sites. In a similar vein, Okubo et al. [24] (for

* Corresponding author at: Department of Mathematical Sciences, The University of Montana, Missoula, MT 59812, United States. Tel.: +1 4062435365.
E-mail address: stone@mso.umt.edu (E. Stone).

0025-5564/$ - see front matter © 2012 Elsevier Inc. All rights reserved.
http://dx.doi.org/10.1016/j.mbs.2012.07.004

Please cite this article in press as: E. Stone et al., Identifying neurotransmitter spill-over in hippocampal field recordings, Math. Biosci. (2012), http://dx.doi.org/10.1016/j.mbs.2012.07.004

a review see [25]) have developed another type of fluorescent glutamate indicator that allows for the detection of glutamate in intact brain tissue. The family of indicators, dubbed EOS (Excitatory Optical Sensor) are used to study glutamate dynamics in intact brain structures. This imaging method has been used to visualize the release of extra-synaptic glutamate adjacent to excitatory synapses at the parallel fiber-Purkinje cell synapse. A quantitative measurement of the time dependent spread of glutamate with this method remains problematic, because the kinetics of the EOS are slow compared to that of relevant physiological processes, reading the signal from the response of the indicator involves a deconvolution step. We note, also, that as of yet, it is not possible to directly resolve the time course of glutamate *within* a synaptic cleft.

There has been a parallel effort in the mathematical modeling of spill-over in many of these experiments. In Barbour and Hausser [4], a simple model of inter-synaptic diffusion of neurotransmitter is constructed, to predict the likelihood of activation of nearby sites, referred to as "crosstalk". A more complex model is developed in Rusakov and Kullman [29], including three dimensional details of the neuropil, and other factors affecting glutamate diffusion, in order to create a spatiotemporal profile of glutamate in the extra-synaptic space and its effect upon receptors. Large scale Monte Carlo modeling of neurotransmitter release and receptor activation in physiologically realistic simulations of neuropil was pioneered by Sejnowski and his group (see http://www.mcell.cnl.salk.edu). In Coggan et al. [7], there is an example of such a study that addresses glutamate spill-over at the ciliary ganglion synapse. In Mitchell et al. [23], glutamate spill-over at the cerebellar mossy fiber-granule cell synapse was modeled by combining glutamate diffusion models (in restricted fractional two and three dimensional spaces) with probabilistic models of receptor activation. The effect of glutamate transporters on signal transmission in the CA1 region of the hippocampus was recently analyzed with a Monte Carlo model of a typical synaptic environment in Zheng et al. [39]. This work incorporates an estimate of diffusion made in situ with a two-photon excitation technique.

Glutamate transporters, known as excitatory amino acid transporters, or EAATs, are transmembrane proteins that bind free glutamate in the extracellular space and actively move it to the intercellular side of the membrane, a process that involves the binding and transport of other ions in a complex cascade (see [38,26] for more details). Three major subtypes of EAATs in the central nervous system are expressed in the forebrain on both astrocytes (glial: EAAT1 and EAAT2), and neurons (neuronal: EAAT3). In general they regulate glutamate homeostasis by taking up synaptically released transmitter, and are speculated to shape glutamate receptor dynamics during synaptic transmission. The role of neuronal and glial transporters in controlling receptor dynamics can be investigated through the use of glutamate uptake inhibitors. The glutamate uptake blocker DL-TBOA, blocks both neuronal and glial transporters, and a newer transport blocker, L-threo-beta-benzylaspartate, L-TBA, exhibits a slight selectivity for EAAT3 over both EAAT1 and EAAT2. A recent paper by Sun et al. [31], studies the characteristics of L-TBA in detail.

The exact role of the neuronal and glial transporters a subject of current debate. Recent experimental evidence suggests that the density of transporter molecules in hippocampal tissue is lower than originally thought, raising the question of how so few can affect the signaling characteristics of the receptors at the synapses so significantly [10]. The amount of glutamate released itself is debated, with estimates as low as 500 molecules, for instance see [36], who fitted a 3-D glutamate diffusion model to data from patch clamp mossy fiber terminal-CA3 pyramidal cell synapse experiment [17]. In the synapses we will be considering, it is generally accepted that the number is 3000–5000 molecules per vesicle [4,6,28] and that upon stimulation generally a single vesicle is released.

In this paper we study spill-over phenomena in glutamatergic synapses, specifically in the CA1 region of the hippocampus. In particular, the action of glutamate transporters to limit spill-over, as reported by Diamond [11], Scimemi et al. [30], and Arnth-Jensen [1], is examined from a modeling perspective. Diamond infers the presence of spill-over from the response of receptors that are pharmacologically blocked by a low affinity competitive antagonist. The effect of the blocker on the measured signal depends on the local concentration of glutamate, having a larger effect when lower concentrations of glutamate are present. Hence, the fact that it blocks the slow component of the signal to a greater degree than the fast component, implies that the slow component is a response to lower concentrations of glutamate. He also found that simultaneously blocking neuronal glutamate transporters increases the activation of receptors responding to low concentrations of glutamate, indicating that the low concentrations of glutamate are normally removed by the transporters. Mechanistically speaking, transporters appear to "clean up" after a release of glutamate molecules, preventing the occurrence of spill-over. Here we use a formal mathematical approach to gain insight into the spatial scales of transporter actions in limiting spill-over. To do so we model electrophysiological experiments in hippocampal slices that utilize the glutamate uptake inhibitor L-TBA.

Both transporter and receptor function are thought to be important in plasticity effects, where neurons are more or less sensitive to stimuli dependent on their previous firing history. To investigate short term synaptic plasticity, experiments are carried out in which a series of electrical stimuli are delivered to axon fibers, while the response (voltage change) is measured in the dendrites of the cells on the receiving side. Two equal impulses, delivered in quick succession, can generate either a short lived increase in the response (paired pulse facilitation) or decrease (paired pulse depression), depending on brain region/synapse and inter-pulse interval. These short term changes are mechanistically distinct from long-term potentiation and depression, phenomena that may underlie more permanent forms of memory storage In each case, however, neurons exhibit responses that are sensitive to the history of stimulation previously received.

In the experiments we model in this paper, paired pulse facilitation in rodent hippocampal slices is used to study the phenomenon of spill-over. Upon stimulation with a second, equal amplitude pulse, the probability of release of neurotransmitter is increased, which causes more synapses to release vesicles of glutamate into the synaptic cleft, so more glutamate is released overall in the slice. Transporter molecules will normally pick up any excess of glutamate, but when they are inhibited by a pharmacological blocker, a prolongation of the response is seen upon the second pulse [11]. This is presumed to be the effect of neurotransmitter leaking away from active sites and stimulating receptors at adjacent synapses or extra-synaptic regions. The evidence for this is indirect, since, as mentioned above, the concentration of glutamate within the cleft, and in many cases, outside the cleft, cannot be directly measured. Even though the amount of glutamate per vesicle (and hence per synapse) is small, if many postsynaptic densities are stimulated, and transporters are inhibited, spill-over of neurotransmitter could be significant.

The experimental data presented in Fig. 1 are recordings of the effect of electrical stimulation of transverse hippocampal slices (350 μm) from CD1 mice of 3–5 weeks of age. Stimuli are delivered to axon fibers arising from pyramidal cells in CA3, while the response is measured in the dendrites of the pyramidal cells of CA1. Recordings were performed at 30 °C. Field excitatory postsynaptic potentials (fEPSPs) were evoked by 100 μs duration stimuli in stratum radiatum. Stimulus strength (typically 50–100 μA) was adjusted to elicit responses 30–40% of maximum to avoid the occurrence of population spikes (action potentials). A paired pulse

Please cite this article in press as: E. Stone et al., Identifying neurotransmitter spill-over in hippocampal field recordings, Math. Biosci. (2012), http://dx.doi.org/10.1016/j.mbs.2012.07.004

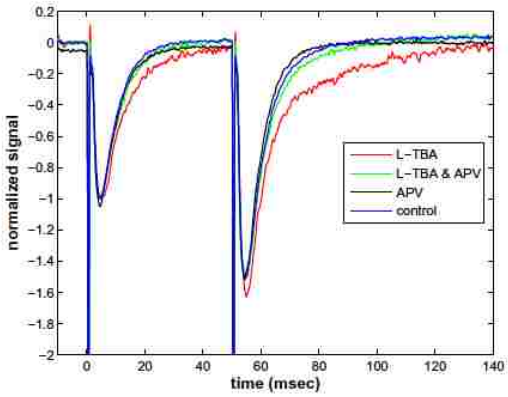

Fig. 1. The effect of transporter blocker L-threo-β-benzylaspartate (L-TBA) on field EPSP decay kinetics during paired pulse stimulation. The NMDA receptor antagonistic APV almost completely removes the effect.

stimulation was delivered 50 ms apart, every 20 s. The final five traces were averaged to arrive at the trace shown for a given experimental protocol. The resulting signal is shown in Fig. 1 for four different protocols: control, with transporters blocked by L-TBA, with NMDA receptors blocked by APV, and with transporters and NMDA receptors simultaneously blocked.

The following key facts summarize the results of this experiment.

1. The peak amplitude of the second response is larger presumably due primarily to increased glutamate release probability.
2. Blocking transporters and/or NMDA receptors does not significantly affect the relative or absolute peak amplitudes.
3. The rate of decay of the second response is the same as the first if transporters are not blocked.
4. Blocking transporters creates a marked prolonged decay in the second response.
5. Blocking NMDA receptors when transporters are also blocked restores the decay rate of the second response to that of the control.

Table 1
Parameter values for the receptors and transporter kinetics.

Parameter name	Value
k_1	8000 (M ms)$^{-1}$
k_{-1}	2 ms^{-1}
k_2	4000 (M ms)$^{-1}$
k_{-2}	4 ms^{-1}
k_3	4000 (M ms)$^{-1}$
k_{-3}	0.114 ms^{-1}
k_{d1}	0.15 ms^{-1}
k_{d2}	0.16 ms^{-1}
k_{-d1}	0.002 ms^{-1}
k_{-d2}	0.014 ms^{-1}
α	9 ms^{-1}
β	20 ms^{-1}
l_1	10000 (M ms)$^{-1}$
l_{-1}	0.005 ms^{-1}
l_2	5000 (M ms)$^{-1}$
l_{-2}	0.080 ms^{-1}
l_d	0.0084 ms^{-1}
l_{-d}	0.0018 ms^{-1}
a	0.0916 ms^{-1}
b	0.0465 ms^{-1}
k_t	5000 (M ms)$^{-1}$
k_{-t}	0.005 ms^{-1}
k_c	0.01 ms^{-1}
δ	0.1–1.0 ms^{-1}

We develop a general model to examine the implications of these facts, especially relative to the local or spatially extended action of released glutamate.

The organization of the paper is as follows. First we outline the physiological processes involved. Then we develop the theoretical model, and mathematically analyze its behavior to arrive at the assertion that something other than local effects near the synapse must be involved. Numerical simulations are next presented to fill in the picture of the dynamics of the receptors. The time profile of leaking glutamate necessary to produce the results of the experiment is determined by fitting the model to the experimental data, guided by physiological estimates of the kinetic parameters of the receptors and transporters (Table 1). We end with a discussion and summary of the research and its implications, and directions for future work.

2. Model development

2.1. Physiological processes

Most electrochemical signaling in the central nervous system is carried out by chemical synapses with transmitter gated ion channels. When an action potential reaches the pre-synaptic terminal of a nerve cell, it causes an elevation in calcium concentration due to the opening of voltage dependent calcium channels. This rise in calcium ultimately triggers the fusion of a vesicle of neurotransmitter molecules with the cell membrane. The neurotransmitter is released into a narrow region (the synaptic cleft) between the presynaptic membrane of the axon and the postsynaptic membrane of the target dendrite. The neurotransmitter can bind to ion channels in the postsynaptic membrane that are gated by the binding of the signalling molecule. The ion channels then open, thus changing the postsynaptic membrane potential and possibly triggering an action potential in the target cell.

Glutamate is the main excitatory neurotransmitter in the central nervous system, and in what follows we describe the components of excitatory glutamatergic signaling (see Fig. 2).

We consider two types of receptors, named after their synthetic agonists, N-methyl-D-aspartic acid receptor (NMDAR), and α-amino-3-hydroxy-5-methyl-4-isoxazole-propionic acid receptor (AMPAR). Both are glutamate-gated ion channels and as such are transmembrane proteins with binding sites for glutamate on their extracellular side. Both possess two binding sites and require two molecules of glutamate bound for activation. the kinetics of each are different, and AMPARs are thought to possess two desensitized states, while NMDARs have only one.

Re-uptake of neurotransmitter is essential for normal operation of chemical synapses, allowing for recycling of the molecules, and reduction of high levels of neurotransmitter which can cause prolonged receptor activity and excitotoxicity. Rapid clearance of neurotransmitter is also necessary for precision in signalling, and prevents the influence of neurotransmitter on neighboring post-synaptic and extra-synaptic receptors. As described in the introduction, re-uptake is performed by these transporters, the EAATs. In general, transporter function depends on electrochemical gradients of Na+, K+ and H+. They co-transport glutamate with three Na+ ions and one H+, and counter-transport one K+ ion in a thermodynamically coupled manner. For details see Zerangue and Kavanaugh [38].

One possible explanation of the prolongation of the response is the "buffering" of glutamate by transporters within and near the

Please cite this article in press as: E. Stone et al., Identifying neurotransmitter spill-over in hippocampal field recordings, Math. Biosci. (2012), http://dx.doi.org/10.1016/j.mbs.2012.07.004

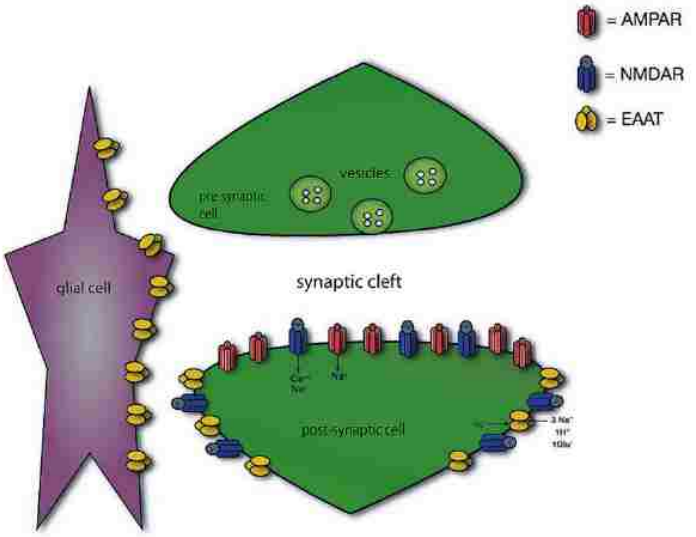

Fig. 2. Components of synaptic transmission: pre- and post-synaptic neurons and a glial cell. Vesicles filled with neurotransmitter (glutamate) fuse with the pre-synaptic membrane and release their contents into the synaptic cleft. The neurotransmitter binds with receptors (NMDA and AMPA) on the post-synaptic membrane and is taken up by transporters (EAATs) in the postsynaptic membrane and glial cells membranes.

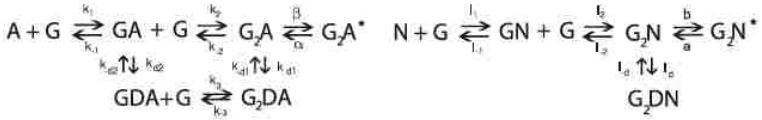

Fig. 3. Kinetic scheme for the state transitions of AMPA and NMDA receptors. See the text for more explanation and parameter values.

synaptic cleft, thus preventing it from lingering and activating the postsynaptic receptors. If so, a simple model of competition between the receptors and transporters for glutamate should be able to reproduce the observed results. To test this, we propose a "well-stirred" model of the concentrations of the constitutive components: the transporter molecules, the two types of receptor molecules, and free glutamate. This is essentially an "average synapse" model, and assumes the measured signal is a linearly rescaling of the signal produced by the receptors of one synapse. This signal is presumed to be proportional to the concentration of activated receptors at any time. We rely on well established kinetic schemes for each receptor, and assume that the equations for the receptors are linked only through the shared glutamate pool. Glutamate is released in a concentration pulse, and is allowed to diffuse away with a realistic time constant (between 1 and 5 ms, see Clements et al. [5]).

The reaction mechanisms and rate constants for the activation of AMPAR and NMDAR we use are reviewed in Attwell and Gibb [2], and a schematic is shown in Fig. 3. Each receptor has binding sites for two glutamate molecules, and can be activated (the ion channel opened) once these are occupied. The activated state is denoted G_2N^* for NMDAR, and G_2A^* for AMPAR. Each can also become desensitized, for instance for the NMDAR the desensitized state has two molecules of glutamate bound and is labeled G_2DN. AMPAR is thought to possess two desensitized states, with one and two molecules of glutamate bound, GDA and G_2DA, respectively. This difference is essential in creating a range of dynamic response, allowing for a richer signalling vocabulary in the neuron, a point which is developed more fully in Section 3.

For the transporters, we assume the simplest possible chemical kinetics. In our model, transporters bind glutamate in the synapse or extracellular space, and in one step move it to the opposite side of the membrane, where it is removed from play. The transporter returns then to its unbound state and is ready to transport another molecule of glutamate. The reaction mechanism is thus

$$G + T \underset{k_{-t}}{\overset{k_t}{\rightleftarrows}} TG,$$

$$TG \xrightarrow{k_c} T + G_{\text{in}}.$$

The simulations follow the concentration of receptor and transporter states in stimulated synapses, where 3000 molecules of glutamate are released into a 0.005 μm³ space, so the initial concentration is about 1 mM. We mimic this release of glutamate by adding a term $\epsilon t^2 e^{-\gamma t}$ to the right-hand side of the ODE for the concentration of glutamate $[G]$, which, by itself, generates a sigmoidal type profile of glutamate concentration rising from zero to the amount $\frac{2\epsilon}{\gamma^3}$. This limit is the maximum concentration of glutamate released (1 mM) and once γ is fixed, this determines the value of ϵ. In the simulations $\gamma = 1.0\ \text{ms}^{-1}$, which, along with the diffusion constant, determines the profile of glutamate concentration of growth and decay. The time to peak and decay can be determined analytically for varying γ and δ, but the expression is cumbersome. For $\gamma = \delta = 1.0$, however, the solution simplifies to $[G](t) = t^3 \exp(-t)$, which peaks at 3 ms (allowing for some latency between the stimulus time and the observed response) and decays with a rate constant of 1, consistent with the observation that glutamate

Please cite this article in press as: E. Stone et al., Identifying neurotransmitter spill-over in hippocampal field recordings, Math. Biosci. (2012), http://dx.doi.org/10.1016/j.mbs.2012.07.004

Table 2
Initial concentrations.

Total/initial concentration	Value	Reference
AMPAR	0.0265 mM	Attwell and Gibb [2]
NMDAR	0.004 mM	Attwell and Gibb [2]
G	1.0 mM	Clements et al. [5]
EAAT	0.0–0.1 mM	Danbolt [9]

clears the cleft within the first 5 ms [5]. The peak amount of glutamate concentration experienced by the receptors also depends on δ, with less reaching the receptors on the post-synaptic side of the cleft for larger values of δ.

The total concentration of the receptor molecules is fixed. AMPAR are assumed more numerous (about 80 molecules in a postsynaptic density) than NMDAR (about 25 molecules in a post-synaptic density) [2]. The number of transporter molecules can be adjusted from zero to several thousand, depending on the situation being simulated. These facts are summarized in Table 2.

2.2. Model equations

In this section we present the equations in dimensional form. The complete set can be written:

$$\frac{d\mathbf{X}}{dt} = F(\mathbf{X}),$$

with initial condition

$$\mathbf{X}(0) = \mathbf{X}_0,$$

where

$$\mathbf{X} \in R^{15}.$$

The components of $\mathbf{X}$ are the concentrations of the species in the reactions listed in the previous section, e.g. $[G]$, $[R]$, $[GR]$, etc.

Invoking the law of mass action, the ODEs for the AMPAR states are

$$\begin{aligned}
\frac{d[A]}{dt} &= -k_1[G][A] + k_{-1}[GA]\\
\frac{d[GA]}{dt} &= k_1[G][A] - k_2[G][GA] - k_{-1}[GA] + k_{-2}[G_2A] - k_{d2}[GA] + k_{-d2}[GDA]\\
\frac{d[G_2A]}{dt} &= k_2[G][GA] - k_{-2}[G_2A] - k_{d1}[G_2A] + k_{-d1}[G_2DA] + \alpha[G_2A^*] - \beta[G_2A]\\
\frac{d[G_2A^*]}{dt} &= -\alpha[G_2A^*] + \beta[G_2A] \qquad (2.1)\\
\frac{d[G_2DA]}{dt} &= k_{d1}[G_2A] - k_{-d1}[G_2DA] + k_3[G][GDA] - k_{-3}[G_2DA]\\
\frac{d[GDA]}{dt} &= k_{d2}[GA] - k_{-d2}[GDA] - k_3[G][GDA] + k_{-3}[G_2DA].
\end{aligned}$$

For the NMDAR, the equations describing the evolution of all states are

$$\begin{aligned}
\frac{d[N]}{dt} &= -l_1[G][N] + l_{-1}[GN]\\
\frac{d[GN]}{dt} &= l_1[G][N] - l_{-1}[GN] - l_2[G][GN] + l_{-2}[G_2N] \qquad (2.2)\\
\frac{d[G_2N]}{dt} &= l_2[G][GN] - l_{-2}[G_2N] - l_d[G_2N] + l_{-d}[G_2DN] + a[G_2N^*] - b[G_2N]\\
\frac{d[G_2N^*]}{dt} &= -a[G_2N^*] + b[G_2N]\\
\frac{d[G_2DN]}{dt} &= l_d[G_2N] - l_{-d}[G_2DN].
\end{aligned}$$

The time evolution of the states of the transporters are given by

$$\begin{aligned}
\frac{d[T]}{dt} &= -k_t[G][T] + k_{-t}[TG] + k_c[T]\\
\frac{d[TG]}{dt} &= k_t[G][T] - k_{-t}[TG] - k_c[TG] \qquad (2.3)\\
\frac{d[G_{in}]}{dt} &= k_c[TG].
\end{aligned}$$

The concentration of glutamate obeys the following ODE

$$\begin{aligned}
\frac{d[G]}{dt} &= -l_1[G][N] + l_{-1}[GN] - l_2[G][GN] + l_{-2}[G_2N] - k_1[G][A]\\
&\quad + k_{-1}[GA] - k_2[G][GA] + k_{-2}[G_2A] - k_3[G][GDA]\\
&\quad + k_{-3}[G_2DA] - k_t[G][T] + k_{-t}[GT] - \delta[G]. \qquad (2.4)
\end{aligned}$$

Note that it is this equation that couples all the other chemical species. We add a linear diffusion term, $-\delta[G]$, to model the loss of glutamate from the cleft due to diffusion.

2.3. Analysis

In these equations, the receptors and transporters interact only through the shared pool of glutamate, and this imposes a simplifying structure on the phase space. There are four invariant subspaces, namely the NMDAR states + glutamate, the AMPAR states + glutamate, the transporter states + glutamate, and the direction representing the concentration of glutamate alone.

There is a conserved quantity in the equations for the transporter, AMPAR and NMDAR subspaces, e.g. the total number of molecules of each species must remain constant. If the reaction is started with glutamate being introduced into a glutamate-free solution, the three conserved quantities are

$$\begin{aligned}
&[A] + [GA] + [GDA] + [G_2A] + [G_2DA] + [G_2A^*] = [A](0)\\
&[N] + [GN] + [G_2N] + [G_2DN] + [G_2N^*] = [N](0)\\
&[T] + [TG] = [T](0)
\end{aligned}$$

Table 3
Coefficient matrix M for the linear system.

GA	G_2A	G_2A^*	G_2DA	GDA	GN	G_2N	G_2N^*	G_2DN	TG	G
$-(k_{-1}+k_{d2})$	k_{-2}	0	0	k_{-d2}	0	0	0	0	0	0
0	$-(k_{-2}+k_{d1}+\beta)$	α	k_{-d1}	0	0	0	0	0	0	0
0	β	$-\alpha$	0	0	0	0	0	0	0	0
0	k_{d1}	0	$-(k_{-3}+k_{-d1})$	0	0	0	0	0	0	0
k_{d2}	0	0	k_{-3}	$-k_{-d2}$	0	0	0	0	0	0
0	0	0	0	0	$-l_{-1}$	l_{-2}	0	0	0	0
0	0	0	0	0	0	$-(l_{-2}+l_d+b)$	a	l_{-d}	0	0
0	0	0	0	0	0	b	$-a$	0	0	0
0	0	0	0	0	0	l_d	0	$-l_{-d}$	0	0
0	0	0	0	0	0	0	0	0	$-(k_{-t}+k_c)$	0
k_{-1}	k_{-2}	0	k_{-3}	0	l_{-1}	l_{-2}	0	0	k_{-t}	$-\delta$

Please cite this article in press as: E. Stone et al., Identifying neurotransmitter spill-over in hippocampal field recordings, Math. Biosci. (2012), http://dx.doi.org/10.1016/j.mbs.2012.07.004

We can then express the concentration of N, A, T as

$$[N] = [N](0) - ([GN] + [G_2N] + [G_2DN] + [G_2N^*])$$
$$[A] = [A](0) - ([GA] + [GDA] + [G_2A] + [G_2DA] + [G_2A^*])$$
$$[T] = [T](0) - [TG].$$

The ODEs for $[N], [A]$ and $[T]$ are thus not needed to compute the full solution, giving a reduction from 15 to 12 dimensions. A further reduction to 11 equations is achieved by noting that the equation for $[G_{in}]$ can be solved by direct integration once the concentration $[TG]$ is known.

The reduced system possesses a fixed point at $[A] = [A](0)$, $[N] = [N](0)$, $[T] = [T](0)$, and the rest of the concentrations set to zero. A linear change of coordinates to shift the origin to this fixed point further simplifies the system. The result is an 11 dimensional set of equations for the concentrations of NMDAR states, AMPAR states, transporter states and glutamate:

$$\begin{aligned}
\frac{d[GA]}{dt} &= k_1[G]([A](0) - ([GA] + [GDA] + [G_2A] + [G_2DA] + [G_2A^*])) \\
&\quad - k_{-1}[GA] - k_2[GA][G] + k_{-2}[G_2A] - k_{d2}[GA] + k_{-d2}[GDA] \\
\frac{d[G_2A]}{dt} &= k_2[GA][G] - k_{-2}[G_2A] - k_{d1}[G_2A] + k_{-d1}[G_2DA] + \alpha[G_2A^*] - \beta[G_2A] \\
\frac{d[G_2A^*]}{dt} &= -\alpha[G_2A^*] + \beta[G_2A] \\
\frac{d[G_2DA]}{dt} &= k_{d1}[G_2A] - k_{-d1}[G_2DA] + k_3[G][GDA] - k_{-3}[G_2DA] \\
\frac{d[GDA]}{dt} &= k_{d2}[GA] - k_{-d2}[GDA] - k_3[G][GDA] + k_{-3}[G_2DA] \qquad (2.5) \\
\frac{d[GN]}{dt} &= l_1[G]([N](0) - ([GN] + [G_2N] + [G_2DN] + [G_2N^*])) \\
&\quad - l_{-1}[GN] - l_2[G][GN] + l_{-2}[G_2N] \\
\frac{d[G_2N]}{dt} &= l_2[G][GN] - l_{-2}[G_2N] - l_d[G_2N] + l_{-d}[G_2DN] \\
&\quad + a[G_2N^*] - b[G_2N] \\
\frac{d[G_2N^*]}{dt} &= -a[G_2N^*] + b[G_2N] \\
\frac{d[G_2DN]}{dt} &= l_d[G_2N] - l_{-d}[G_2DN] \\
\frac{d[TG]}{dt} &= k_t[G]([T](0) - [TG]) - k_{-t}[TG] - k_c[TG] \\
\frac{d[G]}{dt} &= -l_1[G]([N](0) - ([GN] + [G_2N] + [G_2DN] + [G_2N^*])) + l_{-1}[GN] \\
&\quad - l_2[G][GN] + l_{-2}[G_2N] - k_1[G]([A](0) - ([GA] + [GDA] + [G_2A] \\
&\quad + [G_2DA] + [G_2A^*])) + k_{-1}[GA] - k_2[G][GA] + k_{-2}[G_2A] - k_3[G][GDA] \\
&\quad + k_{-3}[G_2DA] - k_t[G]([T](0) - [TG]) + k_{-t}[TG] - \delta[G].
\end{aligned}$$

Following the release of a vesicle of neurotransmitter, modeled by an increase in glutamate concentration, the dynamics of the above system is simple: after an initial peak in the concentration of activated receptors, the diffusion of glutamate results in the decay of the trajectory to the attracting fixed point. In the full 11 dimensional phase space the trajectory follows a path that ultimately collapses on the subspace spanned by the slowest eigendirections of the attracting fixed point. This means that the long term decay rate seen in the response of the receptors is governed by the least negative eigenvalues. To determine the eigenvalues and eigendirections we must linearize the equations about the fixed point. The result can be expressed

$$\mathbf{X}' = M\mathbf{X},$$

where $\mathbf{X} = ([GA], [G_2A], [G_2A^*], [G_2DA], [GDA], [GN], [G_2N], [G_2N^*], [G_2DN], [TG], [G])^T$, and M is the 11×11 coefficient matrix. The invariant subspaces are evident in M, see Table 3.

From the structure of M it is clear that the linearized dynamics of the receptors are uncoupled from one another, and from the transporters. Near the fixed point the trajectory can be approximated by the solution $\mathbf{X}(t)$ to the linearized system, which can be written

$$\mathbf{X}(t) = \sum_{i=1}^{11} c_i \mathbf{v}_i e^{\lambda_i t},$$

where $\mathbf{v}_i$ are the eigenvectors and λ_i are the eigenvalues of the coefficient matrix. While it is possible to compute these (using computer algebra) for general parameter values, the result is intractable. Instead we compute them for the physiological parameter values listed in Table 1, the result is shown in Table 4.

The invariant subspaces are obvious again from the structure of the eigenvectors, e.g. the G subspace is spanned by an eigenvector with eigenvalue $-\delta = -0.9$. The transporter + glutamate subspace is spanned by the $[G]$ eigenvector and one with components in both directions. The AMPAR + glutamate subspace is spanned by two eigenvectors in the $[GA]$, $[GDA]$, $[G]$ subspace, one in the $[GA]$, $[G_2A]$, $[G_2A^*]$ subspace, and two eigenvectors with components in all directions. The most negative eigenvalues, −31.2745, −2.0805, and −1.126, appear in the AMPAR + Glut subspace. There are also two less negative eigenvalues, the least negative (−0.0135) for decay in the $[GA]$, $[GDA]$, $[G]$ subspace, and the other, −0.1161, which corresponds to a decay constant of 8.62 ms, is mainly in the $[G_2DA]$, $[GDA]$ direction.

The NMDAR + glutamate subspace has eigendirections with the three least negative eigenvalues of the whole system, −0.0009, −0.005 and −0.0125 (with time constants 1111, 200, 80 ms, respectively). Two of these eigenvalues (−0.0009 and −0.0125) have eigenvectors with components in the $[G_2N^*]$ direction and will control the slowest decay in the $[G_2N^*]$ signal. By contrast, in the AMPAR subspace, the eigendirections containing a component in the $[G_2A^*]$ direction have eigenvalues −31.2745, −1.126 and −0.1161. All are more negative than any of those associated with the $[G_2N^*]$ direction. It is a fact that a trajectory of a linear system near a stable node will ultimately collapse onto the subspace spanned by eigenvectors with the least negative eigenvalues. The

Table 4
Eigenvalues (first row) and eigenvectors (columns) for the trivial solution of the complete system, organized by subspace.

λ	−31.2745	−2.0805	−1.126	−0.1161	−0.1449	−0.0135	−0.0125	−0.005	−0.0009	−0.134	−0.9
GA	−0.1039	−140.789	1.464	0.0486	−0.6849	0.0	0.0	0.0	0.0	0.0	0.0
G_2A	0.7584	0.0	0.3497	−0.0035	0.0	0.0	0.0	0.0	0.0	0.0	0.0
G_2A^*	−0.6517	0.0	1.0173	−0.0089	0.0	0.0	0.0	0.0	0.0	0.0	0.0
G_2DA	0.0	0.0	−0.138	−7.0262	0.0	0.0	0.0	0.0	0.0	0.0	0.0
GDA	0.0	5.4502	−0.91	7.8277	−101.10	0.0	0.0	0.0	0.0	0.0	0.0
GN	0.0	0.0	0.0	0.0	0.0	−0.538	−0.9956	1.0	−0.0293	0.0	0.0
G_2N	0.0	0.0	0.0	0.0	0.0	0.7286	0.7448	0.0	−0.0120	0.0	0.0
G_2N^*	0.0	0.0	0.0	0.0	0.0	−0.6567	0.4377	0.0	−0.0613	0.0	0.0
G_2DN	0.0	0.0	0.0	0.0	0.0	−0.0442	−0.5857	0.0	−1.1318	0.0	0.0
TG	0.0	0.0	0.	0.0	0.0	0.0	0.0	0.0	0.0	1.0	0.0
G	−0.09	238.5	−19.1031	−0.9183	−1.5451	0.0096	0.0028	0.0056	−0.0030	0.1553	1.0

Please cite this article in press as: E. Stone et al., Identifying neurotransmitter spill-over in hippocampal field recordings, Math. Biosci. (2012), http://dx.doi.org/10.1016/j.mbs.2012.07.004

final decay to the fixed point will occur on the time scale of those eigenvalues. Consequently the decay in the signal obtained by adding the $[G_2N^*]$ and $[G_2A^*]$ together will be determined at long times by the $[G_2N^*]$ eigenvalues, since $[G_2A^*]$ decays much more rapidly. If the NMDAR are removed, the dynamics will be restricted to the AMPAR + G subspace, and the slow decay component of the signal will also be removed, as borne out by the experimental run with the NMDAR blocked by APV.

The transporter + G subspace has eigenvalues of -0.9 and -0.134, corresponding to time constants 1.11 and 7.46 ms, respectively. The dynamics in this subspace evolves on an intermediate time scale. *If the transporters are removed, the long term decay of the signal must be unchanged, since it occurs in the NMDAR + glutamate subspace.* This is the basis for our assertion that local synaptic phenomena cannot be responsible for the experimental observations.

2.3.1. Nonlinear analysis: NMDAR

The linear analysis in the previous section provides some insight into the structure of the phase space, but is not the whole picture by any means. To analyze the full time course of the reaction, not just the decay back to unbound receptor states, we make approximations that allow us to solve the nonlinear equations in closed form. To do so we consider two separate phases of the reaction: (1) the very fast binding of two glutamate molecules and (2) the population of the doubly bound states and subsequent decay back to the attracting fixed point.

During the initial phase of the reaction the concentration of glutamate is very high in comparison to that of the free receptors ($[G](0) = G_0 = 1$ mM vs. $[N](0) = N_0 = 0.007$ mM). Accordingly, we rescale time by defining $\tau = l_1 G_0 t$. The receptor state variables are rescaled by the initial concentration of unbound receptors N_0, while we rescale $[G]$ by its initial concentration, G_0. The result is

$$
\begin{aligned}
y_0' &= -g y_0 + \bar{l}_{-1} y_1 \\
y_1' &= g y_0 - \bar{l}_{-1} y_1 - \bar{l}_2 g y_1 + \bar{l}_{-2} y_2 \\
y_2' &= \bar{l}_2 g y_1 - \bar{l}_{-2} y_2 - \bar{l}_d y_2 + \bar{l}_{-d} y_4 - \bar{b} y_2 + \bar{a} y_3 \\
y_3' &= \bar{b} y_2 - \bar{a} y_3 \\
y_4' &= \bar{l}_d y_2 - \bar{l}_{-d} y_4 \\
g' &= \frac{N_0}{G_0}(-g y_0 - \bar{l}_2 g y_1 + \bar{l}_{-1} y_1 + \bar{l}_{-2} y_2) - \bar{\delta} g
\end{aligned}
$$

with $y_0 = \frac{[N]}{N_0}$, $y_1 = \frac{[GN]}{N_0}$, $y_2 = \frac{[G_2N]}{N_0}$, $y_3 = \frac{[G_2N^*]}{N_0}$, $y_4 = \frac{[G_2DN]}{N_0}$, and $g = \frac{[G]}{G_0}$. The rescaled parameter $\bar{l}_2 = \frac{l_2}{l_1}$; and the rest follow the convention $\bar{p} = \frac{p}{l_1 G_0}$, e.g. $\bar{l}_{-1} = \frac{l_{-1}}{l_1 G_0}$. The initial conditions are $y_0(0) = 1$, $g(0) = 1$, $y_1(0) = y_2(0) = y_3(0) = y_4(0) = 0$. Note $\frac{N_0}{G_0} \ll 1$, and if we look on a time scale much less than $1/\bar{\delta} = \frac{l_1 G_0}{\delta}$, we can assume that $g' \cong 0$, so g is approximately constant, and therefore substitute $g = 1$ into the remaining equations. Referring to the parameter values from Attwell and Gibb in Table 2, we see that $l_1 G_0 = 10\ \mathrm{ms}^{-1}$, while a, b and l_{-2} are $\mathcal{O}(10^{-2})$, and l_d, l_{-d}, l_{-1} are $\mathcal{O}(10^{-3})$, so the rescaled version of each is $\mathcal{O}(10^{-3})$ and $\mathcal{O}(10^{-4})$, respectively. Thus, during this first brief phase we make the further approximation that terms involving these parameters can be ignored.

The resulting system is

$$
\begin{aligned}
y_0' &= -g y_0 \\
y_1' &= g y_0 - \bar{l}_2 g y_1 \\
y_2' &= \bar{l}_2 g y_1 \\
y_3' &= 0 \\
y_4' &= 0 \\
g' &= 0.
\end{aligned}
$$

In this approximate system the variables y_3 and y_4 will remain zero, and g is fixed at 1. The equations are then reduced to three, with linear terms only:

$$
\begin{aligned}
y_0' &= -y_0 \\
y_1' &= y_0 - \bar{l}_2 y_1 \\
y_2' &= \bar{l}_2 y_1.
\end{aligned}
$$

This set of ODEs is easily solved in closed form, yielding

$$
\begin{aligned}
y_0(\tau) &= e^{-\tau} \\
y_1(\tau) &= 2(e^{-\bar{l}_2 \tau} - e^{-\tau}) \\
y_2(\tau) &= -2e^{-\bar{l}_2 \tau} + e^{-\tau} + 1.
\end{aligned}
$$

In terms of the original variables we have

$$
\begin{aligned}
[N](t) &= N_0 e^{-l_1 G_0 t} \\
[GN](t) &= 2N_0(e^{-l_2 G_0 t} - e^{-l_1 G_0 t}) \\
[G_2N](t) &= N_0(-2e^{-l_2 G_0 t} + e^{-l_1 G_0 t} + 1).
\end{aligned} \tag{2.6}
$$

To illustrate the validity of this approximation during short time intervals, we plot the numerical solution to the full system over the first millisecond along with the approximate solution in Fig. 4.

Note that almost all receptors are double-bound with glutamate at the end of this phase. Thus the first, rapid part of the reaction can be completely replaced by setting the concentration of all receptor states to zero, with the exception of $[G_2N]$, which is set to N_0. This will be the initial condition for the second phase.

In the second phase we assume that all the free glutamate has diffused away, that is, the characteristic unbinding time for glutamate is much longer than its residence time in the cleft. At first the receptor states are redistributed between fully bound and deactivated, activated, and desensitized. Thus we rescale time by a rate representative of the redistribution, namely, $\tau = at$. We again rescale the concentrations of the receptor states by N_0, and since the initial concentration of glutamate is very small, we rescale it by N_0 also. The equation for $g = [G]/N_0$ is

$$
g' = -\frac{l_1 N_0}{a} g y_0 - \frac{l_2 N_0}{a} g y_1 + \frac{l_{-1}}{a} y_1 + \frac{l_{-2}}{a} y_2 - \frac{\delta}{a} g
$$

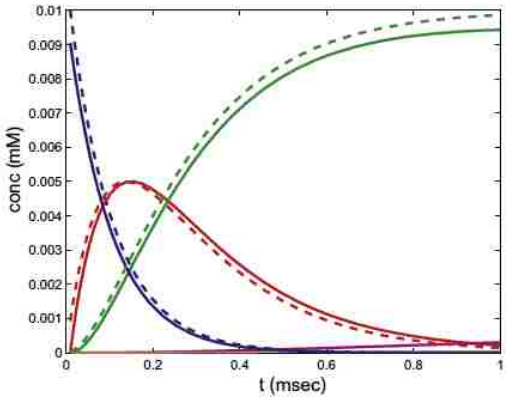

Fig. 4. Comparison of the exact solution to the approximation for the fast binding phase of NMDAR, Eq. (2.6), and the numerical solution of the NMDAR states in the full system, Eq. (2.5). Blue: $[N]$, green: $[G_2N]$, red: $[GN]$, purple: $[G_2N^*]$, solid lines: full simulation, dashed lines: approximation. $[G_2N^*]$ is not included in the approximation, and is just beginning to grow in the first millisecond of the reaction. (For interpretation of the references to color in this figure legend, the reader is referred to the web version of this article.)

Please cite this article in press as: E. Stone et al., Identifying neurotransmitter spill-over in hippocampal field recordings, Math. Biosci. (2012), http://dx.doi.org/10.1016/j.mbs.2012.07.004

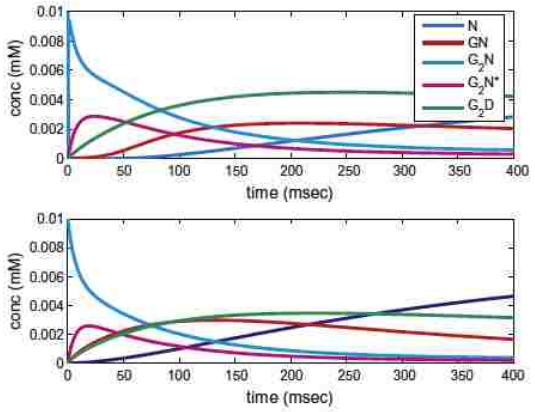

Fig. 5. Simulation of the NMDAR reaction equations (2.5) (top) and the solution to the approximation equations (2.7) (bottom) in the second phase of the reaction.

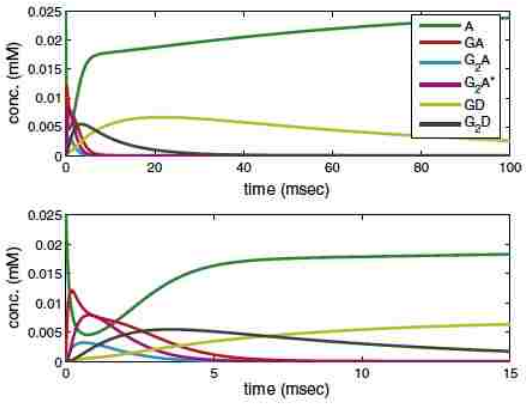

Fig. 6. Simulation of the AMPAR reaction, from Eq. (2.5), for 100 ms and 15 ms.

We assume that g begins very small, so that the first two binding terms (whose coefficients are order 1) can be neglected. Further, because the diffusion term has a much larger coefficient than the unbinding terms (order 10 vs. order 10^{-1}), we assume that any free glutamate created by unbinding is immediately diffused away. This keeps the concentration of g almost zero, and setting $g = 0$ in the other ODEs results in

$$\begin{aligned} y_0' &= \bar{l}_{-1} y_1 \\ y_1' &= -\bar{l}_{-1} y_1 + \bar{l}_{-2} y_2 \\ y_2' &= -\bar{l}_{-2} y_2 - \bar{l}_d y_2 + \bar{l}_{-d} y_4 - \frac{b}{a} y_2 + y_3 \\ y_3' &= \frac{b}{a} y_2 - y_3 \\ y_4' &= \bar{l}_d y_2 - \bar{l}_{-d} y_4. \end{aligned} \tag{2.7}$$

with rescaled parameters following the convention $\bar{p} = \frac{p}{a}$. The system can be reduced to four linear equations by noting that y_0 can be found by invoking the conserved quantity $y_0 + y_1 + y_2 + y_3 + y_4 = 1$. We solve the resulting system by finding the fundamental matrix of solutions, composed from the eigenvalues and eigenvectors of the coefficient matrix. We plot the result with parameter values from Table 2, in terms of the original variables, along with a simulation of the full nonlinear system, in Fig. 5.

Note that the overall behavior of the nonlinear system is captured by this linearization. G_2N decays quickly and G_2N^* is formed. Following this the desensitized state is populated, and G_2N^* decays. Finally the unbound state is recovered from G_2D and GN. The recovery of the unbound state occurs more quickly in the approximation, since there is no free G available. However, for the purpose of creating the measured signal G_2N^*, the approximation would give a reasonable facsimile; for instance, the characteristic decay rate of G_2N^* is approximately the same.

2.3.2. Nonlinear analysis: AMPAR

In Fig. 6 we plot a simulation of all the states in the full AMPAR reaction process, for 15 ms and 100 ms to resolve the fast binding and slow recovery part of the reaction, respectively. These suggest a time rescaling to isolate the early phase, namely $\tau = k_1 G_0 t$, with $z' = \frac{dz}{d\tau}$. We also rescale the receptor states by total number of receptors, A_0, and the glutamate by the initial amount of glutamate, G_0. The resulting equations are

$$\begin{aligned} g' &= \frac{A_0}{G_0}\left(\left(-z_0 - \frac{k_2}{k_1} z_1 - \frac{k_3}{k_1} z_5\right) g + \bar{k}_{-1} z_1 + \bar{k}_{-2} z_2 + \bar{k}_{-3} z_4\right) - \bar{\delta} g \\ z_0' &= -g z_0 + \bar{k}_{-1} z_1 \\ z_1' &= g z_0 - \bar{k}_{-1} z_1 - \frac{k_2}{k_1} g z_1 + \bar{k}_{-2} z_2 - \bar{k}_{d2} z_1 + \bar{k}_{-d2} z_5 \\ z_2' &= \frac{k_2}{k_1} g z_1 - \bar{k}_{-2} z_2 - \bar{k}_{d1} z_2 + \bar{k}_{-d1} z_4 - \bar{\beta} z_2 + \bar{\alpha} z_3 \\ z_3' &= \bar{\beta} z_2 - \bar{\alpha} z_3 \\ z_4' &= \frac{k_3}{k_1} g z_5 - \bar{k}_{-3} z_4 + \bar{k}_{d1} z_2 - \bar{k}_{-d1} z_4 \\ z_5' &= -\frac{k_3}{k_1} g z_5 + \bar{k}_{-3} z_4 + \bar{k}_{d2} z_1 - \bar{k}_{-d2} z_5 \end{aligned}$$

with $g = [G]/G_0$, $z_0 = [A]/A_0$, $z_1 = [GA]/A_0$, $z_2 = [G_2A]/A_0$, $z_3 = [G_2A^*]/A_0$, $z_4 = [G_2D]/A_0$, $z_5 = [GD]/A_0$, and rescaled parameters of the form $\bar{p} = \frac{p}{k_1 G_0}$.

We note that $\bar{k}_{-1}$, $\bar{k}_{-2}$, $\bar{k}_{-3}$, $\bar{\alpha}$, $\bar{\beta}$ are all $O(1)$ and $\frac{k_2}{k_1} = \frac{1}{2}$, while $\bar{\delta}$ is order 10^{-1}, $\bar{k}_{d1}$, $\bar{k}_{d2}$ are order 10^{-2}, and $\bar{k}_{-d1}$, $\bar{k}_{-d2}$ are order 10^{-3}, 10^{-4}, respectively. Assuming $G_0 > A_0$ by a factor of 10, $\frac{A_0}{G_0}$ is $O(10^{-1})$. For a coarse approximation to the reaction in the first millisecond after the release of glutamate we consider only the $O(1)$ terms (which neglects the transitions involving the desensitized states that are initially unpopulated) arriving at

$$\begin{aligned} g' &= -\bar{\delta} g \\ z_0' &= -g z_0 + \bar{k}_{-1} z_1 \\ z_1' &= g z_0 - \bar{k}_{-1} z_1 - \frac{k_2}{k_1} g z_1 + \bar{k}_{-2} z_2 \\ z_2' &= \frac{k_2}{k_1} g z_1 - \bar{k}_{-2} z_2 - \bar{\beta} z_2 + \bar{\alpha} z_3 \\ z_3' &= \bar{\beta} z_2 - \bar{\alpha} z_3 \\ z_4' &= \frac{k_3}{k_1} g z_5 - \bar{k}_{-3} z_4 \\ z_5' &= -\frac{k_3}{k_1} g z_5 + \bar{k}_{-3} z_4. \end{aligned}$$

Furthermore, for the first instance of the reaction (for t less than the unitless time scale set by $\frac{1}{\delta}$), $g' \cong 0$ and g can be fixed at 1. Since the equations for z_4 and z_5 are uncoupled from the rest of the system and $z_4(0) = z_5(0) = 0$, they must remain zero. Incorporating these approximations leads to the following system:

Please cite this article in press as: E. Stone et al., Identifying neurotransmitter spill-over in hippocampal field recordings, Math. Biosci. (2012), http://dx.doi.org/10.1016/j.mbs.2012.07.004

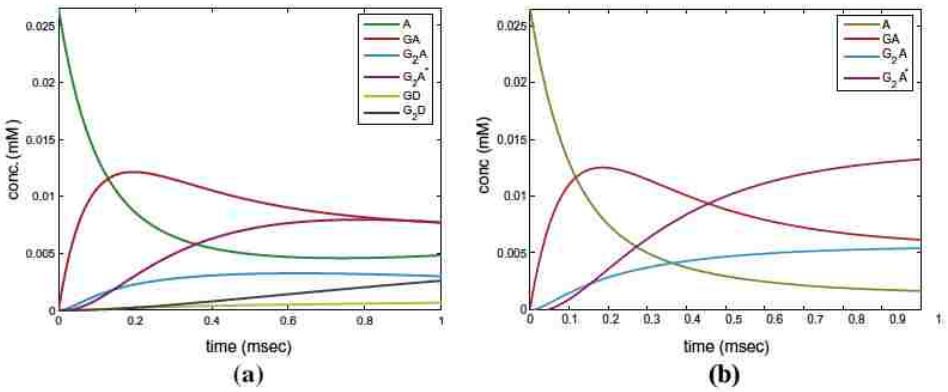

Fig. 7. (a) Numerical simulation of full system of ODEs (2.5) for the first millisecond of the AMPAR reaction. (b) Solution to the approximate system of ODEs for the first phase of the AMPAR reaction, Eq. (2.8).

$$\begin{aligned} z_0' &= -z_0 + \tilde{k}_{-1} z_1 \\ z_1' &= z_0 - \tilde{k}_{-1} z_1 - \frac{k_2}{k_1} z_1 + \tilde{k}_{-2} z_2 \\ z_2' &= \frac{k_2}{k_1} z_1 - \tilde{k}_{-2} z_2 - \tilde{\beta} z_2 + \tilde{\alpha} z_3 \\ z_3' &= \tilde{\beta} z_2 - \tilde{\alpha} z_3. \end{aligned} \tag{2.8}$$

This system can be solved exactly by finding the fundamental matrix of solutions as for the NMDAR reactions. In Figs. 7(a) and (b) we plot the numerical solution to the full system and the exact solution to the approximate system. The duration of this phase of the reaction depends on the time constant $G_0 k_1/\delta \sim O(1) - O(10)$, which is on the order of the 1 ms time window utilized in graphing both. The phase is characterized by decay of the free receptor population, growth and subsequent decay of $[GA]$, followed closely by the growth of $[G_2A]$, and transition from $[G_2A]$ to $[G_2A^*]$. Note that the approximation necessarily will not capture the growth in the desensitized states. This reduction involves more states than the first phase of the NMDAR reaction, because the binding rate of glutamate at physiological concentrations is smaller and comparable to the transition rate to the "on" receptor state. Therefore it includes both the binding of G and the redistribution in the non-desensitized states.

The relative sizes of the four states at the end of the phase are given approximately by the fixed point for the system above, $(\bar{z}_0, \bar{z}_1, \bar{z}_2, \bar{z}_3)$. Because of the conserved quantity $(z_0 + z_1 + z_2 + z_3 = 1)$ the fixed point is non-trivial and depends on the initial concentrations. Solving for this fixed point yields the following relationships:

$$\bar{z}_0 = \frac{\tilde{k}_{-1}}{G_0} \bar{z}_1 = \frac{1}{4} \bar{z}_1; \quad \bar{z}_2 = \frac{\beta}{\alpha} \bar{z}_3 = \frac{8}{20} \bar{z}_3,$$

where we see that the fixed point component values are related by the ratio of the forward to the backward rates. See Fig. 7(b), where at the end of the phase the states are approaching equilibrium, and $z_1 > z_0$ and $z_3 > z_2$, e.g. $[GA] > [A]$, $[G_2A^*] > [G_2A]$.

For the remainder of the reaction we assume that diffusion of free glutamate occurs rapidly enough to remove it as quickly as it is released, so that the forward glutamate binding terms in the equations are negligible and $[G]$ can be set to zero. We then rescale time by k_{-1}, and the concentrations of the reactants by the total amount of receptors A_0. The resulting equations are

$$\begin{aligned} z_0' &= z_1 \\ z_1' &= -z_1 + \tilde{k}_{-2} z_2 - \tilde{k}_{d2} z_1 + \tilde{k}_{-d2} z_5 \\ z_2' &= -\tilde{k}_{-2} z_2 - \tilde{k}_{d1} z_2 + \tilde{k}_{-d1} z_4 - \tilde{\beta} z_2 + \tilde{\alpha} z_3 \\ z_3' &= \tilde{\beta} z_2 - \tilde{\alpha} z_3 \\ z_4' &= -\tilde{k}_{-3} z_4 + \tilde{k}_{d1} z_2 - \tilde{k}_{-d1} z_4 \\ z_5' &= \tilde{k}_{-3} z_4 + \tilde{k}_{d2} z_1 - \tilde{k}_{-d2} z_5, \end{aligned}$$

where the z_i's are as defined for first phase, and $\tilde{p} = p/k_{-1}$. This phase of the reaction can be further divided into three epochs. During the first epoch the quantities $[GA]$, $[G_2A]$, $[G_2A^*]$ decay, while $[GD]$ grows initially and then decays as $[G_2D]$ is formed. The concentration of free receptors, $[A]$, also grows as glutamate unbinds and is removed by diffusion. We can approximate the dynamics during this epoch by noticing that the backward rates of desensitization $\tilde{k}_{-d1}$, $\tilde{k}_{-d2}$ are one to two orders of magnitude smaller than the other reaction rates. We therefore neglect those terms to arrive at

$$\begin{aligned} z_0' &= z_1 \\ z_1' &= (1 - \tilde{k}_{d2}) z_1 + \tilde{k}_{-2} z_2 \\ z_2' &= -(\tilde{k}_{-2} + \tilde{k}_{d1} + \tilde{\beta}) z_2 + \tilde{\alpha} z_3 \\ z_3' &= \tilde{\beta} z_2 - \tilde{\alpha} z_3 \\ z_4' &= -\tilde{k}_{-3} z_4 + \tilde{k}_{d1} z_2 \\ z_5' &= \tilde{k}_{-3} z_4 + \tilde{k}_{d2} z_1. \end{aligned} \tag{2.9}$$

The structure of these equations is sufficiently simple to allow us to solve them analytically. First the two coupled equations for z_2 and z_3 can be solved, and the result for z_2 is used to solve the ODEs for z_1 and z_4. z_5 and z_0 can be computed by direct integration once z_1 and z_4 are determined. The result is plotted in Fig. 8(b), to be compared with a simulation of the full equations during this epoch in Fig. 8(a).

We see that the essentials of the reaction are captured by the approximation, but perhaps it is more informative to examine the decay rates of the different species, as determined analytically. For instance, the decay rates for z_2 and z_3 are -0.6 and -15.75, respectively. The larger rate corresponds to a time constant of 0.025 ms, which is not resolved at this scale. The smaller rate governs the longer term decay with a time constant of 1.66 (or 0.833 in ms). Moving to z_1, the solution will necessarily have decay rates from the z_3 solution and $1 - \tilde{k}_{d2} = 1 - 0.16/2 = 0.92 = 0.46\ \text{ms}^{-1}$, which is roughly half the smaller decay rate of z_3 and z_2, hence the slightly longer decay profile. z_0 can be determined by direct

Please cite this article in press as: E. Stone et al., Identifying neurotransmitter spill-over in hippocampal field recordings, Math. Biosci. (2012), http://dx.doi.org/10.1016/j.mbs.2012.07.004

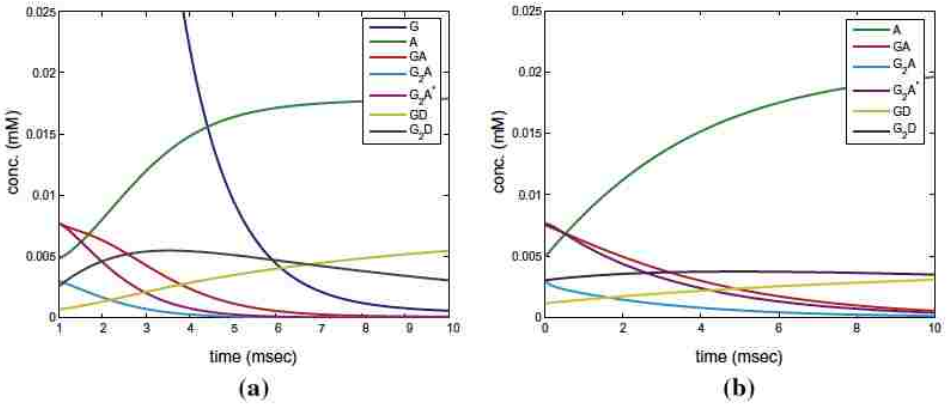

Fig. 8. (a) Numerical simulation of full system of ODEs (2.5) for the second phase, first epoch of the AMPAR reaction. Note the time shift that leaves out the first millisecond. (b) Solution to approximate system of ODEs (2.9) for the second phase, first epoch, of the AMPAR reaction.

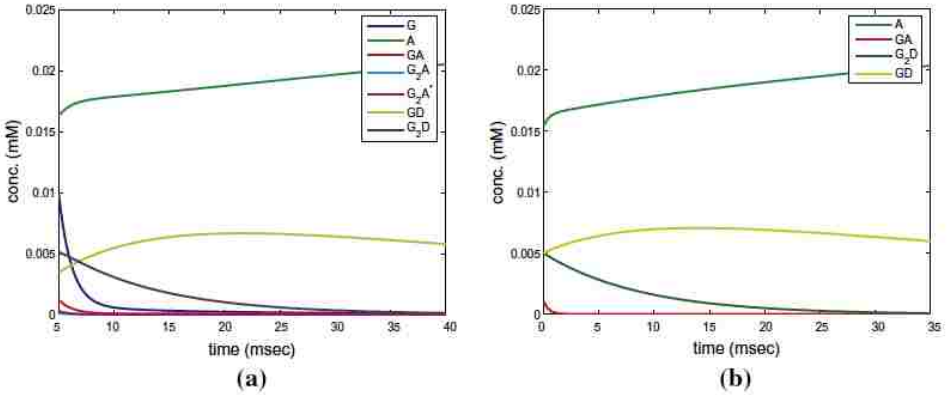

Fig. 9. (a) Numerical simulation of full system of ODEs (2.5) for the AMPAR reaction showing the second epoch of the second phase. (b) Solution to approximate system of ODEs (2.10) for the AMPAR reaction in the second epoch of the second phase.

integration of z_1, and so is governed by the same rates, although in this case they are growth rates as the unbound receptor is recovered over time. The solution to the ODE for z_5 is found by solving another first order linear ODE, driven by z_1, so it will inherit those rates, but what is evident from the figure is the much slower rate of $\tilde{k}_{-3} = 0.057\ \text{ms}^{-1}$, which determines the long-term growth of z_5 toward a stationary value.

The second epoch in phase two occurs for $5 < t < 30$ ms, and is characterized by the decay of $[G_2D]$, growth and slow decay of $[GD]$, and subsequent growth of $[A]$. Interestingly, the concentration of $[GA]$ decays to almost zero and remains near zero through the rest of the reaction, though it is necessarily populated as $[A]$ is formed from $[GD]$.

We consider the rescaled equations from the first epoch:

$$
\begin{aligned}
z_0' &= z_1 \\
z_1' &= -z_1 + \tilde{k}_{-2}z_2 - \tilde{k}_{d2}z_1 + \tilde{k}_{-d2}z_5 \\
z_2' &= -\tilde{k}_{-2}z_2 - \tilde{k}_{d1}z_2 + \tilde{k}_{-d1}z_4 - \tilde{\beta}z_2 + \tilde{\alpha}z_3 \\
z_3' &= \tilde{\beta}z_2 - \tilde{\alpha}z_3 \\
z_4' &= -\tilde{k}_{-3}z_4 + \tilde{k}_{d1}z_2 - \tilde{k}_{-d1}z_4 \\
z_5' &= \tilde{k}_{-3}z_4 + \tilde{k}_{d2}z_1 - \tilde{k}_{-d2}z_5.
\end{aligned}
$$

First we assume z_2 and z_3 remain zero for all time, which is consistent with the z_3 ODE. For the z_2 ODE, $\tilde{k}_{-d1}$ (which multiplies z_4) is several orders of magnitude less than the other parameters and thus can be ignored. That small backward rate effectively blocks one pathway of the reaction, but does not appear appreciably in the actual solution for any of the species. Ignoring the terms multiplied by $\tilde{k}_{-d1}$ in the remaining ODEs creates the following system:

$$
\begin{aligned}
z_0' &= z_1 \\
z_1' &= -(1 + \tilde{k}_{d2})z_1 + \tilde{k}_{-d2}z_5 \\
z_4' &= -\tilde{k}_{-3}z_4 \\
z_5' &= \tilde{k}_{-3}z_4 + \tilde{k}_{d2}z_1 - \tilde{k}_{-d2}z_5.
\end{aligned}
$$

This system has a conserved quantity, and we use that to determine the solution for z_0, e.g. $z_0 = 1 - z_1 - z_4 - z_5$. The ODE for z_4 is uncoupled and yields the solution

$$z_4(\tau) = z_4(0)e^{-\tilde{k}_{-3}\tau}.$$

With this, the equations for z_1 and z_5 are a set of coupled, linear non-homogenous ODEs, which can be solved exactly. Doing so via Maple generates an intractable expression, so to simplify it we substitute the rescaled parameter values, and choose as initial

Please cite this article in press as: E. Stone et al., Identifying neurotransmitter spill-over in hippocampal field recordings, Math. Biosci. (2012), http://dx.doi.org/10.1016/j.mbs.2012.07.004

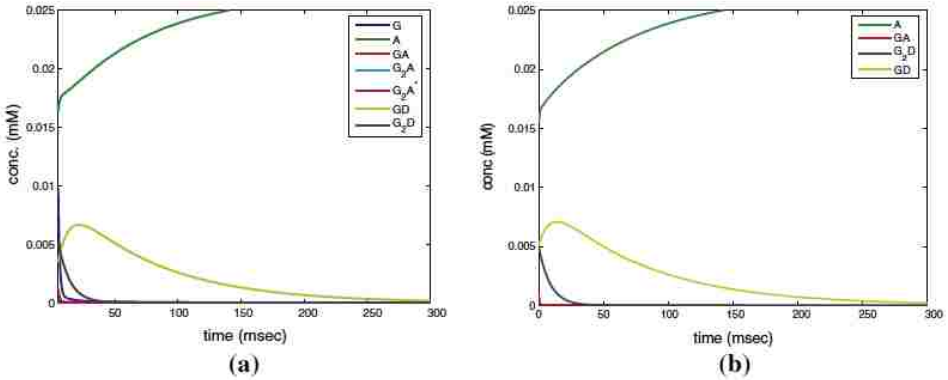

Fig. 10. (a) Numerical simulation of full system of ODEs for AMPAR in the third epoch of phase two. (b) Solution to approximate system of ODEs for AMPAR in the third epoch of phase two.

conditions the values from the end of the first epoch from Fig. 8(b). The result is:

$$z_1(\tau) = 0.0023e^{-0.0065\tau} + 0.037e^{-1.08\tau} - 0.001164e^{-0.057\tau} \qquad (2.10)$$
$$z_5(\tau) = 0.3616e^{-0.0065\tau} - 0.00273e^{-1.08\tau} - 0.17e^{-0.057\tau}.$$

This approximation is plotted in Fig. 9(b) (in the original variables), to be compared with the full simulation in Fig. 9(a). The approximation captures the essential features of the reaction, that is, decay of G_2D, slow growth and decay of GD, and recovery of A. Note that GA, which must be populated, is so at a very low level. The relatives rates $k_{-d2} \ll k_{-1}$ ensures that the transition to A from GA happens very rapidly compared to the recovery from the desensitized state, so GA never has a chance to accumulate.

This approximation is also valid on the longest time scale, which we illustrate in Fig. 10(a) and (b). The recovery of all receptors to the deactivated state occurs on a much longer time scale than that of the paired pulse experiments in question, where the inter-pulse interval is 50 ms.

The additional desensitized state and the relative size of the reaction rates creates a different signalling behavior in AMPAR than NMDAR, namely a significant proportion of the receptor population can be caught in a desensitized state over a much longer time period for AMPAR. With a large pulse of glutamate there is first a spike in the "on" receptor state, but the rebound reaction is preferentially through the pathway of the desensitized states, which recover to the deactivated state at a very slow rate. In the next section we will contrast this with what occurs when a long low profile of glutamate is imposed upon the receptors.

3. Results

3.1. Paired pulse experiments

Synapses in which paired pulse facilitation occurs are thought to possess an increased release probability (through the presence of an elevated level of calcium) and hence an increase in the number of active release sites when a second stimulus closely follows the first. Our linear analysis indicates that synapse-level effects near the stable equilibrium cannot capture the observed behavior in the experiments, since removing the transporters does not, and cannot, change the slower decay rates of the signal. We confirm this with numerical simulations of the paired pulse experiment.

For these, we use the linked kinetic equations for the receptor states, transporter states and glutamate to represent the average behavior in a single synapse (2.5). The concentration of "on" receptors (sum of $[G_2A^*]$ and $[G_2N^*]$), is presumed to be proportional to the observed signal from the field recordings. Since the field recordings are essentially averaging the response over many neurons with many thousands of synapses, we feel that this is a reasonable way to model the data in these sub-threshold experiments (i.e. no action potential is created). Furthermore, we normalize the amplitude of the experimental signal by the peak amplitude of the response to the first stimulation, so the peak amplitude of the second gives the paired pulse ratio directly. The simulation responses are similarly normalized, which makes data fitting and parameter estimation straight-forward, as it removes the constant of proportionality between the concentration of the activated states and the signal.

In paired pulse experiments the brain slice is stimulated twice with an electrical input at one position (in our experiments it is the stratus radium), and the response is measured at another location (the CA1 pyramidal cell dendrites). If the second response is larger than the first (facilitation), the number of activated synapses is presumed to have increased. This effect depends on the length of the time interval between the pulses. The fractional amount of facilitation is used by experimentalists to measure the increase in so-called probability of release of glutamate. An action potential arriving at the presynaptic membrane of a terminal bouton may or may not trigger release of a vesicle of glutamate into the synaptic cleft, hence the probabilistic component. The probability of release in the simulations is controlled by the fraction of activated synapses that release glutamate. We perform simulations of receptors and transporters responding to glutamate release, under varying conditions, corresponding to the different experimental protocols. Glutamate vesicle release is modeled by including a pulse of glutamate concentration to the state equations, as described in the modeling section. Two such increases in glutamate occur 50 ms apart, mimicking the paired pulse stimulation protocol. Initially all the receptors and transporters are in their unbound state.

Since there is a different release probability in response to the first and second pulses, to capture the field response to this stimulation three separate pools of target molecules (each containing AMPAR, NMDAR and transporters) are created. One receives a pulse of glutamate upon the first stimulus only, another upon the second stimulus only, and a third upon both the first and second stimuli. The measured signal is made up of activated receptor concentrations from these pools in fractions that represent the probability of release in each instance. E.g., if the probability of release is p_1 for the first pulse and p_2 for the second pulse (p_1 and

Please cite this article in press as: E. Stone et al., Identifying neurotransmitter spill-over in hippocampal field recordings, Math. Biosci. (2012), http://dx.doi.org/10.1016/j.mbs.2012.07.004

$p_2 \in [0,1]$), and the concentration of activated receptors (both NMDAR and AMPAR) for the three pools is r_1 for first pulse only, r_2 for second pulse only, and r_3 for the receiving both the first and second pulse, the signal would be proportional to $p_1 r_1 + p_1 p_2 r_2 + p_2(1-p_1)r_3$. This is a general expression, in these experiments it is assumed that $r_1 = r_2$.

A control simulation, with initial transporters and receptors in the concentrations listed in Table 2, is shown in Fig. 11. The signal is the sum of the concentrations of activated NMDAR and AMPAR. To correspond to the experimental data, the amplitude of this sum is scaled by the peak response to the first glutamate pulse. The increased amplitude of the response is achieved by increasing p_2. For the control run this increase from the first to the second pulse is roughly twofold. The initial concentrations of free receptors and glutamate are as in Section 2, e.g. the total amount of glutamate released is 1 mM and the rate constant γ is 0.85 ms^{-1}. The total number of transporters is considered to be an order of magnitude larger than that of the receptors. Another important fitting parameter is the linear diffusion coefficient, δ, set at 0.8 (ms^{-1}) for all of the following runs. This corresponds to an almost complete removal of free glutamate in about 5 ms, which, as pointed out in Section 2, is consistent with the work of Clements et al. [5]. The simulation, thus tuned, is compared to the experimental signal in Fig. 11(a).

Next we determine the effect of pharmacologically blocking the transporter molecules. Leaving all other simulation parameters unchanged, the concentration of transporters is set to zero, and the simulation repeated. The resulting signal is shown in Fig. 11(b), compared with the experimental data from a typical run with transporters blocked. From this it is evident that removing the transporters does not create the extended response seen after the second stimulus of the experiment. Recall that it *cannot*, since the slow decay rates occur in an invariant subspace that does not involve the transporters. The structure of the equations, which reflects the fact that the receptors and transporters are linked only through shared glutamate, subdivides the phase space into invariant subspaces associated with each molecule type, plus glutamate. The linear analysis of these subspaces in Section 4 demonstrates that the slowest decay rates occur in directions restricted to the NMDAR-Glutamate subspace, so that the slowest decay is entirely NMDAR dependent. This is consistent with the experimental result that when the NMDAR are blocked by APV, the extended decay after the second stimulation is removed.

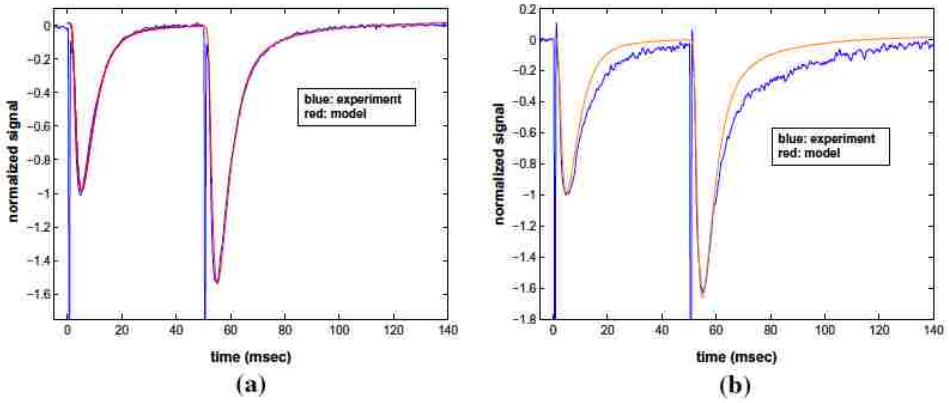

Fig. 11. (a) Control experimental data set overlaid with paired pulse simulation, parameters listed in Tables 1 and 2. (b) Transporters blocked: model run with the same parameters, but with $T(0) = 0.0$.

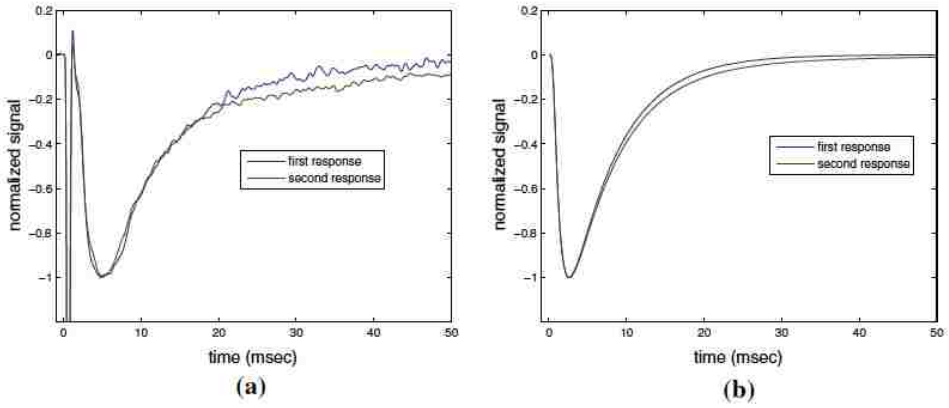

Fig. 12. Overlaid first response and second response, rescaled to same minimum value in order to compare decay rates. (a) Data set from experiment with transporters blocked and (b) model with zero transporter concentration (parameters as in Table 2).

Please cite this article in press as: E. Stone et al., Identifying neurotransmitter spill-over in hippocampal field recordings, Math. Biosci. (2012), http://dx.doi.org/10.1016/j.mbs.2012.07.004

To further highlight this result we plot the first and second pulses overlaid, each rescaled to have a (negative) peak amplitude equal to unity, in order to compare the decay rates. Fig. 12(a) shows the data set, while Fig. 12(b) plots the model simulation results. Removing the transporters in the model clearly does not result in the same prolongation seen in the experiments with the transporters blocked. The inability of this computational model to capture the experimental phenomenon illustrates the theoretical result that simple competition for glutamate between receptors and transporters at or near the synapse cannot be responsible for the prolonged response seen in the experiments.

If a well-mixed population of transporters and receptors and glutamate, presumably within or near a synaptic cleft, cannot reproduce the experimental data, some other mechanism must be responsible. If we believe that the transporters and receptors are linked only through their dependence on shared free glutamate, a non-homogeneous/spatial effect should be invoked to explain the experiment. In the next section we show that the inclusion of a pool of receptors that receives a long low concentration profile of imposed glutamate upon the second stimulus is sufficient to fit the experimental result. This could be caused by leaking glutamate for high release probability events, in other words, spill-over after the second stimulus.

3.2. Numerical results: adding spill-over

In Section 3.1 we showed that simply blocking transporters in the simulations could not duplicate the experimental results, the prolonged decay upon the second pulse was only marginally affected. This confirms the results of our linear analysis in Section 2. However, if the neuronal transporters are blocked and a long low concentration profile of glutamate is then imposed on the receptors, we can demonstrate prolonged decay of the signal upon the second stimulation. The prolonged low concentration profile of glutamate is presumed to be the result of neurotransmitter from other release sites reaching the modeled synapses due to the simultaneous block of glial transporters. The transporters would act to keep this leaking glutamate from reaching other neighboring sites, hence unblocking the transporters turns off the leak. We do not see a sizable increase in the amplitude of the second response when the transporters are blocked, so this leak must affect the receptors in such a way that the fast responding AMPARs (responsible for the large fast peak) do not create a significant signal. This, in turn, is due to the different reaction mechanisms of the two receptors, which make NMDAR much more sensitive to a long low influx of glutamate.

To generate a long low glutamate profile, the solution to the diffusion equation in a domain between by two parallel planes of infinite extent, with no-flux boundary conditions on the planes, e.g.

$$\frac{\partial G}{\partial t} = D\left(\frac{\partial^2 G}{\partial x^2} + \frac{\partial^2 G}{\partial y^2} + \frac{\partial^2 G}{\partial z^2}\right);$$

$$-\infty < x < \infty; \quad -\infty < y < \infty; \quad 0 < z < w; \ \frac{\partial G}{\partial z}(0, w) = 0,$$

is computed. We consider eight sources of diffusing glutamate, located on the corners and the middle of each side of a square on one plane ($z = 0$). The concentration of glutamate is measured at a point in the middle of this square, on the opposing plane ($z = w$). Referring to electron micrograph images of the CA1 region of the hippocampus by Ventura and Harris [35], the spacing between neighboring synapses generally is less than a micron, and the extracellular space itself is on the order of a tenth of a micron. In what follows we vary the spacing between leaking synapse sites, essentially altering the number of synapses that release glutamate after receiving the stimulus. In Fig. 13(a) we illustrate this geometry with the leak sources at a spacing of 6.0 μm, and the width of the gap (w) of 0.1 μm.

This mimics diffusion in a narrow extracellular space, but physiologically it could be convoluted and contain barriers. Following Barbour and Hausser [4], to account for the tortuosity, we adopted an effective diffusion constant, $D = \bar{D}/\lambda^2$, where $\bar{D}$ is the diffusion constant for glutamate in water, and $\lambda > 1$ is the ratio of the average diffusion path compared to unrestricted diffusion, or tortuosity factor. Modeling the extracellular space as a narrow region avoids the complication of adding barriers to diffusion, hence we do not include a volume fraction factor. The solution can be expressed in terms of Fourier Series as

$$G(x, y, z, t) = \frac{Q}{4\pi w D t}\sum_{i=1}^{M} \exp\frac{(x - x_i)^2 + (y - y_i)^2}{4Dt} \times \left(1 + 2\sum_{n=1}^{N} \cos\left(\frac{n\pi z}{w}\right)\cos\left(\frac{n\pi z_i}{w}\right)\exp\left(-\frac{(n\pi)^2 D t}{w^2}\right)\right). \tag{3.1}$$

M is the number of Fourier modes taken in the approximation, N is the number of release sites, x_i, y_i and z_i are the coordinates of the ith

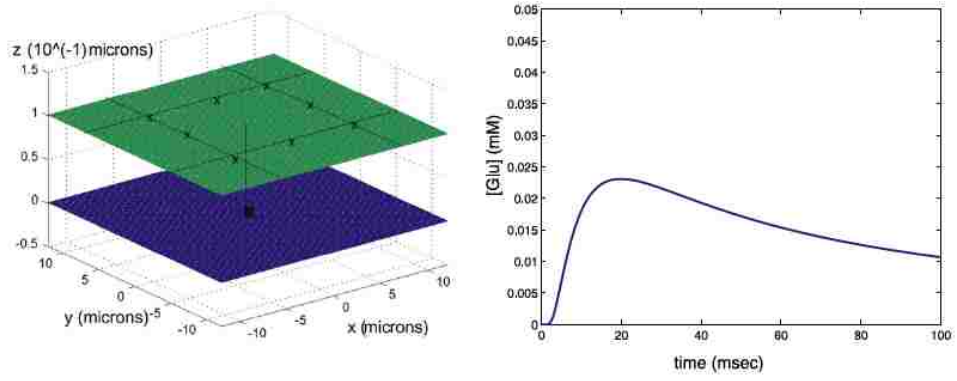

(a) (b)

Fig. 13. (a) Geometrical space of diffusion simulation, x's are leak sites, filled central square is the point at which glutamate concentration is measured. (b) Glutamate concentration at the center point as a function of time.

Please cite this article in press as: E. Stone et al., Identifying neurotransmitter spill-over in hippocampal field recordings, Math. Biosci. (2012), http://dx.doi.org/10.1016/j.mbs.2012.07.004

To further highlight this result we plot the first and second pulses overlaid, each rescaled to have a (negative) peak amplitude equal to unity, in order to compare the decay rates. Fig. 12(a) shows the data set, while Fig. 12(b) plots the model simulation results. Removing the transporters in the model clearly does not result in the same prolongation seen in the experiments with the transporters blocked. The inability of this computational model to capture the experimental phenomenon illustrates the theoretical result that simple competition for glutamate between receptors and transporters at or near the synapse cannot be responsible for the prolonged response seen in the experiments.

If a well-mixed population of transporters and receptors and glutamate, presumably within or near a synaptic cleft, cannot reproduce the experimental data, some other mechanism must be responsible. If we believe that the transporters and receptors are linked only through their dependence on shared free glutamate, a non-homogeneous/spatial effect should be invoked to explain the experiment. In the next section we show that the inclusion of a pool of receptors that receives a long low concentration profile of imposed glutamate upon the second stimulus is sufficient to fit the experimental result. This could be caused by leaking glutamate for high release probability events, in other words, spill-over after the second stimulus.

3.2. Numerical results: adding spill-over

In Section 3.1 we showed that simply blocking transporters in the simulations could not duplicate the experimental results, the prolonged decay upon the second pulse was only marginally affected. This confirms the results of our linear analysis in Section 2. However, if the neuronal transporters are blocked and a long low concentration profile of glutamate is then imposed on the receptors, we can demonstrate prolonged decay of the signal upon the second stimulation. The prolonged low concentration profile of glutamate is presumed to be the result of neurotransmitter from other release sites reaching the modeled synapses due to the simultaneous block of glial transporters. The transporters would act to keep this leaking glutamate from reaching other neighboring sites, hence unblocking the transporters turns off the leak. We do not see a sizable increase in the amplitude of the second response when the transporters are blocked, so this leak must affect the receptors in such a way that the fast responding AMPARs (responsible for the large fast peak) do not create a significant signal. This, in turn, is due to the different reaction mechanisms of the two receptors, which make NMDAR much more sensitive to a long low influx of glutamate.

To generate a long low glutamate profile, the solution to the diffusion equation in a domain between by two parallel planes of infinite extent, with no-flux boundary conditions on the planes, e.g.

$$\frac{\partial G}{\partial t} = D\left(\frac{\partial^2 G}{\partial x^2} + \frac{\partial^2 G}{\partial y^2} + \frac{\partial^2 G}{\partial z^2}\right);$$

$$-\infty < x < \infty; \quad -\infty < y < \infty; \quad 0 < z < w; \ \frac{\partial G}{\partial z}(0, w) = 0,$$

is computed. We consider eight sources of diffusing glutamate, located on the corners and the middle of each side of a square on one plane ($z = 0$). The concentration of glutamate is measured at a point in the middle of this square, on the opposing plane ($z = w$). Referring to electron micrograph images of the CA1 region of the hippocampus by Ventura and Harris [35], the spacing between neighboring synapses generally is less than a micron, and the extracellular space itself is on the order of a tenth of a micron. In what follows we vary the spacing between leaking synapse sites, essentially altering the number of synapses that release glutamate after receiving the stimulus. In Fig. 13(a) we illustrate this geometry with the leak sources at a spacing of 6.0 μm, and the width of the gap (w) of 0.1 μm.

This mimics diffusion in a narrow extracellular space, but physiologically it could be convoluted and contain barriers. Following Barbour and Hausser [4], to account for the tortuosity, we adopted an effective diffusion constant, $D = \bar{D}/\lambda^2$, where $\bar{D}$ is the diffusion constant for glutamate in water, and $\lambda > 1$ is the ratio of the average diffusion path compared to unrestricted diffusion, or tortuosity factor. Modeling the extracellular space as a narrow region avoids the complication of adding barriers to diffusion, hence we do not include a volume fraction factor. The solution can be expressed in terms of Fourier Series as

$$G(x, y, z, t) = \frac{Q}{4\pi w D t}\sum_{i=1}^{M} \exp\frac{(x - x_i)^2 + (y - y_i)^2}{4Dt} \times \left(1 + 2\sum_{n=1}^{N} \cos\left(\frac{n\pi z}{w}\right)\cos\left(\frac{n\pi z_i}{w}\right)\exp\left(-\frac{(n\pi)^2 D t}{w^2}\right)\right). \tag{3.1}$$

M is the number of Fourier modes taken in the approximation, N is the number of release sites, x_i, y_i and z_i are the coordinates of the ith

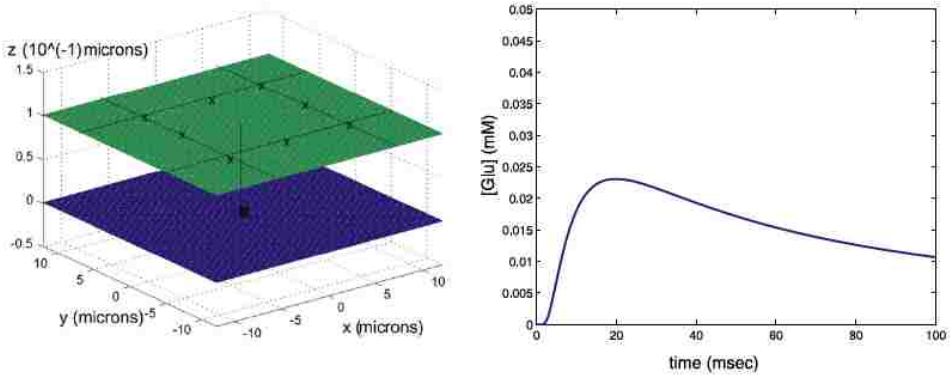

(a) (b)

Fig. 13. (a) Geometrical space of diffusion simulation, x's are leak sites, filled central square is the point at which glutamate concentration is measured. (b) Glutamate concentration at the center point as a function of time.

Please cite this article in press as: E. Stone et al., Identifying neurotransmitter spill-over in hippocampal field recordings, Math. Biosci. (2012), http://dx.doi.org/10.1016/j.mbs.2012.07.004

release site and Q is the number of glutamate molecules leaking out of each release site.

In the synapse simulations in the next section the amount of glutamate leaking from each site ranges between 20 and 50 molecules. The distance between release sites in such a region of the hippocampus will be variable, but is expected to be in the range of single digit microns, depending on how many sites are active during an EPSC. The parameter D is estimated to be less than the diffusion constant for glutamate in free solution of 0.75 [20], around 0.6 $\mu m^{-2}\, s^{-1}$. This follows the results of Cory and Glavinovik [8], who use molecular dynamics simulations to determine how spatial confinement and membrane charges affect the diffusion constants of glutamate in a gap similar to a synaptic cleft. They concluded that the diffusion of glutamate is slower than its free diffusion in water only if the cleft is very narrow (<5 nm). The extracellular space between the two planes is wider than that, hence glutamate diffusion should not be significantly slowed by confinement.

At this point it is necessary to make a comment about the uniqueness of the parameter set used to generate the glutamate profile. The variables of space and time and the diffusion constant in the equation cannot be independently varied, which can be confirmed by simple scaling arguments. Time can be made dimensionless by creating the variable $\bar{t} = \frac{t}{Dl^2}$, where l is a representative length in the problem. Hence a change in D can be compensated for by a reciprocal change in l^2. In the same vein, if the spacing between release sites is increased and the width of the space is decreased in such a way as to keep the distance between the release site and the measurement point the same, the resulting profile will be unaltered. Hence we cannot claim to unambiguously resolve the physical space and diffusion constant required to generate a certain profile of diffusing glutamate, we can only be guided by known physiological constraints on these values.

That said, the concentration of glutamate at the center location as a function of time for the release of 60 molecules is shown in Fig. 13(b). The distance between the release sites is 6.0 μm, the width of the gap is 0.1 μm and the corrected diffusion constant is 0.6. For a more complete picture of the glutamate concentration in space see Fig. 14 where the concentration of glutamate on the plane opposing the leak sites is plotted at $t = 3$ and $t = 10$ ms.

We next examine the response of the receptors to this leaking glutamate profile. In Fig. 15(a) we plot a series of such applied glutamate profiles, the total amount of glutamate ranging between 20 and 50 molecules. The activated (b) AMPAR and (c) NMDAR concentration vs. time, responding to the applied glutamate profiles are also shown. The initial concentration of free NMDAR and AMPAR receptors is 0.03 mM. From these plots it is clear that the NMDAR are preferentially stimulated by long low glutamate profiles, which plays a key role in explaining the experimental results. To understand this further we examine the population of the different states of each receptor exposed to this profile.

3.2.1. AMPAR: effect of leaking glutamate

We analyze the time evolution of the AMPAR states in Fig. 16(b) by decomposing the reaction into phases. The fastest nonlinear phase of the response is missing, because the concentration of glutamate initially is very low. Since glutamate binding proceeds more slowly, as GA is formed the conversion to GD can compete effectively with the formation of G_2A. The back reaction from GDA to GA occurs at a much slower rate than the forward reaction, and GDA accumulates. GDA can also add glutamate to become G_2DA, further tying up the receptor in desensitized states. Subsequently a much smaller amount of G_2A and G_2A^* is created. This is illustrated in the time course of the reaction, where the states with the smallest concentrations are G_2A and G_2A^*. Note also that the imposed glutamate profile is not sufficient to saturate the receptor, a large fraction remains in an unbound state.

To compare this quantitatively to the response of the NMDAR we analyze the reaction dynamics when a constant concentration of glutamate is added at a level much less than that of the concentration of receptors. Hence we begin with the equations for the receptor states (2.5), and set $[G] = G_0 < A_0$ arriving at

$$\begin{aligned}
\frac{d[GA]}{dt} &= k_1 G_0([A](0) - ([GA] + [GDA] + [G_2A] + [G_2DA] + [G_2A^*])) \\
&\quad - k_{-1}[GA] - k_2 G_0[GA] + k_{-2}[G_2A] - k_{d2}[GA] + k_{-d2}[GDA] \\
\frac{d[G_2A]}{dt} &= k_2 G_0[GA] - k_{-2}[G_2A] - k_{d1}[G_2A] + k_{-d1}[G_2DA] + \alpha[G_2A^*] - \beta[G_2A] \\
\frac{d[G_2A^*]}{dt} &= -\alpha[G_2A^*] + \beta[G_2A] \\
\frac{d[G_2DA]}{dt} &= k_{d1}[G_2A] - k_{-d1}[G_2DA] + k_3 G_0[GDA] - k_{-3}[G_2DA] \\
\frac{d[GDA]}{dt} &= k_{d2}[GA] - k_{-d2}[GDA] - k_3 G_0[GDA] + k_{-3}[G_2DA].
\end{aligned}$$

The forward reaction from A to GA now proceeds much more slowly than the back reaction, since the rate is $k_1 G_0$, and if $G_0 < A_0$, $k_1 G_0 < 8 \times 0.0265 = 0.212\ ms^{-1}$ while $k_{-1} = 2\ ms^{-1}$. Also, the rate from $[GA]$ to $[GDA]$, $k_{d2} = 0.16\ ms^{-1}$, now competes effectively with the rate that takes $[GA]$ to $[G_2A]$, which is less than $4 \times 0.0265 = 0.106\ ms^{-1}$, hence the accumulation in the desensitized state. To

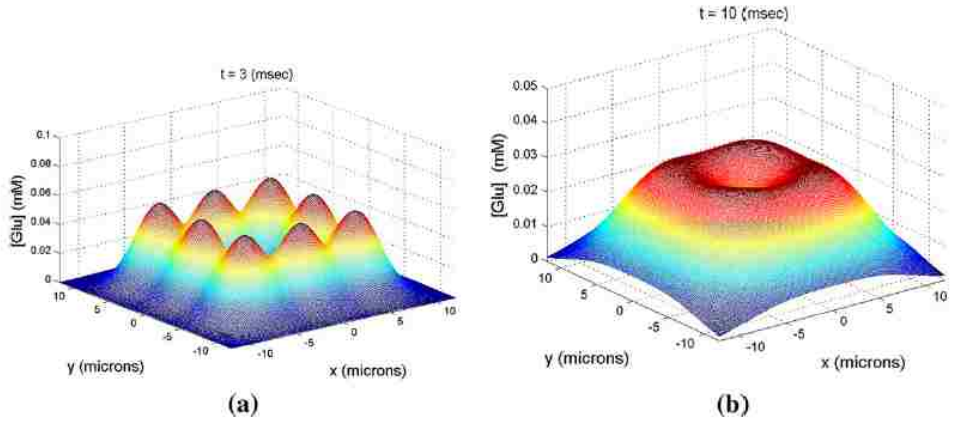

(a) (b)

Fig. 14. Concentration of glutamate on the plane opposing the leak sites ($z = w$), (a) $t = 3$ ms and (b) $t = 10$ ms.

Please cite this article in press as: E. Stone et al., Identifying neurotransmitter spill-over in hippocampal field recordings, Math. Biosci. (2012), http://dx.doi.org/10.1016/j.mbs.2012.07.004

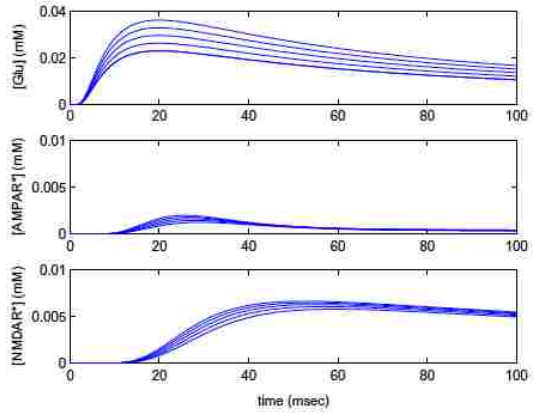

Fig. 15. Varying intensity of leaking glutamate. (a) Profile of applied glutamate concentration, varying total amount, (b) corresponding activated AMPAR concentration [AMPAR*] vs. time, and (c) corresponding activated NMDAR concentration [NMDAR*] vs. time.

quantify how these rates determine which state "wins" this competition, we compute the fixed point for the above set of ODEs analytically. The symbolic expression is intractable, so we present it evaluated with physiological parameter values and $G_0 = 0.01$: $[A] = 0.6118A_0$, $[GA] = 0.0244A_0$, $[G_2A] = 0.0003A_0$, $[G_2A^*] = 0.0007A_0$, $[GDA] = 0.2694A_0$, $[G_2DA] = 0.0932A_0$. From this it is clear that $[A]$, $[GDA]$, and $[G_2DA]$ dominate, and the concentration of "on" receptors is several orders of magnitude lower. This result is reflected in the relative sizes of the states in the simulation shown in Fig. 16(a). The low concentration of glutamate drives the receptor into desensitized states at a greater rate than it turns it "on".

3.2.2. NMDAR: effect of leaking glutamate

Next we take up the response of NMDAR to the same long low profile of glutamate. Since NMDAR is postulated to become desensitized only when two molecules of glutamate are bound, there is no initial accumulation of a desensitized state. Thus the dynamics of NMDAR very different from that of AMPAR. In the simulation shown in Fig. 16(c) we see an initial growth of GN and G_2N, followed by a shift to G_2N^* and finally an accumulation of G_2DN. The peak concentration of G_2N^* is a factor of 10 greater than that of G_2A^* in the same experiment, and it persists over the duration of the simulation.

Taking the reaction equations for NMDAR in (2.5) with $[G] = G_0$ a constant, the resulting linear system is reduced from five to four equations.

$$\frac{d[GN]}{dt} = l_1 G_0(N_0 - ([GN] + [G_2N] + [G_2DN] + [G_2N^*])) - l_{-1}[GN] - l_2 G_0[GN] + l_{-2}[G_2N]$$

$$\frac{d[G_2N]}{dt} = l_2 G_0[GN] - l_{-2}[G_2N] - l_d[G_2N] + l_{-d}[G_2DN] + a[G_2N^*] - b[G_2N]$$

$$\frac{d[G_2N^*]}{dt} = -a[G_2N^*] + b[G_2N]$$

$$\frac{d[G_2DN]}{dt} = l_d[G_2N] - l_{-d}[G_2DN]$$

The fixed point for the above set of ODEs is computed analytically and again the symbolic expression is intractable, so we present it evaluated with physiological parameter values, and $G_0 = 0.01$ mM: $[N] = 0.0016N_0$, $[GN] = 0.03N_0$, $[G_2N] = 0.16N_0$, $[G_2N^*] = 0.08N_0$, $[G_2DN] = 0.73N_0$. In this case the forward reaction rates are such that very little $[N]$ and $[GN]$ remain, and because a is half b, $[G_2N^*]$ is roughly half $[G_2N]$. Both are much smaller than $[G_2DN]$, but still two orders of magnitude larger than the steady state AMPAR "on" concentration. However, for NMDAR the fixed point is approached over the time scale of hundreds of milliseconds, and because the imposed glutamate profile is effectively zero after 50 ms, this fixed point is not evident in the paired pulse simulation. Instead, see Fig. 17 where we show a simulation with constant glutamate concentration over 1000 ms and 100 ms, under similar conditions to those in Fig. 16(b).

3.2.3. Fitting the paired pulse data

We next repeat the paired pulse simulations including a diffusing glutamate component. This is administered to receptors upon

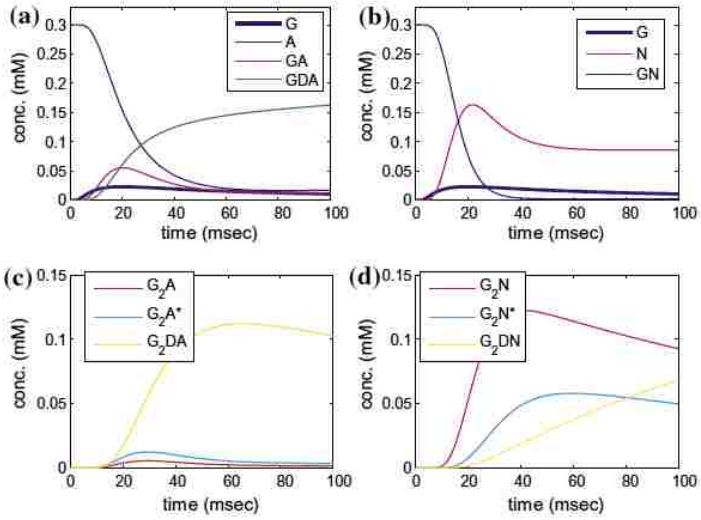

Fig. 16. Receptor states upon stimulation with a prolonged low concentration of glutamate. (a, c) AMPAR states and (b, d) NMDAR states. The AMPAR 'on' concentration is an order of magnitude less than NMDAR 'on' concentration for the same total receptor concentration and imposed glutamate profile.

Please cite this article in press as: E. Stone et al., Identifying neurotransmitter spill-over in hippocampal field recordings, Math. Biosci. (2012), http://dx.doi.org/10.1016/j.mbs.2012.07.004

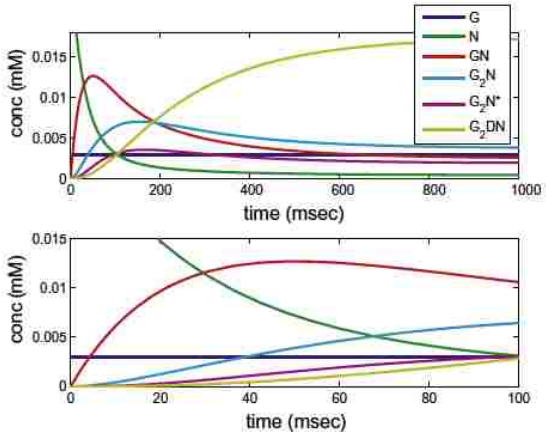

Fig. 17. Simulation of NMDAR reaction with an imposed constant concentration of glutamate, over long time (1000 ms, top) and shorter time (100 ms, bottom).

the second pulse, mimicking spill-over to adjacent sites for high release probability events. The simulation has three more pools of receptors: one that receives leaking glutamate upon the first pulse, one that receives leaking glutamate upon the second pulse, but no direct glutamate release upon the first pulse, and one that is activated upon the first pulse, and then receives a leak upon the second pulse. It is assumed the effect of the leaking glutamate upon sites that simultaneously receive a direct pulse is small enough to be neglected. The fraction of the signal made up from these pools is related to the probability of release, and an additional scaling factor that represents the relative size of these pools compared to those encountering a direct release of glutamate.

Four data sets are fitted: control, transporters blocked with L-TBA, NMDAR blocked with APV, and both transporters and NMDAR blocked (L-TBA+APV). We use the kinetic parameters for the receptors from before. The common parameters for all four data sets are summarized in Table 5.

The initial transporter concentration is set to 0.0 mM for the cases with L-TBA applied, and the initial free NMDAR concentration is set to 0.0 mM when APV is applied. The proportion of receptors receiving a leaking component of glutamate varies between the first and second pulse. Denoting the proportion for the first pulse as γ_1, and the second pulse as γ_2, Table 6 shows the values used in fitting the four experiments. These were determined by a combination of hand identification of potential ranges of parameters, and the nonlinear fitting program *lsqnonlin*, in Matlab.

With these parameter choices the data can be very closely fit, as seen in Fig. 18. Note that some leaking glutamate is also present upon the first pulse. This result is meant as a proof of principle: glutamate diffusing from other sites *could* be responsible for the prolongation of the response to the second pulse. We cannot say precisely what time course of glutamate would be necessary for this, since the response is tuned by the exact receptor parameters, and the diffusion constant for glutamate. Furthermore, we cannot say what exact geometry of the release sites is necessary to create a given time course. There an infinitude of configurations that could create a single time course. For instance, if the width of the space is decreased, the spacing between sites can be increased to compensate, or the number of molecules or number of sites could be decreased, resulting in the same profile of glutamate seen at the central site. However, the parameters we have chosen are physiologically reasonable, so it is plausible that glutamate released from adjacent sites and diffusing to other synapses or extra-synaptic

Table 5
Common parameters used in fit for all data sets.

Parameter name	Value
Concentration of AMPAR	0.0265 mM
Total concentration of Glu released directly	1.0 mM
Rate constant for direct release of Glu	0.85 ms^{-1}
Probability of release for first pulse	0.2
probability of release for second pulse	0.36–0.38
Distance of release grid	6.0 μm
w	0.1 μm
D/λ^2	0.6
Q	60

Table 6
Fitted parameter values for the four experiments.

Experiment	$T(0)$	$N(0)$	γ_1	γ_2
Control	0.1	0.003	0.0	0.0
APV	0.1	0.0	0.0	0.0
L-TBA	0.0	0.003	0.12	0.3
L-TBA+APV	0.0	0.0	0.12	0.3

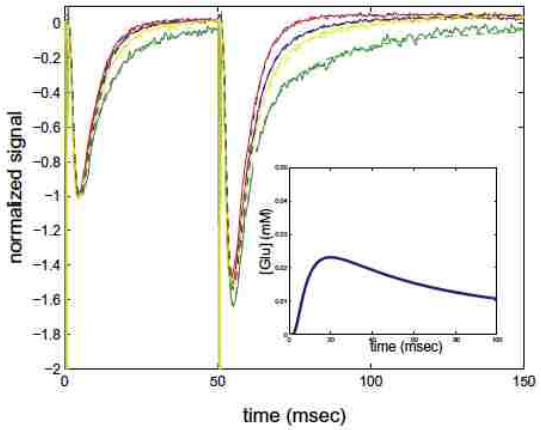

Fig. 18. Paired pulse experiment compared with simulation in four cases: with transporters blocked by BA (green, model-dashed), and NMDAR blocked by APV (red, model-dashed), transporters blocked by BA and NMDAR blocked by APV (yellow, model-dashed), and control (blue, model-dashed). The imposed glutamate concentration profile shown as an inset on the second response with a solid blue line. Details of the simulation runs can be found in the text. (For interpretation of the references to color in this figure legend, the reader is referred to the web version of this article.)

receptors, could be occurring in these experiments. Our mathematical analysis demonstrates that dynamics at the local synaptic level only *cannot* be responsible, and something else (such as "leaking glutamate") is required.

4. Discussion

While the existence of neurotransmitter spill-over at different synapses in the central nervous system is taken for a fact [1,4,7,11–13], the experimental evidence for it is generally indirect. A prolonged response to a sequence of stimuli in subthreshold electrophysiological experiments is one such indirect indicator of spill-over. An example of more direct evidence is the recent work of Okubo et al. [24], where fluorescent markers for glutamate have been developed and used in experiments on cultured neurons, in

Please cite this article in press as: E. Stone et al., Identifying neurotransmitter spill-over in hippocampal field recordings, Math. Biosci. (2012), http://dx.doi.org/10.1016/j.mbs.2012.07.004

slice preparations, and in vivo. However, because the kinetics of the marker are slow, deconvolution is required to resolve the signal, and the time course of glutamate in the extracellular regions cannot be precisely resolved. Furthermore, the marker is not evident within the synapse itself.

Using an average synapse model, we tested the assumption that a prolonged response to a second pulse in a paired pulse experiment is a hallmark of glutamate spill-over. The data being field potential measurements, average the electrical activity of many cells and many thousands of synapses. The paired pulse protocol is given repeatedly (on the order of 20 times) on a single slice, and the traces are averaged. The experiment is then repeated with several slices (4–8), and those results are also averaged. It is because of this averaging that the data are comparatively smooth, and we feel justified in using an average synapse representation of the dynamics. There is obviously a stochastic component to the process, which is represented by the probability of release of vesicles at an individual synapse. Hence we invoke different pools of synapses in creating the signal, e.g., those that have released glutamate only once or twice during a paired pulse stimulation.

Through analysis of the components in the average synapse model, we show that the phenomena observed cannot be explained by a local mechanism. Linear analysis of the fixed point to which the dynamics decays establishes that the addition or removal of local (synaptic) transporters cannot effect the decay rate on the longest time scales, hence the prolongation of the response upon the second stimulus cannot be due to the inactivity of transporters located within or very near the synapse. Recently, the density of neuronal transporters has been shown to be quite low, [10], which is consistent with the analysis. However, a secondary source of glutamate, potentially from spill-over from adjacent synapses, that is limited by extra-synaptic transporters, can account for the prolongation. Nonlinear analysis of the receptor reaction mechanisms demonstrates why the peak response remains unchanged upon transporter blockage, and highlights the importance of the AMPAR's second desensitized state, and relative reaction rates, in its signalling signature.

Because the linear analysis sets the basis for our assertion that this experiment must be explained by something other than local effects, we have not carried out extensive parameter sensitivity testing for our model. Certainly there are more than one parameter set that fit the data as presented, both at the receptor level, and the model of the paired pulse experiment and glutamate spill-over. In particular, we make no claims of being able to deconvolve the glutamate profile in spill-over, this is clearly not a well-posed problem. However, the results of the diffusion model do not contradict other direct measurements of spill-over, see for instance [15]. The glutamate profile interacts non-trivially with the receptor dynamics, which emphasizes the importance of having the two types of receptors to shape the temporal response at these synapses.

The relative simplicity of the model allows to us understand the dynamic effect of removing or adding components in a structured way. We conclude that, consistent with the results in [31], non-local glial transporters are primarily responsible for limiting spill-over of synaptically released glutamate, and we establish mathematically that a model of co-localized transporters and receptors (as would be the case with neuronal transporters) cannot reproduce the paired pulse experimental results with L-TBA.

5. Conclusion

The study of the action of neurotransmitter in and around the synaptic cleft of neurons in the central nervous system is crucial to the understanding of brain function and neuronal organization. Elucidating how the levels of glutamate are regulated in the extracellular space is central to the study of both glutamate-mediated neuronal signaling and glutamate-mediated neuropathology. Cellular transporters rapidly translocate extracellular glutamate into neurons and glia, contributing to signal termination, and the maintenance of sub-pathological levels of glutamate. An interplay between dynamics of receptors that signal the presence of glutamate, and the glutamate transporters, determines both the spatial and temporal signalling characteristics of neurons.

Prolongation of decay rates of synaptic currents and potentials are often seen as hallmarks of spill-over of neurotransmitter, especially in the case where transporters that remove excess neurotransmitter are disabled or blocked. This implies that a spatial component is necessary to explain the result, and that cross-talk between synapses is at work. But are there alternative explanations of the experimental results that cannot be ruled out? For instance, could direct competition for glutamate between receptors and transporters in or near the synapse be responsible for the result, without invoking any sort of spatially extended spill-over of neurotransmitter? The transporters are clearly shaping the response of the neurons in conditions of increased probability of glutamate release, but is it through the re-uptake of diffusing glutamate, or the fast buffering and removal of glutamate within the synaptic cleft?

The paired pulse experiment that we study, with its controls, outlines a clear modeling pathway for testing the spill-over hypothesis. In this paper we determine what aspects of the simplest mathematical model are required to explain the experimental results. In the process we show that simple competition for glutamate between receptors and transporters is not consistent with these results, and that an additional factor is required. Modeling spill-over as a prolonged glutamate concentration profile, we are able to fit the experimental data in control, with transporters and NMDAR pharmacologically blocked, in way that is not possible with simple pulses of glutamate that mimic vesicular release at each synapse. We establish analytically that homo-synaptic processes cannot account for the observed receptor behavior, and postulate a probable mechanism for the observed results. Moreover, the result hinges on the different reaction mechanisms employed by the AMPAR and NMDAR receptors. The two reaction mechanisms allow for the differentiation of a single spike in neurotransmitter concentration from an extended low concentration profile, characteristic of inter-synaptic spill-over.

Acknowledgements

E.S. would like to acknowledge the support of NSF-DMS-IGMS number 0621830. This project was supported by NIH grants numbered P20RR015583 and R01 NS033270.

References

[1] N. Arnth-Jensen, D. Jabaudon, M. Scanziani, Cooperation between independent hippocampal synapses is controlled by glutamate uptake, Nat. Neurosci. 5 (2002) 325.
[2] D. Attwell, A. Gibb, Neuroenergetics and the kinetic design of excitatory synapses, Nat. Rev. 6 (2005) 841.
[3] F. Asztely, G. Erdemli, D.M. Kullmann, Extrasynaptic glutamate spillover in the hippocampus: dependence on temperature and the role of active glutamate uptake, Neuron 18 (1997) 281.
[4] B. Barbour, M. Hausser, Intersynaptic diffusion of neurotransmitter, TINS 20 (9) (1997) 377.
[5] J.D. Clements, R.A. Lester, G. Tong, C.S. Jahr, G.L. Westbrook, The time course of glutamate in the synaptic cleft, Science 258 (5087) (1992) 1498.
[6] J.D. Clements, Transmitter timecourse in the synaptic cleft: its role in central synaptic function, TINS 19 (1996) 163.
[7] J. Coggan, T. Bartol, E. Esquenazi, J. Stiles, S. Lamont, M. Martone, D. Berg, M. Ellisman, T. Sejnowski, Evidence for ectopic neurotransmission at a neuronal synapse, Science 309 (5733) (2005) 446.
[8] S.M. Cory, M.I. Glavinovik, Molecular dynamics simulations of glutamate diffusion in synaptic cleft, Crit. Rev. Neurobiol. 18 (2006) 61.
[9] N.C. Danbolt, Glutamate uptake, Prog. Neurobiol. 65 (1) (2001) 1.

Please cite this article in press as: E. Stone et al., Identifying neurotransmitter spill-over in hippocampal field recordings, Math. Biosci. (2012), http://dx.doi.org/10.1016/j.mbs.2012.07.004

[10] S. Holmseth, Y. Dehnes, Y. Huang, B. Follin-Arbelet, N. Grutle, M. Mylonakou, C. Paches, Y. Zhou, D. Furness, D. Bergles, K. Lehre, N. Danbolt, The density of EAAC1 (EAAT3) glutamate transporters expressed by neurons in the mammalian CNS, J. Neurosci. 32 (2012) 6000.
[11] J. Diamond, Neuronal glutamate transporters limit activation of NMDA receptors by neurotransmitter spillover on CA1 pyramidal cells, J. Neurosci. 21 (2001) 8328.
[12] J. Diamond, A broad view of glutamate spillover, Nat. Neurosci. 5 (2002) 291.
[13] D. DiGregorio, Z. Nusser, R. Silver, Spillover of glutamate onto synaptic AMPA receptors enhnaces fast transmission at a cerebellar synapse, Neuron 35 (2002) 521.
[14] H. Hartzell, S. Kuffler, D. Yoshikami, Post-synaptic potentiation: interaction between quanta of acetylcholine at the skeletal neuromuscular synapse, J. Physiol. 251 (1975) 427.
[15] S. Hires, Z. Yongling, R. Tsien, Optical measurement of synaptic glutamate spillover and reuptake by linker optimized glutamate-sensitive fluorescent reporters, PNAS 105 (11) (2008) 4411.
[16] J.S. Isaacson, J.M. Solis, R.A. Nicol, Local and diffuse synaptic actions of GABA in the hippocampus, Neuron 10 (1993) 165.
[17] P. Jonas, G. Major, B. Sakmann, Quantal components of unitary EPSCs at the mossy fibre synapse on CA3 pyramidal cells of rat hippocampus, J. Physiol. 472 (1993) 615.
[18] D. Kullman, F. Asztely, Extrasynaptic glutamate spillover in the hippocampus: evidence and implications, TINS 21 (1) (1998) 8.
[19] I. Llano, A. Marty, C.M. Armstrong, A. Konnerth, Synaptic- and agonist-induced excitatory currents of Purkinje cells in rat cerebellar slices, J. Physiol. 434 (1991) 183.
[20] L.G. Longsworth, Diffusion measurements, at 25, of aqueous solutions of amino acids, peptides and sugars, J. Am. Chem. Soc. 75 (1958) 5705.
[21] N.A. Lozovaya, M.V. Kopanitsa, V.A. Boychuk, O.A. Krishtal, Enhancement of glutamate release uncovers spillover-mediated transmission by N-methyl-D-aspartate receptors in the rat hippocampus, J. Neurosci. 91 (1999) 1321.
[22] K. Magleby, D. Terrar, Factors affecting the time course of decay of end-plate currents: a possible cooperative action of acetylcholine on receptors at the frog neuromuscular junction, J. Physiol. 244 (1975) 467.
[23] C. Mitchell, S. Feng, R. Lee, An analysis of glutamate spillover on the N-methyl-D-aspartate receptors at the cerebellar glomerulus, J. Neural Eng. 4 (2007) 276.
[24] Y. Okubo, H. Sekiya, S. Namiki, H. Sakamoto, S. Iinuma, M. Yamaksaki, M. Watanabe, K. Hirose, M. Iino, Imaging extrasynaptic glutamate dynamics in the brain, Proc. Nat. Acad. Sci. USA 107 (2010) 6526.
[25] Y. Okubo, M. Iino, Visualization of glutamate as a volume transmitter, J. Physiol. 589 (3) (2011) 481.
[26] T. Otis, M. Kavanaugh, Isolation of current components and partial reaction cycles in the glial glutamate transporter EAAT2, J. Neurosci. 20 (2000) 2749.
[27] D.J. Perkel, S. Hestrin, P. Sah, R.A. Nicoll, Excitatory synaptic currents in Purkinje cells, Proc. Roy. Soc. Ser. B 241 (1990) 116.
[28] N. Riveros, J. Fiedler, N. Lagos, C. Munoz, F. Orrego, Glutamate in rat brain cortex synaptic vesicles: influence of the vesicle isolation procedure, Brain Res. 386 (1986) 405.
[29] D. Rusakov, D. Kullman, Extrasynaptic glutamate diffusion in the hippocampus: ultrastructural constraints, uptake, and receptor activation, J. Neurosci. 18 (1998) 3158.
[30] A. Scimemi, H. Tian, J. Diamond, Neuronal transporters regulate glutamate clearance, NMDA receptor activation, and synaptic plasticity in the hippocampus, J. Neurosci. 29 (2009) 14581.
[31] W. Sun, K. Hoffman, D. Holley, M. Kavanaugh, Specificity and actions of an arylaspartate inhibitor of glutamate transport at the Schaffer collateral-CA1 pyramidal cell synapse, PLoS ONE 6 (2011) e23765.
[32] G. Szapiro, B. Barbour, Multiple climbing fibers signal to molecular layer interneurons exclusively via glutamate spillover, Nat. Neurosci. 10 (2007) 735.
[33] S. Tsukada, M. Lino, Y. Takayasu, K. Shimamoto, S. Ozawa, Effects of a novel glutamate transporter blocker, (2S, 3S)-3-3-4-trifluoromethyl-benzoylamino-benzyloxy-aspartate (TFB-TBOA), on activities of hippocampal neurons, Neuropharmacology 48 (2005) 479.
[34] A. Tzingounis, J. Wadiche, Glutamate transporters: confining runaway excitation by shaping synaptic transmission, Nat. Rev. Neurosci. 8 (2007) 935.
[35] R. Ventura, K. Harris, Three-dimensional relationships between hippocampal synapses and astrocytes, J. Neurosci. 19 (1999) 6897.
[36] F. Ventriglia, V. Di Maio, A Brownian simulation model of glutamate synaptic diffusion in the femtosecond time scale, Biol. Cybern. 83 (2000) 93.
[37] K.E. Vogt, R.A. Nicoll, Glutamate and gamma-aminobutyric acid mediate a heterosynaptic depression at mossy fiber synapses in the hippocampus, Proc. Nat. Acad. Sci. 96 (1999) 1118.
[38] N. Zerangue, M.P. Kavanaugh, Flux coupling in a neuronal glutamate transporter, Nature 383 (6601) (1996) 634.
[39] K. Zheng, A. Scimemi, D. Rusakov, Receptor actions of synaptically released glutamate: the role of transporters on the scale from nanometers to microns, Biophys. J. 95 (2008) 4584.

Please cite this article in press as: E. Stone et al., Identifying neurotransmitter spill-over in hippocampal field recordings, Math. Biosci. (2012), http://dx.doi.org/10.1016/j.mbs.2012.07.004

Chapter 6: Conclusions

Glutamate is the major excitatory neurotransmitter in the brain and mediates a majority of the excitatory synaptic transmission that is required for processes like learning and memory. The concentration of glutamate in the brain is tightly regulated by glutamate transporters. In these studies, I employed several methods to alter the concentration profile of synaptically released glutamate and increasing spillover.

First, I began by characterizing the novel transport blocker L-TBA (Esslinger et al., 2005). The data presented demonstrate that L-TBA has an increased selectivity for glutamate transporters over ionotropic glutamate receptors expressed on pyramidal neurons, as it neither antagonized nor activated ionotropic glutamate receptor responses to equimolar glutamate concentrations (Figure 1.2). The time course and activation of NMDARs during transport block mediated by L-TBA was also mathematically validated. It is important to note that past work generally examined the effect of transporter block on EPSCs elicited under conditions where NMDAR activity is enabled (i.e. depolarized membrane potentials or in Mg^{2+}-free solution), yet these studies focused on more physiologically relevant conditions where magnesium block of the NMDA receptor was intact. We found that EAAT inhibition significantly prolonged EPSCs recorded at the Schaffer-CA1 pyramidal cell synapse in Mg^{2+}-free conditions due to enhanced NMDAR signaling. However, L-TBA had no effect on postsynaptic responses in voltage clamp conditions with NMDARs blocked by physiological [Mg^{2+}]. Because voltage-dependent Mg^{2+} block of NMDARs is dynamic during synaptic transmission, gaining greater insight into the role of glutamate transport in modulating synaptic activity required the use of selective transport blockers in physiological conditions without voltage clamp, which we accomplished by recording fEPSPs.

We addressed this issue and have shown that NMDAR-mediated components of fEPSPs can be isolated that are dependent on glutamate transporter activity in a frequency-dependent manner (Figure 1.5). NMDAR-mediated signaling is primarily limited by voltage-dependent Mg^{2+} block during low-frequency activity, while the relative contribution of glutamate

transporters increases during short bursts of higher frequency signaling. The effect of L-TBA on the kinetics of fEPSPs elicited by low-frequency stimulation in physiological Mg^{2+} was increased during brief bursts of higher frequency synaptic activity, and this prolongation was blocked by the NMDAR antagonist APV. This effect was not likely to be due simply to frequency-facilitation of transmitter release because increasing stimulus strength did not affect the kinetics of fEPSPs elicited by low frequency stimulation.

We also observed a frequency dependent facilitation of NMDARs that occurred only in the presence of Mg^{2+} and followed a decay time constant similar to the unbinding rate of glutamate to an outside out patch. Therefore, we believe a pool of glutamate-bound and Mg^{2+}-blocked NMDARs signal in a phase-shifted manner during repetitive synaptic activity at frequencies governed by NMDAR channel desensitization and glutamate unbinding. This work suggests a potential mechanism contributing to theta frequency-dependent associative LTP.

REFERENCES (cont.)

Arai, A., and Lynch, G. (1998) AMPA receptor desensitization modulates synaptic responses induced by repetitive afferent stimulation in hippocampal slices. Brain Research. 799: 235-242.

Arnth-Jensen N, Jabaudon D, Scanziani M (2002) Cooperation between independent hippocampal synapses is controlled by glutamate uptake. Nat. Neuroscience. 5:325-331

Asztely F, Erdemli G, Kullmann DM (1997) Extrasynaptic glutamate spillover in the hippocampus: dependence on temperature and the role of active glutamate uptake. Neuron 18:281-293

Attwell, D., Gibb, A. (2005) Neuroenergetics and the kinetic design of excitatory synapses. Nature reviews neuroscience. 6: 841-849.

Bailey, C., Giustetto, M., Haung, Y., Hawkins, R., Kandel, E. (2000) Is heterosynaptic modulation essential for stabilizing hebbian plasticity and memory. Nature review neuroscience. 1:11-20.

Bartlett, T.E., Bannister, N.J., Collett, V.J., Dargan, S.L., Massey, P.V., Bortolotto, Z.A., Fitzjohn, S.M., Bashir, Z.I., Collingridge, G.L., Lodge, D. (2007) Differential roles of NR2A and NR2B-containing NMDA receptors in LTP and LTD in the CA1 region of two-week old rat hippocampus. Neuropharmacology. 51(1):60-70.

Bert, PM, O'Shea, RD. (2007) Transports for L-glutamate: An update on their molecular pharmacology and pathological involvement. British Journal of Pharmacology. 150. 5-17.

Bergles DE, Jahr CE (1997) Synaptic activation of glutamate transporters in hippocampal astrocytes. Neuron 19:1297-1308

Bergles DE, Jahr CE (1998) Glial contribution to glutamate uptake at Schaffer collateral-commissural synapses in the hippocampus. J Neuroscience. 18:7709-16
21.

Bendahan A, Armon A, Madani N, Kavanaugh MP, Kanner BI (2000) Arginine 447 plays a pivotal role in substrate interactions in a neuronal glutamate transporter. J Biol Chem 275:37436-42

Bliss, T.V.P, and G.L. Collinridge. (1993) A synaptic model of memory: long term potentiation in the hippocampus. Nature. 361: 31-39.

Boudker O, Ryan RM, Yernool D, Shimamoto K, Gouaux E (2007) Coupling substrate and ion binding to extracellular gate of a sodium-dependent aspartate transporter. Nature 445:387-93

Buzsáki G (2002) Theta oscillations in the hippocampus. Neuron 33:325-340

Christie JM, Jahr CE (2006) Multivesicular release at Schaffer collateral-CA1 hippocampal synapses. J Neuroscience. 26:210-6

Collingridge GL, Herron CE, Lester RA (1988) Frequency-dependent N-methyl-D-aspartate receptor-mediated synaptic transmission in rat hippocampus. J. Physiology. (Lond.) 399:301-312

Danbolt, N.C. (2001) Glutamate uptake. Progress in neurobiology. 65(1): 1-105.

Diamond JS (2001) Neuronal glutamate transporters limit activation of NMDA receptors by neurotransmitter spillover on CA1 pyramidal cells. J. Neuroscience. 21:8328-8338

Diamond, J.S. and Jahr, C.E. (1995) Asynchronous release of synaptic vesicles determines the time course of the AMPA receptor-mediated EPSC. Neuron. 15(5):1097-1107.

Debanne, D., Guerineau, N.C., Gahwiler, B.H., and Thompson, S.M. (1996) Paired-pulse facilitation and depression at unitary synapses in rat hippocampus: quantal fluctuation effects subsequent release. Journal of physiology. 492:163-176.

Dobrunz, L.E., and C.F. Stevens. (1997) Heterogeneity of release probability, facilitation, and depletion at central synapses. Neuron. 18:995-1008.

Esslinger CS, Agarwal S, Gerdes J, Wilson PA, Davis ES, Awes AN, O'Brien E, Mavencamp T, Koch HP, Poulsen DJ, Rhoderick JF, Chamberlin AR, Kavanaugh MP, Bridges RJ (2005) The substituted aspartate analogue L-beta-threo-benzyl-aspartate preferentially inhibits the neuronal excitatory amino acid transporter EAAT3. Neuropharmacology 49:850-61

Furuta A, Rothstein JD, Martin LJ (1997) Glutamate transporter protein subtypes are expressed differentially during rat CNS development. J. Neuroscience. 17:8363-8375

Gersdorff, H. (2005) Glutamate transporter studies reveal the pruning off metabotropic glutamate receptors and absence of AMPA receptor desensitization at mature calyx of held synapses. Journal of neuroscience. 25(37):8482-97.

Hebb, D.O. (1949) The organization of behavior: a neuropsychological theory. Wiley, New York.

Herron CE, Lester RA, Coan EJ, Collingridge GL (1986) Frequency-dependent involvement of NMDA receptors in the hippocampus: a novel synaptic mechanism. Nature 322:265-268

Herman, M.A. and Jahr, C.E. (2007) Extracellular glutamate concentration in hippocampal slice. Journal of Neuroscience, 27(36):9736-9741.

Hjelmstad, G.O., Isaac, J.T., Nicoll, R.A., and R.C. Malenka. (1999) Lack of AMPA Receptor Desensitization During Basal Synaptic Transmission in the Hippocampal Slice. Journal of Neurophysiology. 81:3096-3099.

Huang, F., Meng, K., and Tang, J. (2007) Properties of paired-pulse firing thresholds and the relationship with paired-pulse plasticity in hippocampal CA3-CA1 synapses. European Journal of Neuroscience. 25:3253-3263.

Holley DC, Kavanaugh MP (2009) Interactions of alkali cations with glutamate transporters. Philos Trans R Soc Lond B Biol Sci 364:155-61

Isaacson JS, Nicoll RA (1993) The uptake inhibitor L-trans-PDC enhances responses to glutamate but fails to alter the kinetics of excitatory synaptic currents in the hippocampus. J Neurophysiol 70:2187-91

Isaacson, J.S., Nicoll, R.A. (1991) Aniracetam reduces glutamate receptor desensitization and slows the fast excitatory syanptic currents in the hippocampus. Proc. Natl. Acad. Sci. 88:10936-10940.

Jabaudon D, Shimamoto K, Yasuda-Kamatani Y, Scanziani M, Gähwiler BH, Gerber U (1999) Inhibition of uptake unmasks rapid extracellular turnover of glutamate of nonvesicular origin. Proc. Natl. Acad. Sci. U.S.A 96:8733-8738

Jensen, V., Rinholm, J., Johansen, T., Medin, T., Storm-Mathisen, J., Sagvolden, T., Hvalby, O., Bergersen, L. (2009). N-methyl-d-aspartate receptor subunit dysfunction at hippocampal glutamateric synapses in an animal model of attention-deficit/hyperactivity disorder. Neuroscience. 158(1):353-64.

Jones, M.V., Westbrook, G.L. (1996) The impact of receptor desensitization on fast synaptic transmission. Trends in neuroscience. 19(3):96-101.

Katz, B., and Miledi, R. (1968) The role of calcium in neuromuscular facilitation. Journal of physiology. 195;481-492.

Kampa BM, Clements J, Jonas P, Stuart GJ (2004) Kinetics of Mg2+ unblock of NMDA receptors: implications for spike-timing dependent synaptic plasticity. J. Physiology. (Lond.) 556:337-345

Kim, J., and Alger, B.E. (2001). Random response fluctuations lead to spurious paired-pulse facilitation. The journal of neuroscience. 21(24):9608-9618.

Koike-Tani, M., Kanda, T., Saitoh, N., Yamashita, T., and Takahasi, T. (2008). Involvement of AMPA receptor desensitization in short-term synaptic depression at the calyx of Held in developing rats. Journal of Physiology. 586.9(2263-2275).

Koh,S., Tibayan, F.D., Simpson, J.N., Jensen, F.E. (2004) NBQX or topiramate treatment following prenatal hypoxia-induced seizures prevents later increases in seizure-induced neuronal injury. Epilepsia. 4:569-575.

Kong, S., Qian, B., Liu, J., Fan, M., Chen, G., Wang, Y. (2010) Cyclothiazide induces seizure behavior in freely moving rats. Brain research. epub.

Kullmann, D.M., Erdemli, G., Asztely, F., (1996) LTP of AMPA and NMDA receptor-mediated signals: evidence for presynaptic expression and extrasynaptic glutamate spillover. Neuron. 17: 461-474.

Kullmann, D.M. and Asztely, F. (1998) Extrasynaptic glutamate spillover in the hippocampus: evidence and implications. TINS. 21(1): 8-14.

Kullmann DM, Min MY, Asztély F, Rusakov DA (1999) Extracellular glutamate diffusion determines the occupancy of glutamate receptors at CA1 synapses in the hippocampus. Philos. Trans. R. Soc. Lond., B, Biol. Science. 354:395-402

Larson J, Lynch G (1986) Induction of synaptic potentiation in hippocampus by patterned stimulation involves two events. Science 232:985-988

Lasztoczi, B., Kardos, J. (2006) Cyclothiazide prolongs low [Mg2+]-induced seizure-like events. Journal of neurophysiology. 96(6):3538-44.

Lawrence, J.J., Brenowitz, S., L.O. Trussell. (2003) The mechanism of action of aniracetam at synaptic a-amino-3-hydroxy-5-methyl-4-isoxazolepropionic acide (AMPA) receptors: indirect and direct effects on desensitization. Molecular pharmacology. 64(2):269-268.

Lehre KP, Danbolt NC (1998) The number of glutamate transporter subtype molecules at glutamatergic synapses: chemical and stereological quantification in young adult rat brain. J. Neurosci 18:8751-8757

Lester RA, Clements JD, Westbrook GL, Jahr CE (1990) Channel kinetics determine the time course of NMDA receptor-mediated synaptic currents. Nature 346:565-7

Lester RA, Jahr CE (1992) NMDA channel behavior depends on agonist affinity. J Neuroscience 12:635-43

Lozovaya NA, Kopanitsa MV, Boychuk YA, Krishtal OA (1999) Enhancement of glutamate release uncovers spillover-mediated transmission by N-methyl-D-aspartate receptors in the rat hippocampus. Neuroscience 91:1321-1330

Mainen ZF, Malinow R, Svoboda K (1999) Synaptic calcium transients in single spines indicate that NMDA receptors are not saturated. Nature 399:151-155

Malenka, R.C., and Nicoll, R.A. (1999) Long-term Potentiation--a decade of progress? Science. 285(5435):1870-1874

Miledi, R, Slater, C.R. (1966) The action of calcium on neuronal synapses in the squid. Journal of physiology. 184(2);473-498.

Manita, S., Suzuki, T., Inoue, M., Kudo, Y., Miyakawa, H.. (2007). Paired-pulse ratio of synaptically induced transporter currents at hippocampal CA1 synapses is not related to release probability. Brain research. 1154:71-79.

Mayer ML, Westbrook GL, Guthrie PB (1984) Voltage-dependent block by Mg2+ of NMDA responses in spinal cord neurones. Nature 309:261-263

Mennerick, S. and Zorumski, C.F. (1995). Paired-pulse modulation of fast excitatory synaptic currents in microcultures of rat hippocampal neurons. Journal of physiology. 488.1:85-101.

Otis TS, Wu YC, Trussell LO (1996) Delayed clearance of transmitter and the role of glutamate transporters at synapses with multiple release sites. J. Neuroscience. 16:1634-1644

Qi, J., Wang, Y., Jiang, M., Warren, P., Chen, G. (2006) Cyclothiazide induces robust epileptiform activity in rat hippocampal neurons both in vitro and in vivo. Journal of neurophysiology. 15;571:605-618.

Rusakov DA, Kullmann DM (1998) Extrasynaptic glutamate diffusion in the hippocampus: ultrastructural constraints, uptake, and receptor activation. J. Neuroscience. 18:3158-3170

Sarantis M, Ballerini L, Miller B, Silver RA, Edwards M, Attwell D (1993) Glutamate uptake from the synaptic cleft does not shape the decay of the non-NMDA component of the synaptic current. Neuron 11:541-549

Scimemi, A., Fine, A., Kullmann, D., and Rusakov, D. (2004). NR2B-containing receptors mediate cross talk among hippocampal synapses. The journal of neuroscience. 24(20): 4767-4777.

Scimemi A, Tian H, Diamond JS (2009) Neuronal transporters regulate glutamate clearance, NMDA receptor activation, and synaptic plasticity in the hippocampus. J. Neuroscience. 29:14581-14595

Shimamoto K, Lebrun B, Yasuda-Kamatani Y, Sakaitani M, Shigeri Y, Yumoto N, Nakajima T (1998) DL-threo-beta-benzyloxyaspartate, a potent blocker of excitatory amino acid transporters. Mol. Pharmacology. 53:195-201

Shimamoto K, Shigeri Y, Yasuda-Kamatani Y, Lebrun B, Yumoto N, Nakajima T (2000) Syntheses of optically pure beta-hydroxyaspartate derivatives as glutamate transporter blockers. Bioorg. Med. Chem. Lett 10:2407-2410

Stella, F., Treves, A. (2011). Associative Memory Storage and Retrieval: Involvement of Theta Oscillations in Hippocampal Information Processing. Neural Plasticity. doi:10.1155/2011/683961.

Teichman S, Kanner BI (2007) Aspartate-444 is essential for productive substrate interactions in a neuronal glutamate transporter. J. Gen. Physiol 129:527-539

Thomson, A. (2000) Facilitation, augmentation, and potentiation at central synapses. Trends Neuroscience. 23, 305-312.

Tong G, Jahr CE (1994) Block of glutamate transporters potentiates postsynaptic excitation. Neuron 13:1195-203

Trussell, L.O., Zhang, S., and Ramant, I.M. (1993) Desensitization of AMPA receptors upon multiquantal neurotransmitter release. Neuron. 10(6):1185-1196.

Tsukada S, Iino M, Takayasu Y, Shimamoto K, Ozawa S (2005) Effects of a novel glutamate transporter blocker, (2S, 3S)-3-[3-[4-(trifluoromethyl)benzoylamino]benzyloxy]aspartate (TFB-TBOA), on activities of hippocampal neurons. Neuropharmacology 48:479-491

Tzingounis AV, Wadiche JI (2007) Glutamate transporters: confining runaway excitation by shaping synaptic transmission. Nat. Rev. Neurosci 8:935-947

Wadiche JI, Kavanaugh MP (1998) Macroscopic and microscopic properties of a cloned glutamate transporter/chloride channel. J Neuroscience. 18:7650-61

Weston, M.C., Schuck, P., Ghosal, A., Rosenmund, C., Mayer, M.L. (2006) Conformational restriction blocks glutamate receptor desensitization. Nature structural and molecular biology. 13: 1120-1127.

Yernool D, Boudker O, Jin Y, Gouaux E (2004) Structure of a glutamate transporter homologue from Pyrococcus horikoshii. Nature 431:811-8

Zerangue, N., Kavanaugh, M. (1996) Flux coupling in a neuronal glutamate transporter. Nature. 383(6601):634-7.